Influence of ammonia and water sorption
on the chemical and electrochemical properties
of polyacrylic acid and its derivates

Einfluss von Wasser- und Ammoniaksorption
auf die chemischen und elektrochemischen Eigenschaften
von Polyacrylsäure und deren Derivaten

D I S S E R T A T I O N

der Fakultät für Chemie und Pharmazie
der Eberhard-Karls-Universität Tübingen

zur Erlangung des Grades eines Doktors
der Naturwissenschaften

2008

vorgelegt von

Melanie Hörter

Tag der mündlichen Prüfung: 18.12.2007

Dekan: Herr Prof. Dr. Lars Wesemann

1. Berichterstatter: Herr PD Dr. Udo Weimar

2. Berichterstatter: Herr Prof. Dr. Günter Gauglitz

Contents

1 Introduction

In everyday life the human nose is well adapted for perception of odours in the atmosphere. However, the detection of gases and vapours with the nose is not suitable for industrial applications because it is extremely subjective as human smell assessment is affected by many parameters [1] and inapplicable if odourless or harmful substances have to be detected. For this reason, assistive techniques as for example gas chromatography and mass spectrometry have been employed to control the atmosphere, to raise an alarm if a maximum or minimum value is exceeded or to assess the quality of products through odour evaluation. However, there are several drawbacks of customary analytical techniques: They are not portable and tend to be expensive and furthermore are relatively slow [2]. Compared with these techniques, chemical microsensors have several advantages as small size, low power consumption and the potential to be produced in a low priced batch fabrication manner. Nowadays, chemical sensors are used in and optimised for many applications such as for example the identification of purity, process and quality control, environmental analysis, medical diagnosis [3], food evaluation and flavour and fragrance testing [4], but there are still many applications remaining for which optimal sensors have not yet been developed. Therefore, further research into the area of chemical sensors is required.

1.1 Motivation and scope of the work

The entire field of chemical sensors suffers from a common malady: The development of chemically sensitive and selective interfaces is far behind the technology of the physical transduction platforms, which translate energy from a chemical system to a useful analytical signal [5]. Additionally, to meet the demands on chemical sensors the sensing material must not only have interesting and useful interactions with the key analytes, but they must be cheap and commercially viable in terms of manufacturability, reproducibility, and longevity.

Inorganic sensing materials, e.g. metal oxides show good sensing properties [6] but have the disadvantage to work at elevated temperatures only. The required heating of the sensing layer results in a high power consumption of the sensor making it unsuitably expensive for many applications. In contrast, sensors with polymers as

sensing materials usually work at room temperature. This feature allows cheap operation and makes polymers promising candidates to be included in chemical gas sensing devices. Another advantage of polymers is their suitability for standard IC (integrated circuit) processing which allows the fabrication of small, low cost sensors. However, the major drawback of these materials is the lack of selectivity as they respond to many different gases and vapours. To avoid this problem sensor arrays were constructed, which allow for the determination of a characteristic response pattern for each gaseous species [7, 8]. Another possibility to enhance the selectivity of polymers is the chemical modification of the material. Due to chemical reactions before, during and after the polymerisation process the properties can be tuned so that the material becomes selective for a certain target species.

It is well known that depending on the polymer functional groups the material prefers to interact with a certain type of molecules, for example polar, non-polar, acidic or basic species. Beside the functional groups other parameters such as the polymer structure or the presence of other species may influence the sorption process and, with it, the observed properties for chemical sensing. It is necessary to gain knowledge about the sorption mechanism in detail to purposefully vary the chemical properties of the polymer yielding in a sensor with optimum characteristics [9]. In this work, a sorption model system, the water vapour and ammonia gas sorption process into polyacrylic acid (PAA), is studied in order to allow for the modelling of the single species sorption mechanisms and their mutual influence on the sorption process. This work will aid future attempts to enhance the selectivity of PAA to water and ammonia. Additionally, the gained knowledge is used to explain the sensing properties of PAA already observed in different kinds of chemical sensors.

First experiments with PAA sensitive layers had already been performed by using chemomechanical sensors as quartz microbalances and electrochemical sensors as resistance measurements and Kelvin Probe set-ups. With the same types of devices the mass uptake upon water vapour and ammonia sorption and the potential change determined in the Kelvin Probe set-up were systematically measured in this work. To complete the picture of the sorption process, changes of the electrochemical properties in the bulk of the polymer and at the polymer electrode interface were studied with

impedance spectroscopy, cyclovoltammetry and voltage step measurements; additionally, infrared spectra were aquired at several compositions of the ambient. These measurements were repeated with two derivates of PAA: ammonium polyacrylate (NH_4PA) and sodium polyacrylate (NaPA). The study of the PAA salts demonstrates the considerable influence of small chemical modifications on the chemical and electrochemical properties and deepens the understanding of the sorption processes in PAA.

1.2 The sorption model system

In this work the water vapour and ammonia gas sorption processes into polyacrylic acid are used as a sorption model system because water and ammonia are important target species and polyacrylic acid showed interesting sensing properties in previous measurements. Both the gaseous species and the polymer are described in the following chapter.

1.2.1 Water vapour as target analyte

Water vapour is a natural component of air, and already in the 19th century several methods were used in meteorology to determine the atmosphere humidity. For example the amount of absorbed or condensed water under given experimental conditions can be used to measure humidity [10, 11]; another approach is the hair hygrometer whereby a strain in hairs induced by ambient humidity is used as sensing process [12]. Beside meteorology studies the humidity was measured in living space equipped with heating facilities to keep the humidity in a beneficial range for human beings [13].

With further development of technology and industry the measurement and/or control of humidity are important not only for human comfort but for a broad spectrum of applications: From intelligent control of tumble dryer, over climate control systems in the automotive industry [14], to high temperature catalyst control systems [15] the request for humidity sensors is widespread. Accordingly, various sensors have been investigated and developed to meet the demands. Most humidity sensors in the market are based on the capacitive technique [16] but other sensor principles such as, for

example, resistive, gravimetric or optical techniques are also used. In recent years transduction techniques of various state-of-the-art humidity sensors and sensing materials were reviewed [17-19]. A variety of ceramic, semiconducting, and polymer-based sensing materials are used in humidity sensors; also polyacrylic acid and its copolymers were already employed [20], as discussed in 2.2.4.

The interaction of water vapour with sensing materials is not only advantageous for humidity sensing but can also be a problem if cross-sensitivity to water hinders the detection of other target gases. Due to changes in the ambient humidity, a sensor may respond similarly as in the presence of the target species and falsely indicate a certain gas concentration. Such behaviour is called cross-sensitivity of first kind to humidity while the cross-sensitivity of second kind express the degree of influence of specific background humidity on the sensitivity to the target gas [21]. To compensate for these phenomena it is necessary to understand the interaction of the sensing material, the target species and water vapour with each other. For PAA used as ammonia sensing material, water vapour is a significant interference for measurements with several transducers [22]. The study of ammonia and water sorption interdependence in the polymer accomplished in this work leads to an understanding of the cross-sensitivity to humidity and supports further efforts to reduce it.

After the presentation of water as target of humidity sensors and as interference in other sensors the significance of ammonia as a target species is discussed in the following chapter.

1.2.2 Ammonia gas as target analyte

Ammonia is an important industrial gas with high toxicity. Therefore, in 1886, it was among the first chemical products whose maximum value allowed at the working place was restricted after animal experiments proved the toxicity even at low concentrations [23]. The human nose smells gaseous ammonia down to a concentration of about 55 ppm [24], particularly if the person is exposed to ammonia for the first time. After repeated exposure inurement effects occur and people become less sensitive to ammonia [25]. Up to now it is not clear if this inurement effects are due to a nonhazardous adaptation or are a pathological process [26] and because of the

insufficient toxicological database decisions on occupational exposure limits are difficult to make. In Germany, the maximum value allowed at the working place is regulated by law and given in the "Technische Regeln für Gefahrstoffe 900" (TRGS 900 [27]). According to this the ammonia concentration must not exceed 50 ppm but this value is rather high and a lowering to 20 ppm is advised by the DFG (Deutsche Forschungsgemeinschaft) in accordance with the European Scientific Committee on Occupational Exposure Limits (EU-SCOEL [28]). This issue is under discussion right now.

Irrespective to the specific maximum value, for the use in work place safety, devices capable of detecting ammonia in a concentration range of 1-50 ppm in ambient air are required. Traditionally the detection of ammonia in the gas phase is performed by potentiometric electrodes [29, 30]. They have the disadvantages of high power consumption, being easily poisoned and consumptive of the analyte. Chemical microsensors can solve these problems because of the sensor properties already mentioned above. In addition, such sensors may be employed in other indoor monitoring applications such as the leakage control in refrigeration systems and air conditioners [31]. The great demand for ammonia sensors has stimulated research efforts in this field and many different transducers and sensing materials were presented in literature. To provide insight into the ammonia sensor field, some of the used transducers and sensitive materials are presented in the following section.

Transducers frequently used for ammonia sensing are resistive devices, acoustic wave devices and field effect transducers (FET) or Kelvin Probe set-ups for the measurement of work function changes.

Resistive devices consist in comb electrode structures covered with sensing materials whose resistance depend on the amount of sorbed ammonia. A great variety of materials were used in this set-up as for example Cu_xS films [32], acrylic acid doped polyaniline [33], CuBr thin films [24], nanoporous anodized ammonia [34], and tellurium thin films [35]. The mass increase of a sensing layer upon gas sorption is also used as a sensing principle for ammonia detection and measured with surface acoustic wave devices. This type of transducers were, for example, covered with Langmuir-Blodgett polypyrrole films [36], nanoporous anodized alumina [34] or

polyacrylic acid produced by different methods [37, 38]. The major problem of many of these sensors is the pronounced cross-sensitivity to humidity, which was already mentioned in the previous chapter. Therefore, an increasing interest in another group of sensors based on work function changes induced by interaction with ammonia is observed because this sensors show a remarkable low cross sensitivity to water. The work function changes are measured with Kelvin Probe set-ups or FET devices and examples for sensing layers are titanium nitride [31], iridium oxide [39] or polyacrylic acid [21]. Further sensor types such as optical sensors, which are based on the change of absorbance of an acid-base indicator [40] or other optical effects are useful for ammonia detection; but these approaches are beyond the scope of this work and therefore will not be discussed in detail.

In the following chapter the sensing material PAA is described.

1.2.3 Polyacrylic acid as sensitive material

The monomer of PAA, acrylic acid was first prepared in 1843 by the air oxidation of acrolein obtained from the high temperature cracking of glycerine [41]. But it was not until 1930 when the technical obstacles for the manufacture and handling of this reactive monomer were overcame [42] and polyacrylic acid could be obtained in a controlled chemical reaction and produced on a large scale. Throughout the following years a growing demand for PAA develops from a variety of industries; some application examples are given in the next section.

In pharmaceutical applications cross-linked, water swellable polymers of acrylic acid are used for the controlled release of drugs in tablets. Because of the wide range of viscosities and flow properties these materials are also used in lotions, creams and gels [43]. Some derivates of PAA such as the ionic complexes with metal salts for example $FeCl_3$ or $TiCl_4$ form hydrogels which have a spongy structure containing water up to 90 wt %. These hydrogels are biocompatible, non-toxic materials which are widely used in dental glass-ionomer cements [44] and as antimicrobial agents [45]. Cross linked with polyethylenglycol or diisocyanates polyacrylic acid is used as a superabsorbant in diapers and other hygiene products.
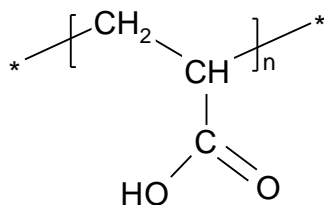
Figure 1.1: Chemical structure of polyacrylic acid

PAA is composed of repeating units bearing carboxyl groups (Figure 1.1) which determine the chemical and electrochemical properties of the material. Being a weak polyelectrolyte, polyacrylic acid partially dissociates in water allowing for electrical conduction in solution [22]. In the solid state, the acid functional groups are capable of hydrogen bonding via the oxygen atom and due to acid / base reactions specific interactions with bases are expected. Because of this chemical constitution the interaction of PAA with water vapour and the base ammonia changes the chemical and electrochemical polymer properties. In combination with appropriate transducers these changes can be utilised in chemical sensors for humidity and ammonia gas detection extending the field of PAA applications beyond the established industrial uses.

To study the sensing properties of PAA some investigations were performed in recent years; PAA was used in: switch-type humidity sensors with electrochemical transducers [20]; in field effect transducers (FET) and Kelvin Probe set-ups for ammonia detection [21, 46]; and in combination with acoustoelectrical transducers for both analytes [22, 37, 38]. The results obtained in these studies are presented in the theoretical part of this work.

Even though impressive changes in the resistance, capacitance and mass of the polyacrylic acid layers have been observed, the sorption mechanism and the influence of the ambient conditions on the electrical transport processes in the polymer have been so far investigated to a limited extent only. In this work, systematic gravimetric and electrochemical measurements were performed and complemented with infrared spectroscopy to obtain a deeper understanding of the sensing mechanisms. For explaining the origin of the work function changes measured in FET and Kelvin Probe set-ups suggestions were made in literature [22, 47], which will be discussed and extended in this work.

7

2 Theoretical background and related work

Several methods have been used in this work to study the chemical and electrochemical properties of PAA and its derivates, which can be monitored in sensing applications. In the following chapters a short introduction into the basics of each method is given and the interpretation is discussed as far as it is required for the measurements performed in this work. A literature survey for already published results obtained for PAA is additionally included.

The discussion starts with gravimetric measurements (2.1) and continues with electrochemical measurements (2.2) and measurements of work function changes (2.3). The chosen methods are supplemented with spectroscopic studies of PAA and its derivates (2.4).

2.1 Gravimetric measurements

Due to the sorption of gases or vapours from the ambient atmosphere the mass of a polymer increases. If it is possible to measure this mass change, useful information can be gained including the polymer / vapour sorption thermodynamics and kinetics [9]; adsorption/desorption isotherms [48]; and vapour/polymer interaction mechanisms [49].

To study the sorption behaviour of thin polymer films, commercial analytical microbalances are inapplicable because the mass increase is less than the current detection limit of the balances (10^{-10} kg). For the measurement of small masses down to 10^{-16} kg Sauerbrey introduced the quartz microbalance (QMB) in 1959 [50]. This device is composed of a thin piezoelectric quartz crystal sandwiched between two metal electrodes (Figure 3.2 a) and its mode of operation is based on the converse piezoelectric effect [51, 52]:

A voltage connected to the electrodes determines a mechanical strain in the piezoelectric material. If the polarity is reversed an identical strain is produced, but in the opposite direction. Therefore, an alternating potential across the quartz causes a vibration of the crystal at its resonant frequency. The resonant frequency depends on the mass of the quartz and the electrodes and therefore, is sensitive to mass changes. This property of the resonant frequency is used in QMBs: The quartz resonator is

adherently coated with a thin polymer layer and the corresponding resonant frequency is chosen as a reference point. Further changes of the resonant frequency indicate the mass change due to sorption of gases or vapours into the polymer layer and hence, the device can be used as a microbalance.

Unfortunately, the resonant frequency does not depend on the mass change only but also on other environmental effects to be discussed, below, in detail. Some authors stress that the QMB is not a mass detector because the sensitivity to mass changes is one property among others only [52]. Therefore, instead of quartz microbalance the name thickness shear mode detector was suggested to be more appropriate [53]. This discussion is still ongoing and in 2006 Mecea formulated three fundamental principles for mass measurements: the field principle, the mass sensitivity principle and the general equivalence principle. With his own work and the results obtained by other authors he demonstrated that QMBs satisfy these principles and hence are really mass detectors [54]. Other effects influencing the resonant frequency are second order only.

The QMBs belong to the family of acoustic wave (AW) devices which are introduced in chapter 2.1.1. In the subsequent chapters the discussion focus on the QMB devices describing their operation method as mass detectors (2.1.2) and further parameters that can influence the QMB signals (2.1.3). The latter chapter examines the experimental conditions under which the QMB results reflect mass changes undisturbed by other parameters. For the interpretation of the gravimetric measurements sorption isotherms, relevant for the studied system are discussed (2.1.4.1) and the Flory-Fox equation for estimation of the polymer static glass transition temperature is deduced (2.1.4.2). The chapter 2.1 closes with a survey of PAA covered SAW devices responses already reported in literature (2.1.5).

2.1.1 Acoustic wave devices [55]

Acoustic wave devices have in common that metal electrodes attached to a piezoelectric material launch acoustic waves into the material at ultrasonic frequencies, which may range from one to hundreds megahertz [55]. Typically a quartz crystal is used as a piezoelectric material but AW devices with other materials

are also known, for example lithium niobate [56], zinc oxide [57], and aluminium nitride [58].

The AW devices are divided into groups according to the following characteristics of the generated acoustic wave: particle displacement relative to the direction of the wave propagation, particle displacement relative to the plate surface, and the wave propagation mechanism. These parameters are determined by the crystal orientation and thickness of the piezoelectric material and the geometry of the metal electrodes.
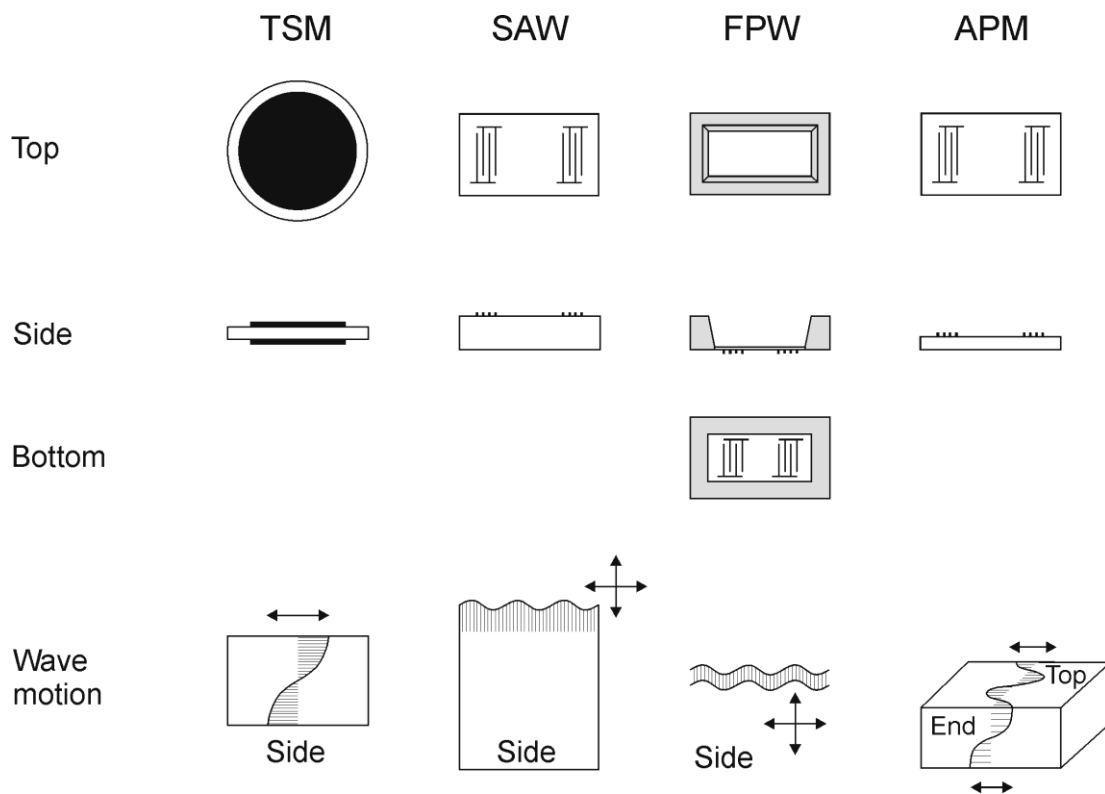
Figure 2.1: Views illustrating the structures of TSM, SAW, FPW, and APM devices and their respective wave motion. The piezoelectric material is white while electrodes are indicated with schematic comb structures or black areas. The side views are cross sections. In the representation of the wave motion the shaded areas illustrate the wave motion or indicate the depth of wave penetration into the plate and the double-headed arrows show directions of surface particle displacements. [55]

In QMBs which are among the group of thickness shear mode (TSM) resonators, the waves generated are bulk transverse waves that travel in a direction perpendicular to the plate surfaces; particle displacements at these surfaces are parallel to the surface. Beside TSM resonators other important groups of the AW family are the Surface

Acoustic Wave (SAW), Flexural Plate Wave (FPW) and Acoustic Plate Mode (APM) devices. Typical setups of these four groups are illustrated in Figure 2.1 and the appropriate type of acoustic wave is sketched.

All these groups are used for applications in chemical sensing and interfacial studies. For this purpose the surface of the AW device is adherently coated with a layer that sorbs gas-phase species [59, 60], for example a polymer film. It is important to carefully tune the thickness of the added layer; the optimal thickness where the device acts as a nearly ideal gravimetric detector depends on the transducer design, the operating frequency and the material chosen as sensitive layer. If the polymeric layer is "acoustically thick" the film does not move synchronously with the substrate surface but the upper film portions lag behind the film/substrate interface, causing nonuniform displacement across the film thickness. This leads to a nonlinear response to the sorbed vapour concentration if the viscosity of the material alters during vapour sorption [61]. Therefore it is necessary that the film remains in the "acoustically thin" regime. Typically, this condition is fulfilled if the mass of the film does not exceed 2% of the mass of the crystal [52]. However, the polymeric film must not be too thin: Coadsorption of analyte molecules at the transducer surface and at the polymer substrate interface could adulterate the response unless the substrate is completely and closely covered [62].

Further discussion in this work will be limited to TSM resonators because these are the devices used in the experimental part. SAW, APM, and FPW devices are mentioned only if it is especially interesting to compare their properties with the ones of the TSM resonator.

2.1.2 Gravimetric measurements with QMBs [50, 52]

If a material is uniformly deposited on the QMB substrate, the acoustic wave will travel across the interface between the quartz and the added material. If it is assumed that the density and the wave transverse velocity associated with the foreign material is identical to those of quartz, the system can be described as a "composite resonator" in which the quartz covered with an additional material is treated as tantamount to a thicker quartz crystal.

12
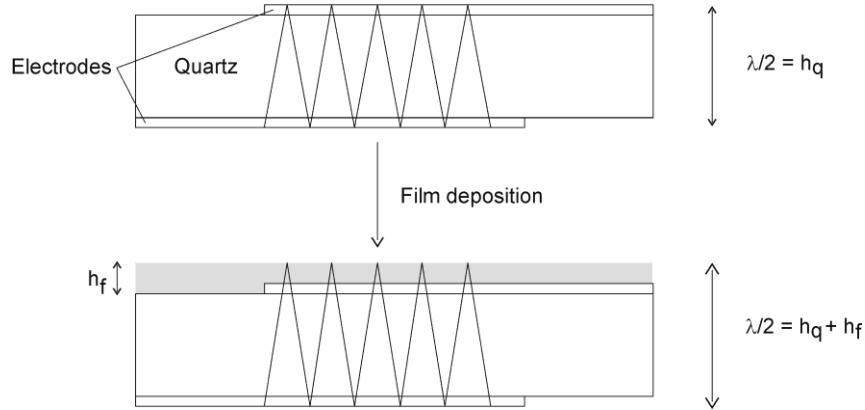
Figure 2.2:   Schematic representation of the transverse shear wave in a quartz crystal and a composite resonator comprising the quartz crystal and a layer of foreign material. The acoustic wavelength is longer in the composite resonator due to the greater thickness, resulting in a low resonant frequency compared to the quartz crystal [52].

The larger the thickness the longer is the acoustic wavelength in the "composite resonator", resulting in a lower resonant frequency (Figure 2.2). Hence, the resonant frequency of a quartz crystal changes proportionally to the mass deposited onto the surface. Sauerbrey set up an equation to quantify this relationship

$$\Delta f = k\, f_0^2\, \frac{\Delta m}{A} \tag{2.1}$$

where Δf is the frequency shift due to added mass, k is a constant, f_0 is the fundamental frequency of the quartz crystal, and $\Delta m/A$ the surface mass loading in grams per square centimetre.

According to this equation and similar equations deduced for other AW devices [63] the sensor response is proportional to the square of the fundamental frequency. In case of QMBs, increasing the operating frequency and therewith the mass sensitivity requires diminishing the plate thickness, with the fragility of the substrate setting the ultimate limit [5]. Because of different setups other devices of the AW family have the advantage to work at higher fundamental frequencies. These devices show higher sensor responses but not necessarily better performance because the higher the fundamental frequency of the devices the thinner the coatings and this results in less vapour being sorbed [64]. Additionally, even if the same amount of foreign material is used to cover AW devices the signal to noise ratio (S/N) increases with increasing operating frequency due to thermal effects and especially electronic interferences at

13

high frequencies. Beside the S/N ratio the limit of detection (LOD), which is the concentration of the analyte corresponding to S/N = 3 may also negatively be influenced. The QMBs used in this work have a fundamental frequency of 30 MHz and show very favourable S/N and LOD values [62].

2.1.3 Further parameters influencing the QMB signals

As mentioned above the response of AW devices is not determined by mass changes only but the sorbed species may, in addition, modify other physical properties of the layer. These modifications would also influence the frequency response of the system [61, 65]. Ricco et al. [56] developed a formula where the frequency change of a SAW device is expressed as a sum of contributions

$$\Delta f = \frac{\partial f}{\partial m} \Delta m + \frac{\partial f}{\partial c'} \Delta c' + \frac{\partial f}{\partial \varepsilon} \Delta \varepsilon + \frac{\partial f}{\partial \sigma} \Delta \sigma + \frac{\partial f}{\partial T} \Delta T + \frac{\partial f}{\partial p} \Delta p + \dots \qquad (2.2)$$

where m is the mass, c' the stiffness, ε the dielectric constant, σ the conductivity, T the temperature, and p the pressure. Similar relationships can be assumed for other AW devices.

The **stiffness modulus**, a measure for the viscoelastic properties of a polymer layer, is affected by volume changes due to thermal expansion of the polymer or vapour sorption, polymer relaxation time, and film resonance effects [66, 67]:

When the polymer film is perturbed by the probing acoustic waves, polymer chain segments relax back to their former conditions. The characteristic relaxation time depends on the temperature and the structure of the polymer possibly altered due to sorption and swelling processes. If the viscosity of the material changes during vapour sorption this effects the resonant frequency of the system and the AW device is no longer a pure mass sensor [68, 69]. Additionally, in relative thick layers film resonance can occur. In this case the films upper surface lags behind the motion at the polymer-substrate interface by 90° and the shear stress applied to the lower film surface interfere constructively with those reflected from the upper film surface leading to a dramatic response of the acoustic wave device at the film resonant frequency [61]. To avoid erroneous conclusions about mass transport in the film Buttry and Ward suggest that QMB investigations of polymer layers should be performed for a range of film

thicknesses [52]. Linearity of response over the chosen range is evidence of the absence of changes in viscoelasticity during the experiment and/or rigid behaviour of the film.

The viscoelastic and the film resonance effect must be considered only in "acoustically thick" films where the polymer behaves rubbery with a modulus of about 10^6 N/m^2. In an "acoustically thin" film where the entire layer of a glassy polymer moves synchronously with the substrate surface the described effects do not occur. Even if the temperature is above the glass transition temperature and the polymer is supposed to be in the rubbery state the material may response "acoustically thin" because the resonant frequency of the AW devices additionally determines if a layer behaves acoustically thick or thin: As soon as the relaxation time is much longer than the period of the acoustic wave the polymer chains cannot relax in between the perturbations and therefore the frequency response is not influenced by changes in viscoelasticity. At acoustic wave frequencies above 1 MHz and room temperature nearly all rubbery polymers show "acoustically thin" film properties with measured moduli typical of polymer glasses (about 10^9 N/m^2) [61, 66].

Not only the mechanical properties of the coating material but also its electric properties (**dielectric constant** and **conductivity**) can affect the resonant frequency of an AW device [70, 71]: The propagation of an acoustic wave in a piezoelectric material generates a layer of electric charges at the surface due to the induced electrical polarisation of the crystal. The magnitude of this effect depends on the electromechanical coupling constant of the piezoelectric material; for example in lithium niobate the effect is more distinctive than in quartz [56, 66]. The resulting electric field extends into the adjacent layer where it may induce movement of ions and dipole reorientation. The energy stored and dissipated in moving these charges and dipoles depends on the dielectric constant and conductivity of the coating film. It is extracted from the wave energy and influences the wave velocity and therefore the resonant frequency of the AW devices. This acoustoelectric effect is not observed if the coating film is either non-conducting, as in most of the polymer layers, or highly conductive, as in metal films [66].

Additionally, the effect of **temperature** and **pressure** variations on the AW device signal must be considered. The temperature influences the resonant frequency of the uncoated transducer, for example the resonance frequency of a 30 MHz QMB device increases by 5 Hz per degree Celsius. However this effect is small compared to the effects resulting from the coatings because the temperature strongly influences the viscoelastic properties of the polymer inducing the effects described above [62, 66]. To perform precise measurements it is necessary to control carefully the temperature and the pressure in the measurement chamber.

In the liquid phase additional effects may occur such as frequency changes due to trapped solvent molecules in the holes of a rough surface, effects due to surface stress or due to interfacial slippage of solvent layers [52]. In contrast gas phase mass detection with acoustic wave devices is usually straightforward if the polymer film is stiff and thin, the added material is non-conducting, and temperature and pressure is kept constant.

2.1.4 Interpretation of the QMB measurements

As discussed in 2.1.2 the raw experimental results are obtained as resonance frequency shifts of the polymer coated QMBs. From them are deduced the corresponding frequency shifts due water vapour and ammonia gas sorption. If this data are plotted against the analyte concentration, sorption isotherms are obtained which can be compared with theoretically deduced sorption isotherms. Depending on the mode of sorption several isotherms have been observed and modelled; in section 2.1.4.1 the discussion is limited to the Langmuir and the BET (Brunauer-Emmett-Teller) isotherm, which are required for the interpretation of the chosen model system.

While the sorption isotherms reflect the mode of sorption they do not take into account any structural changes in the polymer as water vapour or ammonia gas is absorbed. However, it is well known that in amorphous solids water vapour absorption is associated with a significant plasticizing effect, as reflected by significant reductions in the glass transition temperature of the solid [72]. This structural change during gas sorption is very important to understand the sorption mechanism. With the Flory-Fox

equation deduced in 2.1.4.2 the static glass transition temperature can be estimated from the frequency shifts obtained in the QMB measurements.

2.1.4.1 Sorption isotherm

Depending on the sorption site the classical sorption theory draws a formal distinction between **ad**sorption where the sorption phenomenon is confined to the physical interface between a substrate and its environment and **ab**sorption where the sorption process occurs within the substrate.

In 1918 Langmuir proposed a theoretical model to describe the process of surface adsorption [73]

$$\lambda = \frac{\lambda_m b P}{1 + b P}$$

(2.3)

where λ is the current adsorbate loading, λ_m the adsorbate loading at monolayer coverage, P the adsorptive partial pressure and b a constant. According to this model, at low pressure, the amount adsorbed becomes proportional to the pressure whereas at high pressure, λ approaches the monolayer coverage (Figure 2.3). Depending on the properties of substrate and adsorbate other theoretical models were developed [74-76] to obtain a better fit to the experimental results.
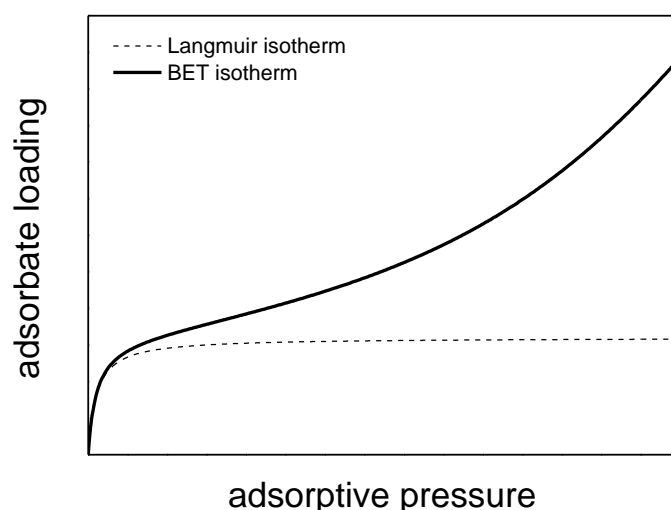
Figure 2.3: Illustration of Langmuir (dashed line) and BET (continuous line) isotherms. The isotherms give a relation between the adsorbate loading and the adsorptive pressure at constant temperature.

Further attempts have been made to extend the analytical treatment of adsorption to cover the formation of multilayers [77-82]; in this work only the well-known Brunauer-Emmett-Teller equation [80] will be discussed. The BET isotherm takes account of the formation of multilayers but usually overestimates the effect at higher adsorbate concentrations. In order to avoid this, the model has been extended by the assumption that multilayer formation is limited to n layers. This leads to a modified equation called finite length BET isotherm where C_{BET} is the BET constant and $x = P/P^*$ (with the saturation pressure of the target gas P^*)[83]:

$$\lambda = \lambda_m \cdot \frac{\left[C_{BET} \cdot x / (1-x)\right]\left[1 - (n+1) x^n + n \cdot x^{n+1}\right]}{1 + (C_{BET} - 1) x - C_{BET} \cdot x^{n+1}} \tag{2.4}$$

The BET constant represents the ratio of the adsorption equilibrium constant of the first layer to that of the subsequent layers. Due to the formation of multilayers the adsorbate loading increases at high pressure (Figure 2.3), at low adsorptive pressure ($x < 0.01$) and sufficient high constant C_{BET} the BET isotherm simplifies to the Langmuir isotherm [84].

These equations are developed for the adsorption process but according to Hayward and Trapnell they can also be used to describe absorption processes because absorption can be regarded as essentially internal adsorption, where the sorbate diffuses from the surface of the substrate into its interior via fine capillaries, crystal grain boundaries, and by penetration of vapour between the atoms of a crystalline network [85].

In this work the Langmuir isotherm is used to fit the ammonia sorption data (e.g. Figure 4.5 b) in 4.2.2) and the finite length BET isotherm proved to be useful to fit the water sorption data (e.g. Figure 4.3 a) in 4.2.1). However, the theoretical models are only nonpredictive curve-fitting exercises that do little to advance the understanding of the molecular processes occurring as water and ammonia is taken up into the polymer [86]. A parameter reflecting structural changes in the polymer is the static glass transition temperature. It can be estimated from the gravimetric measurements as discussed in the following chapter.

2.1.4.2 Dynamic and static glass transition temperature

As mentioned above (see 2.1.3) the temperature affects the viscoelastic properties of the polymer layer. Below the **dynamic glass transition temperature** the glassy polymer film behaves acoustically thin and if the temperature is increased above the glass transition the film becomes rubbery showing acoustically thick behaviour.

There are two phenomena associated with the glass transition that are not observable at the high frequencies at which AW devices operate [61]. These are an increase in specific heat capacity as observed in differential scanning calorimetry (DSC) and an increase in thermal expansion coefficient. It is important to identify the temperature at which these quasi-static effects occur because the properties of the polymer differ below and above this temperature, which is called the **static glass transition temperature** (T_g). It is a controversial issue if the static glass transition temperature can be extracted from the response of polymer-coated AW devices [60, 87-89], however, for the sorption of water into the polymer it can be estimated with the Flory-Fox equation [90] which is deduced in the following section:

A relationship between T_g and the phase composition of mixed amorphous systems can be derived from the polymer free volume theory [91]. By assuming perfect volume additivity at T_g and no specific interaction between the two components the following equation can be set up

$$T_{gm} = \phi_{V1} \cdot T_{g1} + \phi_{V2} \cdot T_{g2} \tag{2.5}$$

where T_{gm} is the static glass transition temperature of the mixed amorphous system, T_{g1} and T_{g2} the static glass transition temperatures and ϕ_{V1} and ϕ_{V2} the volume fraction of each component. The equation is based on a simple mixing rule similar to that used to describe ideal solution behaviour. If it is expressed in terms of weight fraction of each component the result is the well-known Gordon-Taylor equation [92]

$$T_{gm} = \frac{(w_1 \cdot T_{g1}) + (K \cdot w_2 \cdot T_{g2})}{w_1 + (K \cdot w_2)} \qquad \text{where} \quad K = \frac{\rho_1 \cdot \Delta\alpha_2}{\rho_2 \cdot \Delta\alpha_1} \tag{2.6}$$

where for both materials 1 and 2 w is the weight fraction, ρ the true density, and $\Delta\alpha$ the change of thermal expansivity of T_g; K is a constant. This equation has been used to describe the glass transition behaviour of many compatible polymer blends. It is, however, not particularly suitable for the description of the glass transition temperature

dependence on the water content in the polymer layer because T_g of water is very low and $\Delta\alpha$ is subsequently very difficult to measure. In this case it is useful to simplify the Gordon-Taylor equation using the Simha-Boyer rule [93].

$$\Delta\alpha \cdot T_g \approx const \tag{2.7}$$

Hence the constant K can be calculated from the densities of the two components.

$$K = \frac{\rho_1 \cdot T_{g1}}{\rho_2 \cdot T_{g2}} \tag{2.8}$$

For polymers plasticized with water the ratio of densities will be approximately unity and this leads to a further simplification of the Gordon-Taylor equation resulting in the following equation which is commonly referred to as the Flory-Fox equation

$$\frac{1}{T_{gm}} = \frac{w_w}{T_{gw}} + \frac{w_p}{T_{gp}} \tag{2.9}$$

where the indices w and p mark the weight fraction of the water in the polymer film and the polymer respectively. The weight fraction of the water depends on the ambient humidity and can be calculated from the frequency shift of the QMBs, where $\Delta f_{PAA\ layer}$ is the frequency shift due to the added polymer in dry air, and Δf_{water} is the further frequency shift due to sorbed water molecules at a given ambient humidity. The weight fraction of the polymer follows from the same equation.

$$w_w = \frac{\Delta f_{water}}{\Delta f_{PAA\ layer} + \Delta f_{water}} = 1 - w_p \tag{2.10}$$

With the calculated weight fractions and the values for T_{gw} (T_g of water) and T_{gp} (T_g of the dry polymer) taken from literature the Flory-Fox equation can be used to estimate the static glass transition temperature of the humid polymer at several ambient humidities (see Figure 4.4 in 4.2.1).

2.1.5 Literature survey of QMB devices covered with PAA

In 2001 Nanto et al. reported for the first time that QMBs covered with a plasma-polymerized acrylic acid exhibit a high sensitivity and selectivity for gaseous ammonia. While many organic species such as for example methane, ethanol, chloroform, toluene, or trimethylamine induce no sensor response, the injection of gaseous ammonia into the measurement chamber results in a frequency shift which

increases with increasing ammonia concentration. The sensor responded to the gas ammonia at concentrations down to 1 ppm [37]. Even if this study does not consider the influence of relative humidity on the ammonia sensing process, later work highlights that water vapour strongly intensifies the sensor response [22, 38]. This property can be used to detect gaseous ammonia at ppb level with the assistance of pre-adsorbed water in the polymer, as reported for QMBs covered with an electrospun fibrous polyacrylic acid membrane.

Because of the high sensitivity of QMBs with PAA coating to humidity Ding et al. suggested to use this device for water vapour detection [38]. However, up to now no systematic studies of humidity sensors based on acoustic wave devices covered with PAA are reported in literature.

To explain the interactions between polymer, ammonia and, in addition, water molecules it was suggested that a tendency of carboxyl radicals to chemically adsorb ammonia causes the sensitivity to ammonia [33] and that water molecules absorbed into the PAA layer are creating new absorption sites for ammonia explaining the enhanced sensitivity in the presence of humidity [38, 47]. However, so far it was not possible to draw a complete picture of the sorption process and the suggestion concerning the interaction of ammonia with preabsorbed water molecules is challenged by the experiments performed in this work.

2.2 Electrochemical measurements

In chemical gas sensing the electrical resistance and capacitance shifts of polymer layers upon gas exposure can be used to monitor the analyte concentration in the ambient atmosphere [94, 95]. For research into the underlying electrochemical processes the alternating current impedance spectroscopy (AC IS) is particularly suitable because this minimally destructive technique [96] allows insight into the mechanism of charge carrier transport in the polymer layer and into the electrochemical interactions and reactions at the polymer/electrode interface.

After an introduction into the measurement principle and typical results of AC IS in the following chapter the interpretation of the obtained results with equivalent circuits is discussed in 2.2.2 and possible equivalent circuit elements are presented. The

physical meaning of the circuit elements describing the impedance of the polymer bulk and the polymer/electrode interface are given in section 2.2.2.1 and 2.2.2.2 respectively. The impedance measurements are supplemented with voltage step and cyclic voltammetry measurements which are introduced in 2.2.3.

2.2.1 Measurement principle and typical results of AC impedance spectroscopy

The concept of electrical impedance generalizes Ohm's law to AC circuit analyses and analogue to Ohm's law the impedance, Z, results from the ratio of the potential and the current:

$$Z = \frac{E_t}{I_t} \tag{2.11}$$

To measure the impedance of a circuit a sinusoidal alternating electrical potential is applied (equation (2.12)) where E_t is the potential at time t, E_0 the amplitude and ω the radial frequency. As response to this stimulus, a AC current is measured. If the electrical circuit is linear[1], the AC current is a sinusoidal function with the same frequency as the potential but shifted in phase where I_t is the response signal, I_0 the amplitude and ϕ the phase by which the signal is shifted (equation (2.13)).

$$E_t = E_0 \sin(\omega t) \tag{2.12}$$

$$I_t = I_0 \sin(\omega t + \phi) \tag{2.13}$$

Equation (2.13) is also valid for non-linear circuits if the system is pseudo-linear; this means that the current versus voltage plot is at least linear over the measured range. To experimentally fulfil this condition it is necessary to keep the measured range as small as possible and therefore such experiments are performed with very small electric potentials applied (usually 10-30 mV [98] or even below 10 mV [96] depending on the studied circuit). The polymer coated metal electrodes used in this work can be considered as a linear system and hence higher electric potentials (up to 100 mV) are possible [99].

---

[1] "A linear system… is one that possesses the important property of superposition: If the input consists of the weighted sum of several signals, then the output is simply the superposition, that is, the weighted sum, of the responses of the system to each of the signals." [97]

With equations (2.12) and (2.13) the impedance of linear or pseudo-linear systems results in:

$$Z = \frac{E_t}{I_t} = Z_0 \frac{\sin(\omega t)}{\sin(\omega t + \phi)} \qquad (2.14)$$

where Z_0 is the amplitude. The impedance depends on the frequency of the excitation potential and this property is applied in the AC IS.

AC impedance spectroscopy consists in measuring the changes in electrical impedance upon variation in frequency (1 mHz – 1 MHz) of the alternating voltage. To present the data the complex notation of the impedance is introduced which results from equation (2.14) and Eulers relationship:

$$Z(\omega) = Z_0 (\cos\phi + i\sin\phi) \qquad (2.15)$$

with the real part $Z' = Z_0 \cdot \cos\phi$ and the imaginary part $Z'' = Z_0 \cdot \sin\phi$. In the plane spanned by Z' and Z'' each point can be specified by two Cartesian (Z' and Z'') or polar coordinates (r and ϕ, where r is the modulus of impedance). Most electrochemical impedance spectra have been presented with the real impedance plotted against the imaginary leading to the so-called Nyquist impedance spectrum [100] which is sometimes also called Cole-Cole plot; an example is shown in Figure 2.4 a). An alternative presentation is the Bode spectrum where the polar coordinates ϕ and r are plotted as a function of the frequency (Figure 2.4 c) and d). The Bode plot provides a quick survey of the type of spectrum recorded because all measured points are displayed equally, the frequency dependence is directly visible and the resistance and capacitance regions are clearly distinguished [101].

2.2.2 Interpretation of the AC impedance spectroscopy results

Depending on the electrochemical processes in the polymer and at the polymer/electrode interface the Nyquist plot shows a line, an arc and one or more full semicircles. The properties of the studied electric circuit can be deduced from this data by several methods [102]. The resistance of an electrochemical process for example can directly be obtained from the Nyquist plot because the distance from the high-frequency end of the semicircle to the low-frequency end coincides with the resistance. Other methods are the calculation of the resistance from the maximum of the

imaginary impedance, from the absolute impedance and phase angle versus frequency plots or from the equivalent circuit. The values resulting from the different methods are almost identical but in this work the equivalent circuit is exclusively used because this method is simple, fast and can provide a complete picture of the system [103].
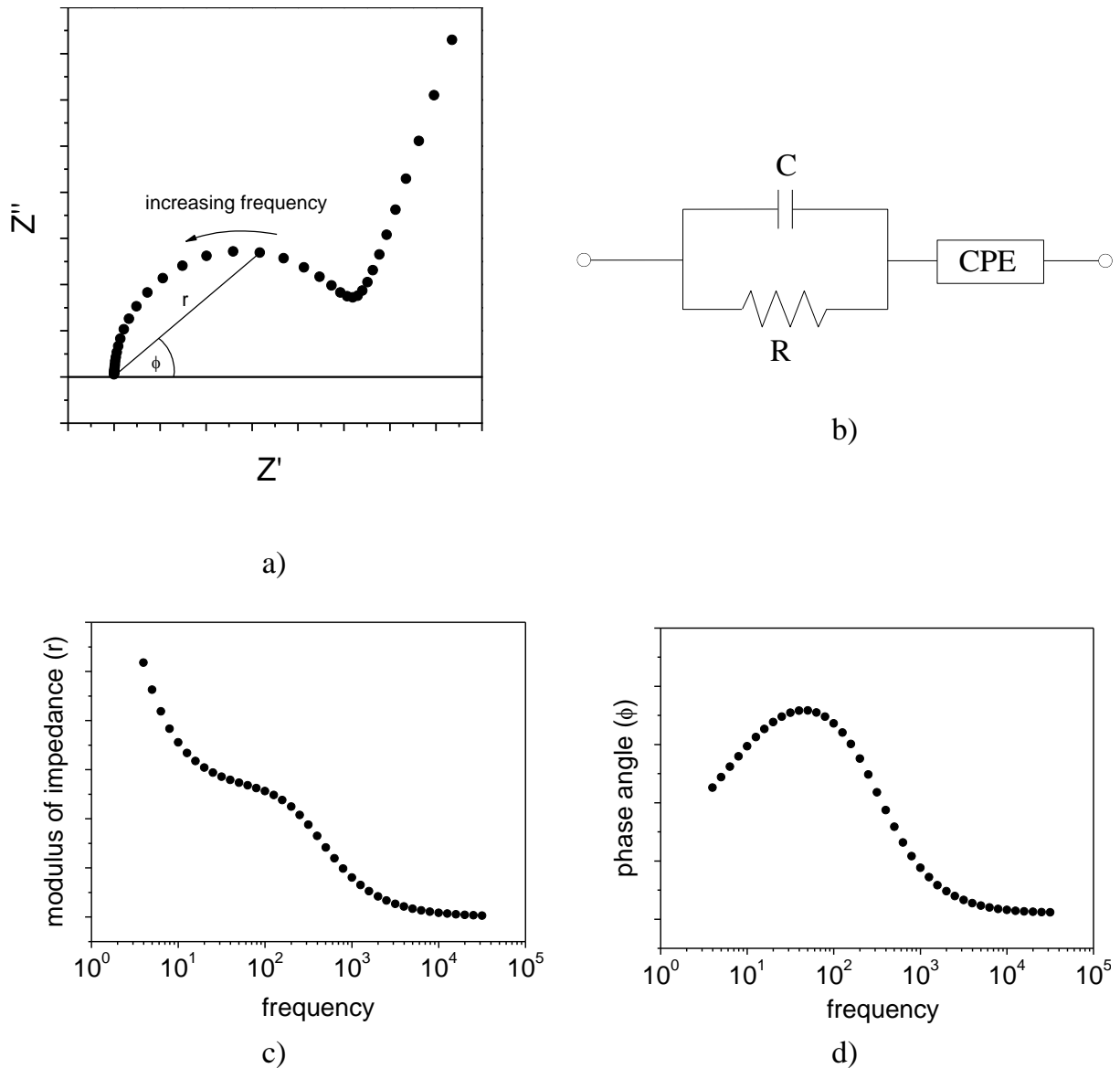
Figure 2.4: Two different representations of impedance spectroscopy results: In the Nyquist impedance spectra (a) the real impedance Z' of the circuit (b) is plotted against the imaginary one Z'' while in the Bode spectrum the modulus of the impedance (c) and the phase angle (d) are plotted against the frequency of the AC circuit. In the equivalent circuit (b) R represents the resistor that charge carrier encounter in the material or in a specific electrochemical process and the capacitor C in parallel is caused by the dielectric constant of the polymer layer or by the accumulation of charged species. The constant phase element CPE describes the behaviour of the sample at low frequencies.

The equivalent circuit model represents the various processes involved in the transport of mass and charge in the polymer. The model usually consists of several elements (resistors and capacitors among others) arranged in series and in parallel in a network [104]. For the dispersion data in Figure 2.4 the equivalent circuit is given in Figure 2.4 b).

The resistor R represents the resistor that charge carrier encounter in the material or in a specific electrochemical process and the capacitor C in parallel is caused by the dielectric constant of the polymer layer or by the accumulation of charged species. The impedance increase at low frequencies cannot satisfactorily be described with a capacitor and for this reason an empirical impedance function, the constant phase element CPE, is introduced

$$Z_{CPE} = Y_0 \cdot (i\omega)^n \tag{2.16}$$

where Y_0 and n are parameters of the CPE impedance. The CPE represents a variety of elements (for example a capacitor ($n = 1$) or a resistor ($n = 0$)) and can describe non-ideal dielectric behaviour ($-1 \leq n \leq 1$). Possible causes that give rise to non-ideal behaviour are the irregular thickness and morphology of the polymeric film [105], the roughness of the electrode surface [106], a distribution of relaxation times [107] or a non-uniform diffusion in the layer [108]. Even though a particular theory may not give exactly CPE behaviour, very often CPE will fit experimentally data very well and can provide a useful modelling element even if it is just treated as an empirical constant with no real physical meaning [109].

Additional elements which can be included in an equivalent circuit are the inductor and the Warburg element. The inductor may represent the deposition of surface layers and the Warburg element is used to model linear semi-infinite diffusion which occurs when the diffusion layer has infinite thickness [109, 110]. Calculations of the impedance due to diffusion show that the real and the imaginary part of the impedance depend on the frequency in the same manner and, hence, in the Nyquist plot it appears as a straight line inclined at 45° to the real axis. In the equivalent circuit the Warburg element is a short form for a semi-infinite resistive-capacitive transmission line (Figure 2.5). This model must be modified in the case of finite-length boundary conditions (reflective and transmissive boundary conditions) which have to be

considered at very low frequencies, for very thin samples or for large diffusion coefficients. In the case of reflective boundary conditions the electroactive species cannot reach the electrode at low frequencies any more and in the equivalent circuit the finite-length transmission line is terminated with an open circuit. If the transmission line ends with a resistance it is an analogue of transmissive boundary condition where the electroactive species reaches the electrode at low frequencies with a constant activity.
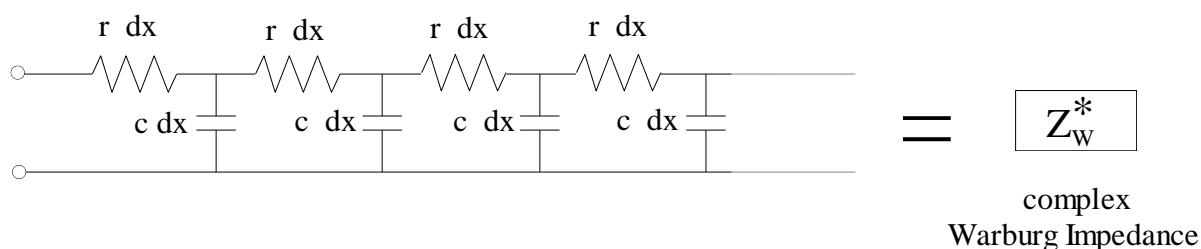
Figure 2.5: A resistive-capacitive transmission line which describes the behaviour of a semi-infinite diffusion process.

With the described elements the equivalent circuit is a useful model to represent the dynamic characteristics of an electrochemical system. However, a major drawback of this method is that the elements of an equivalent circuit often can be rearranged in various ways and still yield exactly the same impedance. This raises the problem: which specific equivalent circuit out of a large number of possibilities has to be chosen [109]? A suitable model of an electrochemical system should not only give a good fit with the experimental data but also be physically meaningful und confirmed by one or two other techniques [104].

The equivalent circuit representing the electrochemical system studied in this work should be able to explain both the impedance of the polymer bulk and the polymer/electrode interface.

2.2.2.1 Impedance of the polymer bulk

The arc or semicircle that appears at the highest frequencies in the electrochemical impedance spectra can be fitted with a parallel $R \parallel C$ circuit with R representing the resistance of the polymer (R_b) and C the capacitance of the electrode structure covered with polymer as a dielectric material (C_b).

26

Ionic conductance of polymers in dry air depends on the ability of the polymer chains to move in the bulk and in doing so to carry charged species through the polymer [111]. This segmental motion of polymer chains is usually observed above the glass transition temperature only and therefore polymers at lower temperatures in dry air do not show ionic conductance. In humid air water molecules diffuse into the polymer adsorbing at critical points by dipole-dipole interaction or hydrogen bonds. With increasing amount of water in the polymer the molecules associate, forming clusters of water molecules and eventually liquid water in the polymer. This process was studied for example for cellulose [112]. Sorbed water molecules allow for the transport of charge by two different mechanisms [113]:

The first transport mechanism is based upon the ability of water molecules to form hydrogen bonds among each other and with the host polymer if the material is able to accept or donate hydrogen bonds. These bonds, which specifically involve a hydrogen atom already covalently or ionically bonded to another atom [114], cause the formation of a chain of water dipoles throughout the polymer providing a path for proton transfer from one water molecule to the neighbouring one. Under the action of an externally applied field the protons undergo a Grotthuss [115] mechanism where the charge is carried through the entire polymer film by a hopping process along the uninterrupted trajectory of water dipoles which is in average aligned to the field direction (Figure 2.6 a). Besides water, other molecules, for example imidazol, may take part in the Grotthuss mechanism acting as proton donor and acceptor in the proton conduction process [116].

This transport mechanism is favoured if the hydrogen bonds are short and strong but it is progressively dominated by a second transport mechanism if the hydrogen bonds are weakened, for example, due to increasing temperature [113]. The second transport mechanism, the so-called vehicle mechanism is a molecular diffusion process where the migration of protons is assisted by the translational dynamics of bigger species (Figure 2.6 b). The protons diffuse together with a vehicle (e.g. H_3O^+ or NH_4^+ ions) while the counterdiffusion of unprotonated vehicles (e.g. H_2O or NH_3) allows the net transport of protons through the polymer [117]. The vehicle mechanism is, for example, observed in solvent swollen polyelectrolytes; this materials can be described

as concentrated solutions in which one ionic species is very large and multiply charged and the mobile ion is solvated and hence mobile in the solution [111].
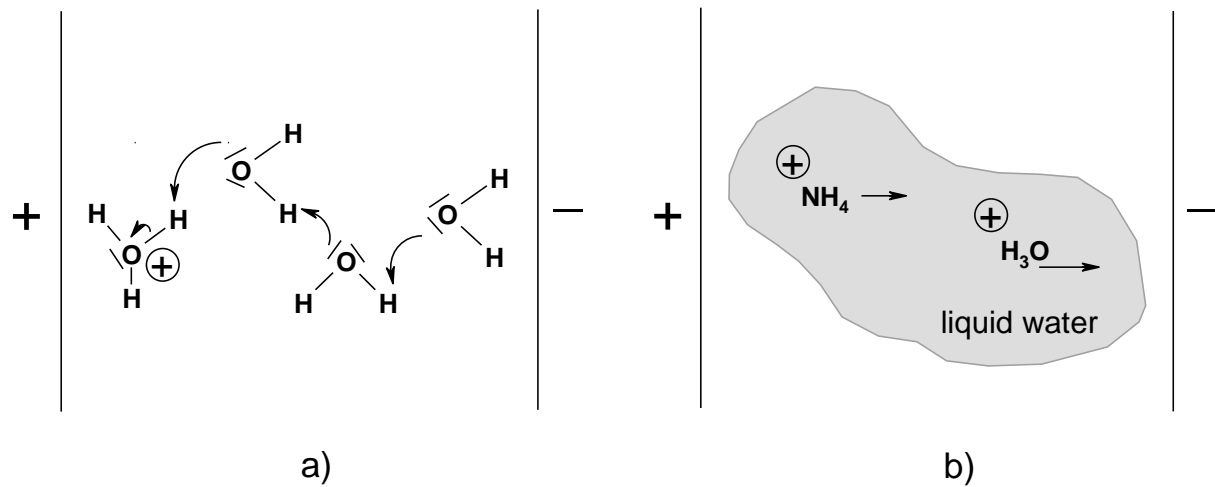
Figure 2.6: Possible charge transport mechanisms in humid polymers: a) Grotthuss mechanism where the charge is carried by a hopping process along the uninterrupted trajectory of water dipoles and b) a molecular diffusion process which is called vehicle mechanism.

Sorption of water not only changes the resistance of the polymer but also influences the capacitance of the coated electrode structure: Since the relative dielectric constant of polymers is typically in the range of 3-8, and for pure water it is 78.3 at 25°C, then the uptake of water shall lead to a rise in the dielectric constant of the coating material, resulting in a higher capacitance [118]. Additionally, due to water induced swelling of the polymer, the capacitance may be further influenced. If the polymer is sufficiently rigid and hence the swelling of the material can be neglected the Brasher-Kingsbury equation [119] has been used to relate the increase in capacitance to the volume fraction of the absorbed moisture (ϕ_{V,H_2O})

$$\phi_{V,H_2O} = \frac{\log(C_t/C_0)}{\log(\varepsilon_W)} \tag{2.17}$$

where C_t is the capacitance at time t, C_0 the initial capacitance of the system in dry air and ε_W the dielectric constant of water. This equation gives a good approach to gravimetric data [120] but, as aforementioned, it assumes that the increase of the coating capacitance is caused by the penetration of water only; to include the swelling

of the polymer or non-uniformities in the distribution of water in the film more advanced equations have to be deduced [33].

2.2.2.2 Impedance of the polymer/electrode interface

To identify whether a semi-circle is due to bulk processes or due to electrode reactions it is useful to apply several bias voltages: A higher voltage should decrease the time constant related to the electrode reaction but should normally not affect the time constant related to the bulk properties of the polymer [121]. The time constant, τ, can be deduced from the impedance measurements by the following relationship:

$$\tau = \frac{1}{\omega_0} \tag{2.18}$$

where ω_0 is the frequency corresponding to the maximum of the imaginary part of the impedance [122]. Variations of the time constant influence the shape of the Nyquist plot and, therefore, that part of the spectra responsible for the slow electrode reaction, depends strongly on the potential. If this arc, usually appearing at low frequencies [104], is fitted with a R$\parallel$CPE equivalent circuit it is observed that R strongly depends on the bias voltage while the parallel CPE is almost unaffected. This indicates that R represents the charge-transfer resistance of an electrochemical process at the electrode/polymer interface (R_{ct}) and CPE represents the double layer capacitance altered due to non-ideal behaviour at the interface (CPE_{dl}) [123].

The charge transfer reaction in water containing polymers is probably the redox reaction of water at the electrodes which was studied for several polymers partly doped with other substances in humid ambient [124]. The following chemical equations were suggested to describe the redox reaction at the polymer/electrode interface in a water swollen polymer:

Cathode reaction: $2\,H_2O + 2\,e^- \rightarrow H_2 + 2\,OH^-$ (2.19)

Anode reaction: $H_2O \rightarrow H_2 + 2\,H^+ + \frac{1}{2}\,O_2 + 2\,e^-$ (2.20)
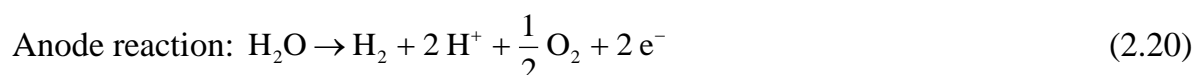
Cathode and anode reaction together result in the decomposition of water as the overall reaction shows:

Overall reaction: $H_2O \rightarrow H_2 + \frac{1}{2}\,O_2$ (2.21)

2.2.3 Voltage step and cyclic voltammetry measurements

In order to study the processes at the electrode it is useful to supplement impedance spectroscopy with other electrochemical techniques. In this work the current decay after the application of a 1 V potential step and cyclic voltammetric measurements were used; they are presented in the following sections.

A schematic representation for a current decay after a constant potential is applied to the electrodes is given in Figure 2.7. In the first millisecond after the charging of the electrode the double layer at the surface develops inducing a linear current decrease with the square root of time. In time other processes as, for example, charge transfer reactions, adsorption and desorption at the electrode surface and coupled chemical reactions may influence the shape of the current decay until after sufficient time the diffusion process exclusively determines the current [125] and a quasi-steady state condition is reached. The dependence of this diffusion current on the exposure to water and water in a background of ammonia is used in this work to determine the electroactive species in the studied system (4.3.2). Similarly, square-wave potentiostatic measurements were used to study charge transfer reactions in several polymers [126].
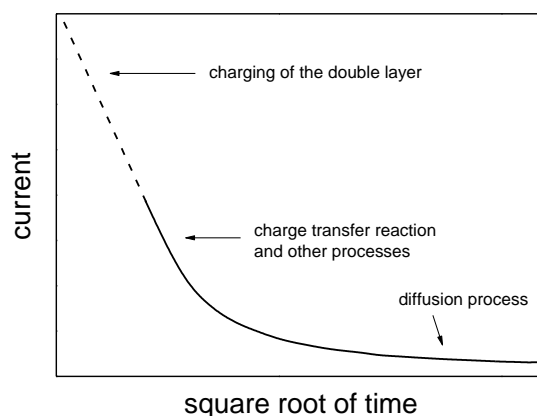
Figure 2.7: Current decay following the application of a constant potential: In the first millisecond the charging of the double layer determines the shape of the curve. With proceeding time charge transfer reactions and other processes influence the current decay until after a sufficient time only the diffusion process determines the current.

In contrast to the method described above, cyclic voltammetry (CV) is a potential sweep method where the potential is not changed in one step but increases or decreases

continuously as shown in Figure 2.8 a): Starting from 0 the voltage linearly increases with time until the maximum value is reached. At this point suddenly the potential scan is reversed and the voltage linearly decreases until no voltage is applied any more; subsequently the polarity of the voltage changes and the run is repeated. The current response upon the applied voltage is measured resulting in a current-potential diagram. Without charge transfer reactions at the electrodes or specific chemisorption processes the current against voltage plot is similar to the solid line plotted in Figure 2.8 b). This current is proportional to the voltage scan rate with the double layer capacitance as proportionality constant. Therefore, from several measurements performed with different scan rates the capacitance of the double layer can be deduced (e.g. Figure 4.23 in 4.3.2) and compared with the information obtained from impedance measurements performed in the frequency range of the CV scan rates (e.g. Figure 4.18 in 4.3.1.2).

If charge transfer reactions or chemisorption at the electrodes take place the charging current is superimposed by a faradaic response leading to the formation of current peaks as observed in the dotted line in Figure 2.8 b). The study of these current peaks was proven very useful in obtaining information about fairly complicated electrode reactions and hence, cyclic voltammetry is a very popular technique for studies of electrochemical systems [127].

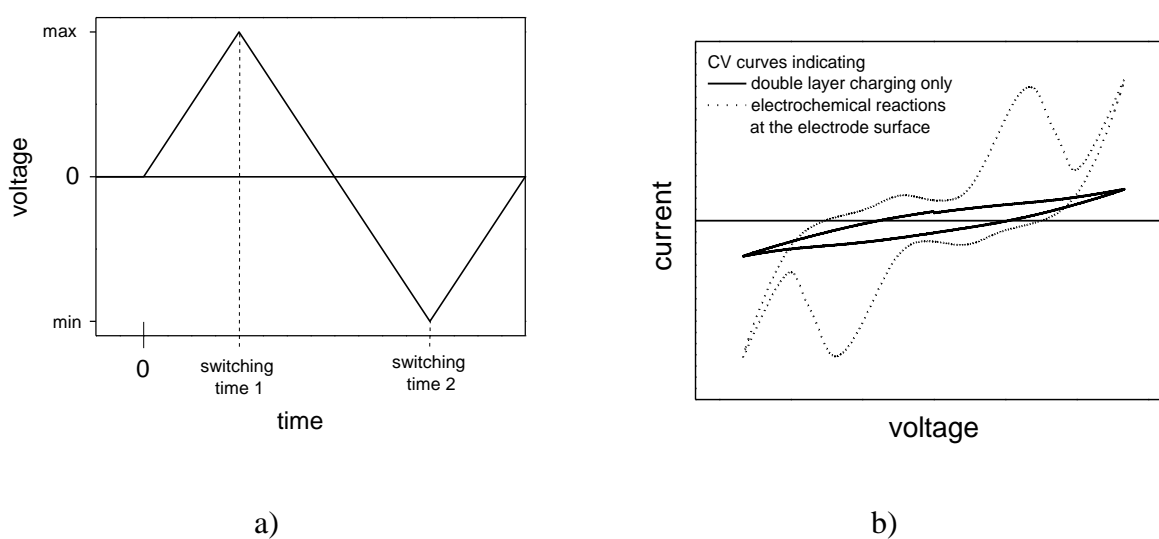

a)   b)

Figure 2.8: Cyclic voltammetry measurements are perfomed applying a triangular voltage sweep (a) to the sample. In the obtained current voltage plot (b) the solid line indicates double layer charging process only while the peaks of the dotted curve represent electrochemical reactions at the electrode surface.

2.2.4 Electrochemical measurements with PAA sensing materials

Variations of the electrochemical properties of PAA and its derivates upon gas exposure have been used to a limited extent in gas sensing devices only, even if, for example, the remarkable water sorption properties suggest that these polymers are promising candidates for humidity sensors. However, a major disadvantage is the water solubility of the materials which may cause destruction of the sensitive layer at high ambient humidities. To solve this problem crosslinked polymers can be used to increase the stability of the material: The more hydrophilic groups participate in the crosslinking reaction the more stable is the polymer but unfortunately the less sensitive it is to water. To adapt the polymer layer to the requirements of a certain sensing problem a balance has to be struck between stability and water sensitivity [20].

In some applications sensors for which the dependence of the electrical resistance on the humidity has an obvious switch point are required. Wu et al. observed such a switch point for the resistance of the PAA layers and discovered that it becomes much more distinctive if polyacrylic acid is used as a copolymer together with acrylamide [20]. Additionally, the switch point of the humidity sensor depends on the content of the crosslinking agent and the amount of alkali metal ions added to the copolymer.

Ammonia sensors based on the resistance and capacitance changes of PAA or its salts have not been reported in literature. For ammonia detection with PAA sensitive layers it is more suitable to use Kelvin Probe or field effect transducer measurements which are discussed in the following chapter.

2.3 Measurement of work function changes

The work function is "the minimum work required to extract an electron from the Fermi level of a conducting phase through the surface and place it in vacuum just outside the reach of the electrostatic forces of that plate" [128]. From the point of view of chemical sensing the work function is a useful parameter because it is influenced by variation of the ambient atmosphere and the work function changes caused by the interaction with gaseous species can easily be detected with Kelvin Probe measurements or field effect transducers (FET).

For ammonia detection the work function changes of several sensitive materials upon ammonia exposure have been used. Sensors made of conducting or semi-conducting inorganic materials as platinum, iridium [129], gallium oxide [130], titanium nitride, titanium oxide [31], iridium oxide [39] or high critical temperature superconductors [131] were described in literature. In addition, it was observed that organic polymer layers deposited on metal substrates, as PAA on gold, show remarkable responses in Kelvin Probe or FET setups [21, 46]. For explaining the origin of these signals, the standard picture valid for, e.g. metal-semiconductor structures does not help because of the lack of electronic conduction in the PAA layer. To understand the sensing mechanism of the polymer / metal structure some experimental work has been performed and possible mechanism suggested [47]. One aim of this work is to deepen the understanding of the PAA / gold system by means of Kelvin Probe measurements of PAA and its derivates on gold substrates.

In the following chapter the basic principle of Kelvin Probe measurements is presented before work function changes of gold and polymer covered gold substrates upon water and ammonia exposure are discussed in 2.3.2.

2.3.1 Basic principle of Kelvin Probe measurements

When two different conducting materials are brought into contact forming an electric junction, electrons flow from the material of low work function to that of the higher work function until the Fermi energies of the materials are adjusted. The charge flow induces a potential change of the materials; the resulting potential difference at the junction of the two materials is the so-called contact potential.

In Figure 2.9 the band structure of two metals without and with electric contact is sketched. Without electric contact the vacuum level of both materials is even and no electric field is observed between the plates. When the metals are electrically connected the Fermi energies reach the same value and the vacuum levels differ by the work function difference of the materials. The work function difference $\left(\Phi_{\text{metal A}} - \Phi_{\text{metal B}}\right)$ divided by $q = -e$ is the measurable contact potential V_{CPD}:

$$V_{\text{CPD}} = \frac{\Phi_{\text{metal A}} - \Phi_{\text{metal B}}}{q} \tag{2.22}$$

33
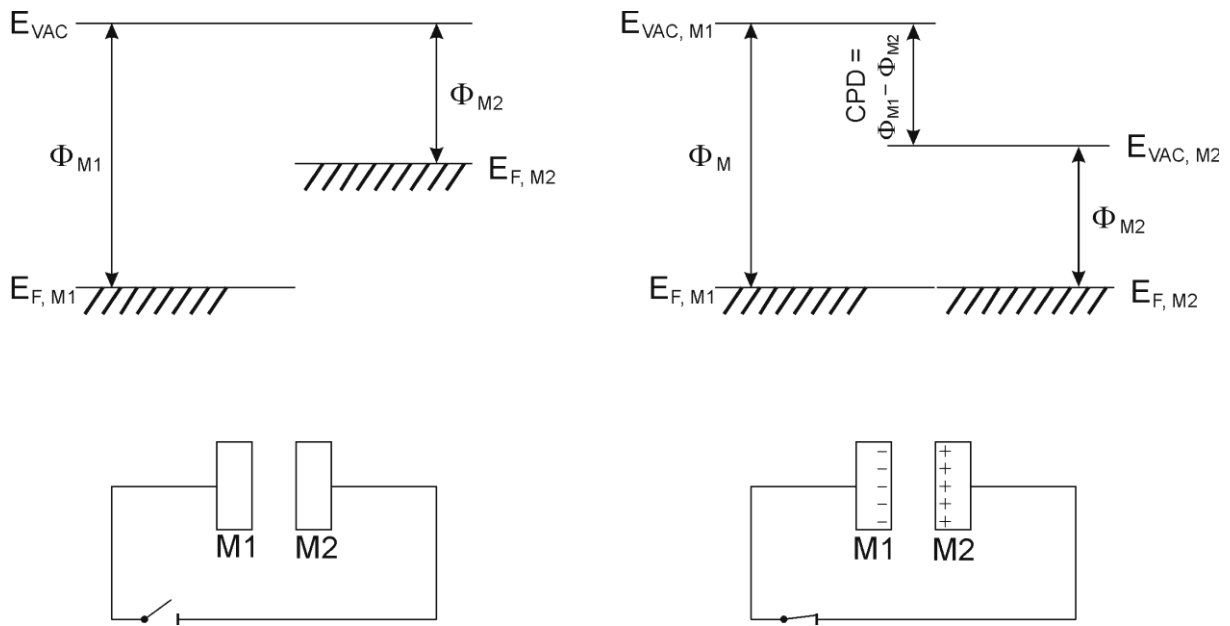
Figure 2.9: Two metals with different work functions are shown in the left side of the figure. When they become electrical connected (right band structure) the Fermi energies reach the same value and this leads to a charging of the two opposing materials and the appearance of a contact potential (CPD).

To determine the contact potential (CPD), Lord Kelvin developed a capacitor method in 1898 [132] which was advanced to the vibrating capacitor method by Zisman in 1932: In the so-called Kelvin Probe setup two metals are arranged as the plates of a capacitor and electrically connected. Due to the work function difference of the materials, a voltage drop appears between the plates of the capacitor. This induces the charging of the plates proportional to the voltage, with the capacitance, C, as the constant of proportionality:

$$Q = C \cdot V_{CPD} \tag{2.23}$$

The capacitance is a function of the plate area, A, the dielectric constant of the material between the plates, ε, the permittivity of free space, ε_0, and the separation distance, d(t):

$$C = \frac{\varepsilon_0 \varepsilon \ A}{d(t)} \tag{2.24}$$

The distance dependence of the capacitance is used in the vibrating capacitor method where one of the capacitor plates moves permanently up and down. A periodic

variation of the separation distance $d(t) = d_0 + \phi \sin(\omega t)$ causes a periodic change of the capacitance and with it of the charges on the capacitor plates (equation (2.23)). The time variable charge is the ac current that is measured in the experimental setup:

$$I = \frac{dQ}{dt} = V_{CPD} \frac{dC}{dt} = V_{CPD} \, \varepsilon_0 \varepsilon \, A \frac{d\left(\dfrac{1}{d_0 + \phi \sin(\omega t)}\right)}{dt}$$

$$= - V_{CPD} \, \varepsilon_0 \varepsilon \, A \frac{\phi \cos(\omega t)}{(d_0 + \phi \sin(\omega t))^2} \tag{2.25}$$

Because of experimental reasons a counter voltage, V_C, is added to the circuit:

$$I = - V_{total} \, \varepsilon_0 \varepsilon \, A \frac{\phi \cos(\omega t)}{(d_0 + \phi \sin(\omega t))^2} \qquad \text{with } V_{total} = V_{CPD} + V_C \tag{2.26}$$

The counter voltage pushes the electrons back to the material of low work function. As a result of this the electric field between the capacitor plates decreases and the ac current vanishes, indicating that the compensating voltage equals exactly the difference of the work functions which caused the displacement of the electrons.

The zero current condition can easily be determined in the Kelvin-Probe set-up and the corresponding counter voltage is used to obtain the contact potential:

$$V_{CPD} = - V_{C\,(zero\,current\,condition)} \tag{2.27}$$

From the measured contact potential differences the work function difference of the materials can be calculated with equation (2.22).

2.3.2 Work function changes

The surface potential of a metal or a semiconductor has to be overcome to transport an electron from the bulk to the vacuum level. Therefore, variations of the surface potential caused by changes of the interfacial dipole layer influence the metal work function. The dipole layer is formed and affected due to physisorption and chemisorption of gaseous species at the metal surface. To study this work function change with Kelvin Probe measurements a capacitor plate of the material to be tested must be electrically connected with a reference plate that remains unaffected by the variation of the gaseous environment. It is assumed that stainless steel, oxidised tungsten or tantalum are materials which are inert against changes of the gaseous environment [133] and hence can be used as reference material. Another commonly

used reference material is gold although metal-gas reactions are observed, which may influence the work function. These reactions have to be compensated by reference measurements of the gold plate with an inert material, for example Si_3N_4, as the second capacitor plate [134] and considered in the interpretation of the Kelvin Probe response.

The contact potential of a system composed of a gas sensitive and an inert material is influenced by the sensitive material work function change only [135]. Therefore the Kelvin Probe is a powerful device to study ambient atmosphere depending work function changes caused due to several interaction mechanisms between adsorbate molecules and sensitive material (Figure 2.10).
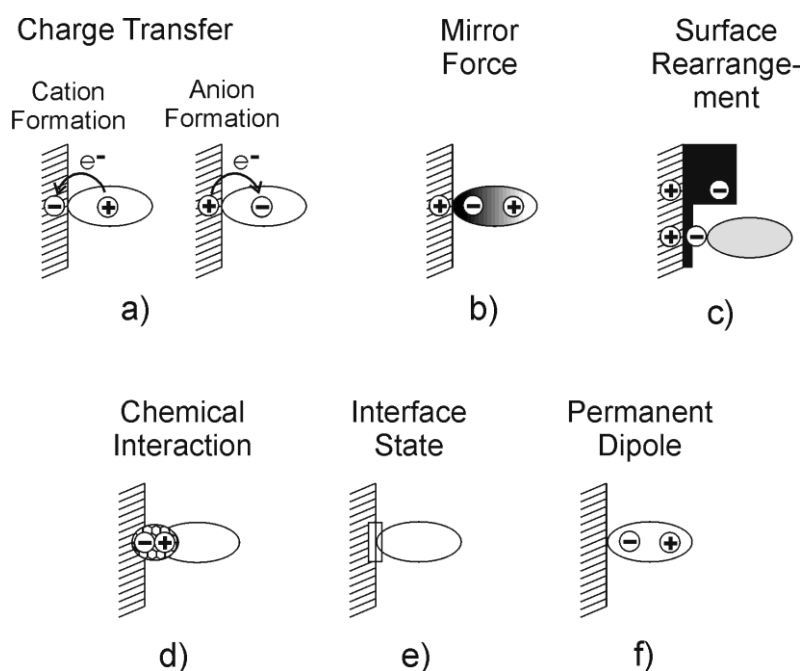
Figure 2.10: Possible factors forming and affecting the interfacial dipole layer: a) Charge transfer across the interface, b) Concentration of electrons in the adsorbate leading to charging of the vacuum side, c) Rearrangement of electron cloud at the metal surface, with the reduction of tailing into vacuum, d) Strong chemical interaction between the surface and the adsorbate leading to the rearrangement of the electronic cloud and also the molecular and surface geometries (both directions of dipoles are possible), e) Existence of interface state serving as a buffer of charge carriers, and f) Orientation of polar molecules or functional groups. [136]

The charge transfer from the gaseous species to the metal or semiconductor across the interface (Figure 2.10 a) occurs when, for example, donor molecules, e.g. alkali atoms, are sorbed at a metal surface. In other cases the adsorbate acts as an electron acceptor. Theoretical studies suggested this behaviour for thiols and disulfides on gold surfaces [137] but there are experimental hints that, at least, the work function change of gold with sorbed methanethiol and dimethyl disulfide are due to other reasons [138]. The formation of an interface dipole on the basis of physical interaction only (Figure 2.10 b) is observed when for example noble gas atoms are being pulled towards a metal surface by van der Waals forces and their electronic wave functions overlap with those of the metal inducing a change of the metal surface potential [139, 140]. An alternative explanation in the case of noble gas adsorption describes the work function change due to the rearrangement of the electron cloud at the metal surface (Figure 2.10 c) [136]. Besides charge transfer, other chemical interactions may occur between the adsorbate and the metal or semiconductor surface (Figure 2.10 d). These give rise to the relocation of the bonds or to the formation of new bonds and are well-known for small molecules like CO and benzene on clean metal surfaces [141]. Differing from the figure, the formation of the dipoles due to chemical interaction is possible in both directions. In Figure 2.10 e) interface states which work as a buffer at the charge exchange between the metal and the added material are sketched. Such interface states are observed at metal / inorganic semiconductor interfaces [142]. Non-polar molecules may interact with a metal surface as discussed till now. Additionally, for polar molecules, the orientation of the dipole moment can lead to a large surface dipole, as shown in Figure 2.10 f).

2.3.2.1 Work function changes of gold due to sorbed ammonia

For most metals, e.g. Ni [143], Ir [144], Pt [145], Al [146], and also Au [147] ammonia is molecularly adsorbed onto the surface and bonded to the substrate via the nitrogen atom with the hydrogens pointing away from the surface (Figure 2.11) so that the threefold axis of the ammonia molecule is perpendicular to the metal surface. In the NH_3/Au system this orientation allows an interaction between the ammonia

molecule and the gold, which is often described with the term "weak chemisorption" [148-150].
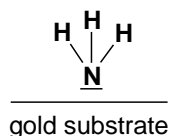

Figure 2.11: Ammonia molecularly adsorbed on a metal surface usually bond to the substrate via the nitrogen atom with the hydrogens pointed away from the substrate so that the threefold axis of the ammonia molecule is perpendicular to the metal surface.

The chemical interactions may be caused by charge transfer from the ammonia to the metal or the other way around (according to Figure 2.10 a) or by covalent bonding via electron sharing involving the ammonia lone-pair orbital and the partially filled gold s band (according to Figure 2.10 d) which both would induce a work function change for the gold.

In a new approach, calculations from first principles of the adsorption process show that charge-transfer or electron sharing contributions are not required to understand the work function changes caused by ammonia sorption [147]: The dipole moment of gaseous ammonia is too small to explain the observed work function changes but ammonia additionally interacts with the gold surface due to electron-correlation effects such as dispersion (according to Figure 2.10 b). Caused by the dipole of the ammonia these effects induce a downward charge flow on the gold surface that result in a dipole moment with the same orientation as that for the ammonia molecule and, in response, a charge flow from nitrogen upwards reducing the ammonia dipole is induced from the gold surface on the ammonia molecule. The obtained over-all dipole moment is in good agreement with the value required to explain the experimentally observed work function decrease.

2.3.2.2 Work function changes of gold due to sorbed water

On metal, semiconductor and ionic compound surfaces at which H_2O does not dissociate, the water molecules are usually chemisorbed. They bound through the oxygen atoms with the hydrogens pointing away from the surface. The bonding is accompanied by net charge transfer to the surface; this manifests itself in a negative

work function change upon adsorption. Isolated single water molecules are not found usually at surfaces but hydrogen bounded water clusters because water molecules are able to form hydrogen bonds with their neighbours and the resulting hydrogen bonding is often energetically competitive with the molecule-substrate bond.

These general features of water sorption on surfaces are taken from [151] and are also confirmed for the sorption on gold surfaces [148, 149, 152]. In contrast to the ammonia sorption, the water molecules remain at the gold surface when the humidity is removed from the ambient, indicating chemisorption.

2.3.2.3 Work function changes of PAA covered gold substrate due to ammonia

Beside the metals and semiconductors described above it was found that organic insulators also show electrical potential outputs when tested as Kelvin Probe samples [153]. One example is PAA that deposited on metal electrodes shows significant Kelvin Probe signals upon ammonia exposure [21, 46]. The observed response logarithmically depends on the ammonia exposure with a logarithmic sensitivity of 30-50 mV/decade of concentration. Having a very high signal to noise ratio the system allows measuring ammonia concentrations down to 50 ppb in a Kelvin Probe and 300 ppb in FET set-up respectively. Other advantages are the good reproducibility of the output signal, whose changes are below 10% in all exposure cycles measured, and minor cross-sensitivity to almost all gases and vapours except humidity and NO_2. The major problem of the humidity cross-sensitivity is that different samples, prepared in the same manner, are giving different responses. If the ammonia measurement is performed in a constant background of humidity in the range of 30-70% r.h. the associated error is below 15%.

The observed Kelvin Probe and FET signals cannot be explained with the standard picture of physisorption and chemisorption (Figure 2.10) at the sample surface because the lack of electronic conduction in the PAA layer prohibits the establishing of an electrical equilibrium between the polymer layer and the reference electrode. An electrical analysis of the system shows that the observed response most probably is based on a process at the PAA / electrode interface [47]. As discussed above for the example of gold (chapter 2.3.2.1), many metal or semiconductor surfaces show some

intrinsic sensitivity to ammonia due to the dipole moment of the ammonia molecule. It is suggested that this feature is improved by the presence of a PAA layer because the polymer significantly concentrates the ammonia through a more or less standard sorption process. In dry air this process explains the signal increasing effect of a deposited polymer layer. The presence of water seems to change the detection mechanism: Water molecules are readily sorbed into the polymer, cluster together, and finally form liquid water in the polymer matrix. Ammonia solves in the liquid water leading to an electrolyte mixture similar to a dilute solution of ammonia in water. It is suggested in literature that, possibly connected with chemical processes in the PAA layer, the electrolyte allows electrochemical reactions at the electrodes. This could give rise to an electrochemical cell potential at the electrodes that can be measured as CPD change in a Kelvin Probe and FET set-up respectively [47].

In this work further investigations are performed in order to check the validity of the considered mechanism.

2.4 Spectroscopic studies of PAA

The infrared (IR) measurement technique is a useful tool to characterize and quantify the interaction between the polymer and the ammonia and water molecules sorbed into the polymer matrix: As the oscillation forces of the intramolecular modes in the polymer are sensitive to the level of interaction with the sorbed molecules the appearance, disappearance or shift of peaks in the IR spectrum allow to draw conclusions about the sorption induced processes in the polymer.

Transmission spectra of PAA and its ammonium and sodium salts are discussed in the literature and the results of these studies are introduced 2.4.1. In addition, first measurements of polyacrylic acid under water and ammonia exposure were already performed [22]; results obtained in this study are presented in 2.4.2.

2.4.1 Transmittance IR spectra in dry air

Transmittance IR spectra of PAA, NH_4PA and NaPA are shown in Figure 2.12. In the following section the PAA spectrum is discussed in detail particularly taking into consideration the region around $1700\,cm^{-1}$ assigned to stretching vibrations of the

carboxyl group. Subsequently the spectra of the ammonium and sodium salts are compared with the one of PAA.
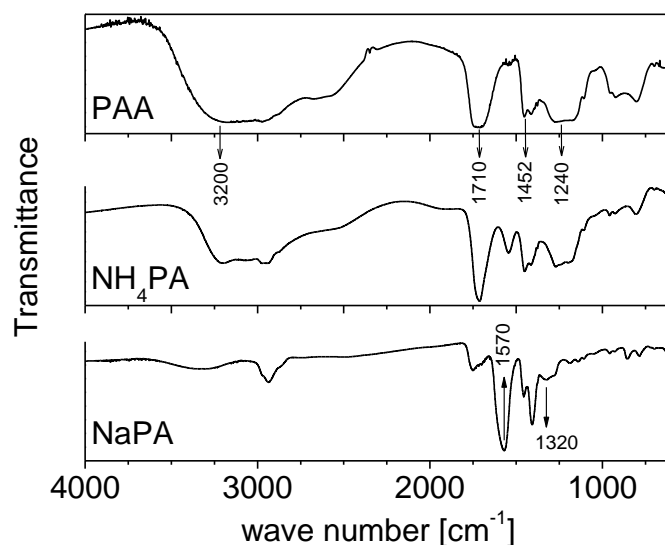
Figure 2.12: IR transmittance spectra of PAA and its ammonium and sodium salts. The marked bands in the spectra are discussed in 2.4.1.

2.4.1.1 Polyacrylic acid

In a dry sample the polymer chains of PAA are connected via hydrogen bonds so that most carboxyl groups form dimers with each other. This results in a shift of the O-H stretching vibrations to lower wave numbers (3200 cm^{-1} in Figure 2.12) if compared to the band of free hydroxyl groups which is expected above 3600 cm^{-1} [154]. The observed band is superimposed by absorption due to symmetric and asymmetric CH_2 stretching vibrations of the polymer backbone appearing between 2950 and 2800 cm^{-1} [155]. The shoulder between 2700 and 2500 cm^{-1} is characteristic of dimer carboxylic acids caused by overtones and combinations of the H-bonded carboxyl groups [156].

The band at about 1710 cm^{-1} is ascribed generally to the C=O stretching vibrations in cyclic dimers [155, 157, 158] without further detailed analysis of it. However, Raman and carefully performed infrared spectroscopy studies pointed out that this band is actually composed of several bands that are due to distinct local environments of the C=O groups in the polymer [156, 159]. The dependence of these bands on the local environment makes the C=O stretching vibration a suitable candidate to study the changes in the polymer upon water and ammonia sorption. Therefore this region is discussed in detail in the following section.

41

According to Ostrowska and Narębska [156] in the neighbourhood of the main band at 1708 cm^{-1} shoulders appear at 1695 cm^{-1}, 1723 cm^{-1} and 1737 cm^{-1}. In agreement with several studies performed [159, 160] the main peak of the band has been attributed to cyclic dimers (Figure 2.13).
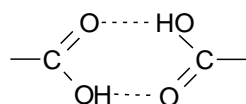
Figure 2.13: Acid groups of adjacent polymer chains form cyclic dimers with each other due to hydrogen bonds.

At 1737 cm^{-1} or even higher wave numbers the vibration frequency of an unassociated carboxyl group appears in the spectra. The contribution of this vibration to the whole C=O band is rather small because to a large extend PAA forms dimers at room temperature [159]. Additionally, in dry air a weak band at 1730 to 1720 cm^{-1} arises from bonded carbonyl stretching mode of a chain structure or a open dimer (as shown in Figure 2.14 a). The band corresponding to the vibration of the terminal carbonyl group of a chain structure ((t) in Figure 2.14 a) should appear at higher wave numbers but it is impossible to differentiate it in the spectra because the characteristic frequency of this species is very close to the vibration frequency of an unassociated carboxyl group. With increasing humidity in the ambient, the water content of the polymer increases and the band at this frequency also may be due to complex compounds composed of acid and water molecules (Figure 2.14 b).

a)   b)
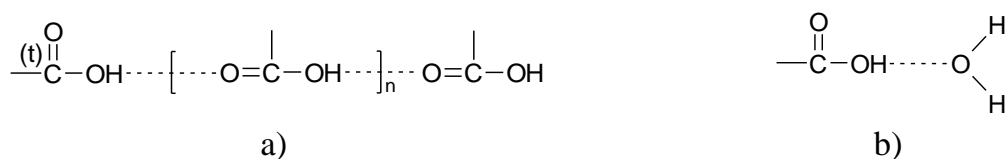
Figure 2.14: Hydrogen bonds between the acid groups of a single polymer chain (a) result in an open dimer (n = 0) or a chain structure (n > 0) and water molecules interact with terminal hydroxyl radicals (b).

The insert ion of water into the polymer may lead to many other structures shifting the C=O stretching vibration to lower wave numbers. The band at 1700 to 1690 cm^{-1} which is not observed in a completely dry sample may be ascribed to dimers with two molecules of water incorporated in the cycle (Figure 2.15 a), three dimensional

structures formed by carboxyl groups and water (Figure 2.15 b) and open dimers or oligomers in which terminal carbonyl groups are hydrogen-bonded with water molecules (Figure 2.15 c) [156]

| a) | b) | c) |

Figure 2.15: In the presence of humidity the acids groups incorporate water molecules into the cyclic dimer (a), form three dimensional structures (b) or open dimers or oligomers in which terminal carbonyl groups are hydrogen-bonded with water molecules.

In this work the influence of ammonia and water sorption on the rather complex process of carboxyl group association is studied and information about the interaction of the gaseous species and the polymer are deduced.

At lower wave numbers the classification of the bands is controversial: While Wu [155] et al. allocate the bands at 1452 and 1415 cm^{-1} to shear mode and bending vibrations of CH_2 and CHCO groups and state that the bands at 1240 and 1180 cm^{-1} are due to the combination of the C-O stretching and O-H bending vibrations of neighbouring carboxyl groups, Santhiya et al. [157] relate the latter ones to CH_2 deformation and the former ones to the O-H bending and C-O stretching. The comparison of the IR spectra of PAA with its derivate NaPA, which is not able to perform O-H bending vibrations, gives a hint that the allocation of Wu is correct because the bands at 1240 and 1180 cm^{-1} do not appear in the spectrum of NaPA any more while the ones at 1452 and 1415 cm^{-1} are still observed (Figure 2.12).

The weak bands at 1107 and 1040 cm^{-1} indicate C-O stretching vibrations [157] and the one at 803 cm^{-1} is associated with the O-C-O deformation vibration; other modes of the O-C-O group cannot be observed in the spectra of PAA because it is difficult to differentiate between the asymmetric stretching vibration (1310-1250 cm^{-1}) and the symmetric stretching vibration (1200-1130 cm^{-1}) and the other bands in these

frequency ranges. The shoulder at 1960 cm^{-1} and weak signals at 960 and 925 cm^{-1} may be caused by some acrylic acid monomer remaining in the material after the polymerisation process.

2.4.1.2 PAA derivates

At high wave numbers the transmittance spectrum of ammonium polyacrylate shown in Figure 2.12, has a similar shape to the one of the pure acid. In both spectra the band caused by O-H stretching vibrations and the characteristic shoulder between 2700 and 2500 cm^{-1} indicate the hydrogen bonds based structure of these materials. Sodium polyacrylate shows quite a different transmission spectrum confirming that this derivate is not able to form hydrogen bonds: The characteristic bands observed in PAA and NH$_4$PA spectra do not appear and only the peak at 2935 cm^{-1} with a shoulder at 2848 cm^{-1} representing the symmetric and asymmetric CH$_2$ stretching vibrations is observed. The very weak and broad band above 3250 cm^{-1} is due to water molecules that remain in the polymer matrix even after keeping the sample in dry air for at least 3 days. The absence of hydrogen bonds is additionally demonstrated by the missing bands at about 1240 cm^{-1}, as mentioned in the previous chapter.

Due to the salt formation process, COO$^-$ ions are generated in the polymer and the two oxygen atoms attached to the carbon atom in these ions keep in resonance equilibrium. As a result, the polymer adsorption bands associated with a protonated carboxylate species disappear (around 1710 cm^{-1}) and are replaced by a strong band in the 1540 to 1610 cm^{-1} range which corresponds to the asymmetric C-O stretching mode and a weaker on representing the symmetric C-O stretching mode in the 1400 to 1300 cm^{-1} range [161]. The former band is generally stronger and more stable in wave number; it is more diagnostic than the latter one which is weaker and has many other skeletal vibrations occurring in the same range. For the identification of the latter band, it is helpful to know that the intensity ratio of the former to the latter band average out at 7.6 : 1 [162].

In the transmission spectrum of NaPA the decrease of the carboxyl bands and the appearance of the carboxylate bands (1570 and 1320 cm^{-1}) can be clearly observed (Figure 2.12). A band caused by the asymmetric C-O stretching mode of COO$^-$

appears also in the spectrum of NH_4PA but it is shifted with about $30 \, cm^{-1}$ to lower wave numbers. As discussed in literature [161], the different size of ammonium and sodium as cations in the PAA salts explain this frequency shift. However, in the case of ammonium polyacrylate the carboxyl bands are still very strong. Lee et al. interpretation is that a large number of carboxylate groups do not bond to ammonium ions because some ammonia evaporates from the polyacrylate leaving behind a hydrogen ion which bonds to a carboxylate group [161]. Another interpretation of these observations is suggested in this work (see chapter 5).

2.4.2 IR spectra changes upon water and ammonia sorption [22]

Water sorption into a PAA layer leads to strong changes in the infrared transmission spectrum. Most obvious is the increase in intensity of the broad band assigned to associated water molecules (at about $3500 \, cm^{-1}$); this increase is in agreement with the known water sorption properties of PAA. In addition, with increasing humidity the band attributed to protonated carboxylate groups decreases and bands caused by carboxylate anions appear, suggesting a higher degree of PAA dissociation with increasing water content of the polymer.

In addition to the interaction of PAA with water vapour, the influence of ammonia sorption on the IR spectra was also studied. In dry air, ammonia induced changes are very small indicating that a proton exchange reaction between PAA and ammonia hardly takes place; in humid air the changes in the spectra are much more intense. Ammonia sorption creates additional sorption possibilities for water molecules reflected by the strong increase of the bands due to O-H vibrations (about $3200 \, cm^{-1}$). Changes of the bands in the carboxyl / carboxylate region indicate a reaction of ammonia molecules with PAA in the presence of water in the polymer matrix.

Even though the published data are very helpful for the understanding of the sorption process, they have a major shortcoming: the band ascribed to the protonated carboxylate groups is discussed without further analysis. A lot more information about the environment of carboxyl groups and the changes of this environment upon water vapour and ammonia gas sorption can be gained if the region around $1710 \, cm^{-1}$ is studied in detail. Therefore, in this work similar measurements were performed

particularly taking into consideration the 1800 to 1600 cm^{-1} range (see 4.5.2) but also discussing in detail other parts of the spectra.

3 Experimental details

As presented in the previous chapters gravimetric, electrochemical, Kelvin Probe and infrared measurements were performed in this work. The following chapters provide comprehensive information about the experimental details of the polymers including the coating process, the study of the film morphology and the instrumental equipment required for the different methods. Special features of the measuring tools, for example the determination of alternating current amplitude for IS measurements or the two different Kelvin Probe set-ups, are discussed in detail and references to additional reading concerning the measuring tools is given.

3.1 Sensitive materials

Polyacrylic acid with a molecular weight of 2000 g/mol was purchased from SigmaAldrich and an aqueous stock solution was prepared. According to Figure 3.1 its derivates were made by neutralization of the PAA solution with diluted ammonia (diluted from: ammonia solution max. 33% NH_3, extra pure, Riedel-de Haën) or sodium hydroxide (analytical reagent, Riedel-de Haën) in water; all chemicals were used as delivered. While the structural unit of the original acid has a molar mass of 72 g/mol the molar mass of the salts is greater than this value: 89 g/mol for NH_4PA and 94 g/mol NaPA, because of the additional cation mass. To the prepared solutions acetone (puriss., Fluka) and water (purified with Milli-Q PF PLUS, Millipore Corporation) were added to obtain the desired polymer concentration in a mixture of acetone and water. The concentrations required for the substrates studied in this work are given below at the method descriptions.

In dry air PAA as well as its ammonium and sodium salts are glassy materials at room temperature. It is not easy to determine the glass transition temperature in dry air because the studied polymers likely sorb water from the ambient. The sorbed water molecules Act as plasticizer and change the glass transition temperature of the polymer (see 2.1.4.2). However, with some experimental effort T_g of PAA in dry air could be determined to 106°C [163]. This procedure is not possible for NaPA because of the great difficulty to obtain this derivate in the dry state. Therefore the glass transition temperature was determined as a function of water content and extrapolation to zero

plasticizer content resulting in a T_g of 251°C in dry air [164]. The glass transition temperature of the ammonium salt is not known.
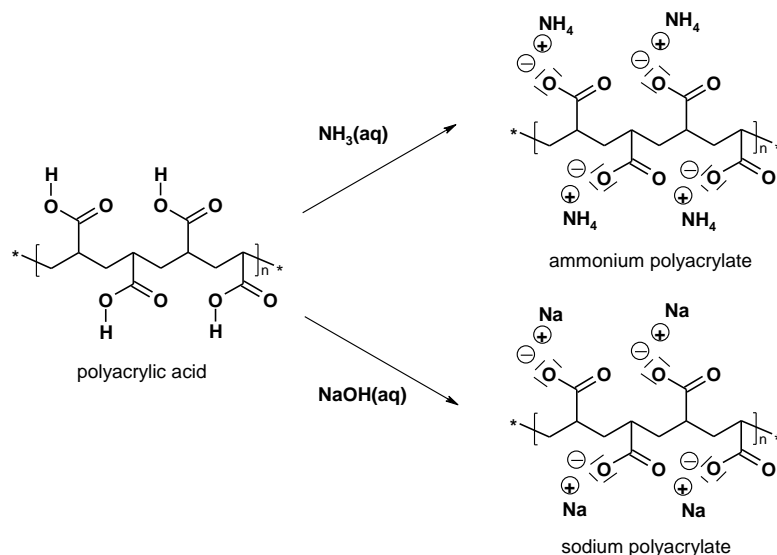

Figure 3.1: The ammonium and sodium salts of polyacrylic acid are prepared by neutralisation of the aqueous acid solution with diluted ammonia and sodium hydroxide solutions in water.

3.1.1 Coating procedures

Depending on the intended polymer layer thickness two different deposition processes, drop and spray coating, were applied to produce the polymer film on the substrates as described in the following sections.

The drop coating is a simple and fast technique as the polymer solved in water and acetone are directly dropped onto the substrates. If the solution amount is accurately defined, for example by the use of an Eppendorf pipette, reproducible polymer films can be obtained with the additional advantage of a very small surface roughness. In this work 50 µl drops of polymer solutions between 6 and 200 mg/ml were deposited onto the substrates resulting in layer thicknesses between 1 and 30 µm. For thinner films this method is suitable to a limited extend only because due to irregular drying, the obtained films are not uniform any more. This especially happens if the wettability of the substrates is poor. In such cases improved polymer layers can be obtained with the spray deposition method.

The spray coating technique uses a conventional spraying nozzle with nitrogen as propellant. This system allows the controlled growth of the polymer film on the

substrate: The concentration and flow of the polymer solution, the spraying pressure, the sample-nozzle distance and the carrier air stream influencing coating rate are parameters which can be adjusted to obtain optimised polymer layers. In this work the optimal parameters determined in [22] were set to obtain uniform films with thicknesses between 0.1 and 1.5 μm.

The progress of the coating process is monitored on-line by a QMB sensor used as a thickness monitor. To obtain polymer films of PAA and its derivates containing the same amount of polymer, i.e. the same number of functional units, the required frequency change of the thickness monitor is determined by the molar mass of the polymer basic units: Therefore, the frequency shift through the derivate coating process must be about 1.24 times larger for NH_4PA and 1.31 times larger for NaPA than the frequency shift observed for polyacrylic acid. The obtained polymer films can be used to study the influence of the derivatisation on the sensing properties undisturbed by effects induced through changes of the polymer amount.

In this work a semi-automatic spray deposition system is used consisting of a two substance nozzle Model 970 S8 manufactured by Düsen-Schlick and a rotating disk as sample holder; it allows the preparation of a large set of samples in one single process. In detail the system is described in literature [22]. The polymers were solved in a mixture of acetone and water (80% to 20%) resulting in a solution of 0.2 or 0.5 mg/ml depending on the substrate to be covered. After preparation the coated samples were heated up overnight at 70°C to remove remaining solvent traces and were openly stored at room temperature in ambient air.

3.1.2 Layer morphology studies

Beside the substrates for the different measurement techniques silicon wafers covered with thin gold layers were coated with polymer for morphology research.

The surface of the films was studied with an optical microscope (Olympus BX60) and images were taken and processed with the AnalySIS software (Soft Imaging Systems GmbH analyses 3.00, 1986). In addition the surface roughness and the thickness of the produced layers were determined with a stylus surface profilometer (KLA Tencor Alpha Stepper 500). The measurement is done by a stylus which touches the surface of

the sample and runs across a prescribed length; details about the method are described in literature [22]. To measure the thickness of a film, a step that is comparable to the film thickness must be produced before the measurement. This can be done for example by scratching the film with a sharp metal piece.

Some optical microscope images and surface profilometer scans are presented in Figure 4.1 in chapter 4.1.

3.2 Instrumental equipment

The experiments performed in this work require controllable and reproducible conditions in terms of air flow and composition of the gas atmosphere. In a computer driven gas mixing station all those parameters can be adjusted with high accuracy and reproducibility. The gas mixing station consists of several gas channels controlled by a set of mass flow controllers (Tylan 2900). The system used in this work is similar to the one described in literature [165] and runs under control of a personal computer equipped with the homemade software programme POSEIDON. In a background of synthetic air the required humidity was adjusted in a thermostated water evaporator and ammonia was supplied from a gas bottle (Air Liquid, 100 ppm and 500 ppm ammonia in synthetic air respectively).

The outlet of the gas mixing station was connected with the gas ports of the measurement chambers providing the desired gas composition. Beside the measurement chambers, the measuring tools, the substrates and the applied polymer deposition procedure are described for each method in the following paragraphs.

3.2.1 Gravimetric measurements

Gravimetric measurements were performed with quartz micro balances as presented in 2.1.2. In Figure 3.2 the QMB substrate is shown; it is composed of the piezoelectric material sandwiched between two gold electrodes. The piezoelectric material used in this work is an AT-cut quartz crystal with a thickness of 56 μm and a fundamental frequency of 30 MHz. The QMBs were manufactured by KVG Quartz Crystal Technology GmbH, Neckarbischofsheim.

QMB substrate   Measurement chamber

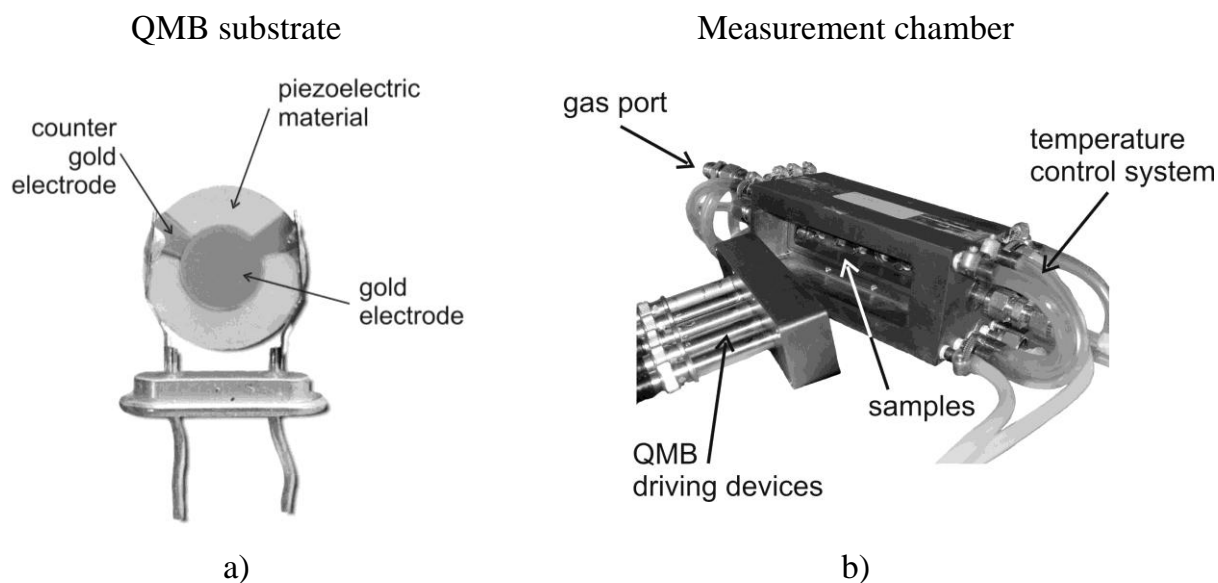a)   b)

Figure 3.2: a) QMB substrate: A piezoelectric material (quartz crystal) plate sandwiched between two gold electrodes. b) Measurement chamber: The polymer coated QMB substrates are placed in a brass measurement chamber designed for a maximum of eleven QMB sensors aligned in two opposite, interlacing rows. A temperature control system which is made up of water filled coils integrated in the walls of the measurement chamber enabling the temperature control as required for precise studies.

The substrates were covered by spray deposition of a 0.2 mg/ml PAA solution in acetone and water (80% to 20%) resulting in polymer film thicknesses of 120 nm, 320 nm, 400 nm, 710 nm and 1.3 µm respectively. Ammonium and sodium polyacrylate solutions were prepared in the same solvent mixture and molarity and spray deposited onto the QMB substrates. In each case, the deposited polymer amount was equal to the amount of PAA in the 400 nm layers. This allows the comparability of the sorption properties observed for the different materials studied. To be able to subtract the interaction of the analyte gases with the uncoated substrate an uncovered QMB was measured as well.

The sensor holder contains the driving oscillator circuitry and a coaxial cable between the sensor holder and the computer provides the driving voltage and transmits the signal which is read out by a frequency counter card. More detailed information on the circuitry can be taken from literature [166]. The data acquisition system allows measuring the resonance frequency shift of ten QMB sensors at a time. The system possesses a very good resolution of 1 Hz but has the disadvantage that absolute

frequencies cannot be determined with it because always the initial frequency is taken as reference.

The polymer covered QMB substrates attached to the sample holder are placed in a brass measurement chamber designed for a maximum of eleven QMB sensors aligned in two opposite, interlacing rows (Figure 3.2 b). The sensors are close to a water filled coil integrated in the walls of the measurement chamber enabling the temperature control of the measurement chamber as required for precise studies (see 2.1.3). For the measurements performed in this work the temperature was kept at 25°C by a Julabo F 32 MH thermostat.

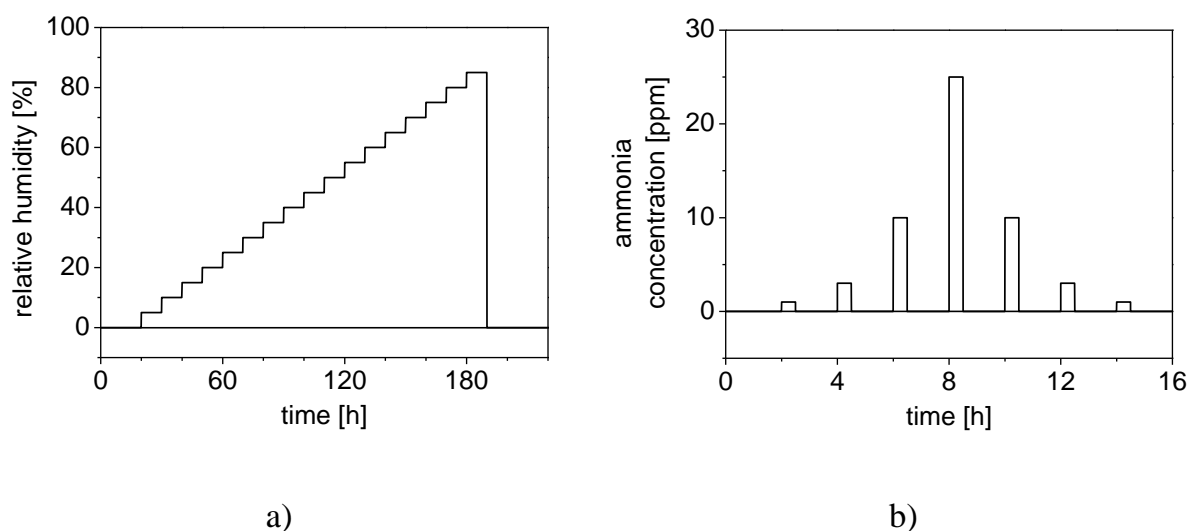a)   b)

Figure 3.3: Measurement schemes usually applied in gravimetric measurements. a) Water exposure with and without ammonia in the ambient: The dried polymer was exposed to humidities starting with 5% r.h. and each 10 hours increased by the same fraction until 85% r.h. was reached and the sample was dried again. The measurements of water sorption in the presence of ammonia followed the same scheme but additionally constant backgrounds of ammonia were added over the whole humidity range. b) Ammonia exposure in dry air: The sample was exposed for 30 min to ammonia concentration steps between 1 and 25 ppm separated by 90 min of dry air without ammonia.

In the measurement chamber the samples were exposed to water vapour and ammonia gas; typical runs are presented in Figure 3.3: Starting from dry air, the relative humidity was increased in steps of 5% r.h. each 10 hours until 85% r.h. was reached (Figure 3.3 a). Afterwards the sample has been exposed to dry air again. For further experiments the scheme was changed so that each level of relative humidity was

separated from the next one by 5 hours of dry air to allow the sensor to recover. The experiments of humidity pulses with ammonia followed the same scheme but additionally constant backgrounds of 1 to 30 ppm ammonia were added over the whole humidity range. In dry air the sample was exposed to ammonia concentration steps running from 1 to 25 ppm ammonia separated by periods of dry air without ammonia (Figure 3.3 b). Additionally, several measurements were performed with longer exposure times and higher ammonia concentrations up to 100 ppm. Examples of the frequency shifts obtained upon the polymer interaction with these analytes are given in Figure 4.2 in chapter 4.2 and Figure 4.5 in chapter 4.2.2 respectively. In this work, the frequency shifts are given as positive values even if the frequency of the QMBs is actually lowered due to the additional mass uptake.

3.2.2 Electrochemical measurements

The samples required for electrochemical measurements were prepared by drop deposition of PAA solution (concentration range between 6 and 200 mg/ml) or corresponding solutions of the derivates in acetone and water (80% to 20%) onto quartz substrates provided with platinum interdigitated electrodes. The electrodes have a width of 50 µm and are separated from the counter electrode by 50 µm quartz resulting in an aspect ratio of 1000 and a 10 mm^2 active area (Figure 3.4 a) and the produced polymer layers have a thicknesses between 1 and 30 µm.

Mounted on a TO-8 socket the sample is placed in a Teflon measurement chamber which is equipped with current linkage for the working and the counter electrode between the sample and the measuring tool (Figure 3.4 b). In all electrochemical experiments performed a two electrode set-up without reference electrode is applied. The measurement chamber is covered with an earthed Cu sheathing, shielding the sample from environmental effects and connected with a gas mixing station to provide the desired gas composition in the ambient. The measurements were performed under equilibrium conditions in dry air and humidities up to 80% r.h. and ammonia concentrations between 1 and 30 ppm in dry and humid air.
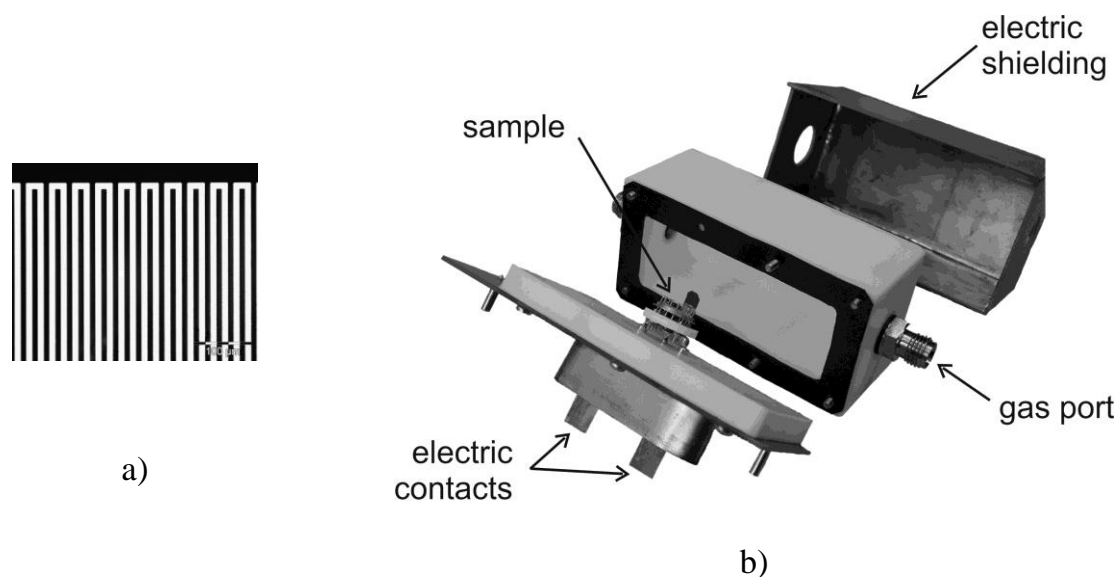
Figure 3.4: Substrate and measurement chamber for electrochemical measurements. a) Optical microscope picture of a quartz substrate applied in these measurements (detail section). The platinum interdigitated electrodes (black in the picture) have a width of 50 μm and are separated from the counter electrode by 50 μm quartz gap. b) Shielded measurement chamber for electrochemical measurements. It is equipped with current linkage for the platinum electrodes of the substrate with the measuring tool.

As measuring tool the computer controlled electrochemical measurement system Autolab (Eco Chemie B.V., Utrecht) was used; it consists of a data acquisition system and a potentiostat (PGSTAT 30) which provides potentials up to 30 V with an accuracy of 0.2% independent of the current in a range of 10 nA to 1 A and an alternating voltage frequency up to 1 MHz. This device was employed for the impedance measurements as well as for the step voltage and cyclic voltammetry experiments as discussed in the following sections.

For AC impedance spectroscopy measurements the potentiostat is driven by the *Frequency Response Analyser* software (FRA, Eco Chemie B.V., Utrecht) were the settings of the measurement as the frequency range, the amplitude of the alternating voltage and possibly an additional direct current bias can be chosen. In this work the electrical impedance is measured upon variation in frequency of the alternating voltage in the range of 1 mHz to 1 MHz. As discussed in 2.2.1 the method requires a linear electrochemical system and therefore the alternating voltage applied should not influence the response of the sample. In contrast to other systems the influence of the

alternating voltage on the spectra obtained is small for polymer covered comb structures as for example shown in Figure 3.5: Potentials below 250 mV do not influence the shape of the spectra suggesting that the system behaves linear at lower voltages. Hence, in this work a relative high alternating voltage of 100 mV (compared with [96] and [98]) could be applied to the sample resulting in accurate determination of the AC current response and with it in a low-noise determination of the impedance. Examples for the obtained impedance spectra are given in Figure 4.10 in 4.3.1 or Figure 4.17 a) in 4.3.1.2 where additionally a direct current bias up to 3 V is applied to the sample.

As presented in 2.2.2 the interpretation of the impedance spectra was performed with equivalent circuits using the software *Equivalent circuit* written by B. Boukamp [167] to fit the circuit parameters to the experimental data. The equivalent circuit describing the measured electrochemical systems is given in Figure 4.11 in 4.3.1.
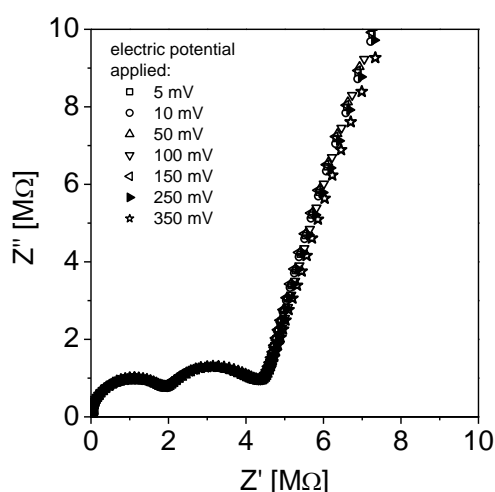

Figure 3.5: Negligible influence of the alternating current amplitude on the impedance of a sample below 250 mV presented in a Nyquist diagram. The measurements were performed with a 2 μm PAA covered sample exposed to 10 ppm ammonia in 50% r.h. and alternating voltages varied between 5 and 350 mV.

Beside the impedance spectroscopy voltage step and cyclic voltammetry measurements were performed with the Autolab set-up driven by the software *General Purpose Electrochemical System* (GPES version 4.7, Eco Chemie B.V., Utrecht).

For the voltage step measurements a DC voltage of 1 V was applied and the current decay upon this perturbation was observed for 30 s. Typical responses for the current decay several seconds after the voltage step started is shown in Figure 4.21 a) in 4.3.2. The cyclic voltammetry measurements were performed in the range of -1 to 1 V and scan rates ranging from 0.01 to 0.5 V/s were applied. Results obtained with this method are shown in Figure 4.21 and Figure 4.22 in 4.3.2.

3.2.3 Kelvin Probe measurements

In this work Besocke and McAllister Kelvin Probe set-ups were used simultaneously; the configurations are discussed in detail below. Both measurement chambers are made of brass covered with a thin Teflon layer allowing the study of the samples in an inert and shielded environment. Additionally, the chambers are equipped with glass windows to make the sample visible during the measurements (Figure 3.6) and allow for the tuning of the tip position. The two measurement chambers were connected in series with the gas mixing station which provides the desired composition of the sample ambient. With this arrangement and two samples prepared in a single spray deposition process it is possible to compare the response of the different Kelvin Probe set-ups.

The Besocke Kelvin Probe as well as the McAllister one has a gold covered counter electrode. As discussed in 2.3.2 it cannot be excluded that especially ammonia but also water molecules interact with the gold surface changing the work function of the counter electrode. This raises the problem that the measured CPD is not only caused by the sample any more. However, this work does not aim to measure the absolute work function change of the sample but to compare the responses of the substrates covered with different polymers. Therefore, a reproducible work function shift of the counter electrode upon analyte exposure does not hinder these studies.

As substrates, silicon wafers covered with a 100 nm gold layer on a 20 nm thin layer of titanium were applied. The wafers with very smooth surfaces reflected in a roughness of less than 10 nm were hand cut to the desired size of about 5x5 mm^2 for the use in Kelvin Probe measurement chambers. By the spray deposition method the substrate gold layers were covered with a solution of 0.2 mg/ml PAA in acetone and

water (80% to 20%) resulting in a porous layer of 700 nm thickness. The same amount of ammonium and sodium polyacrylate respectively is deposited on the substrates to study the response of these materials exposed to ammonia and humidity.
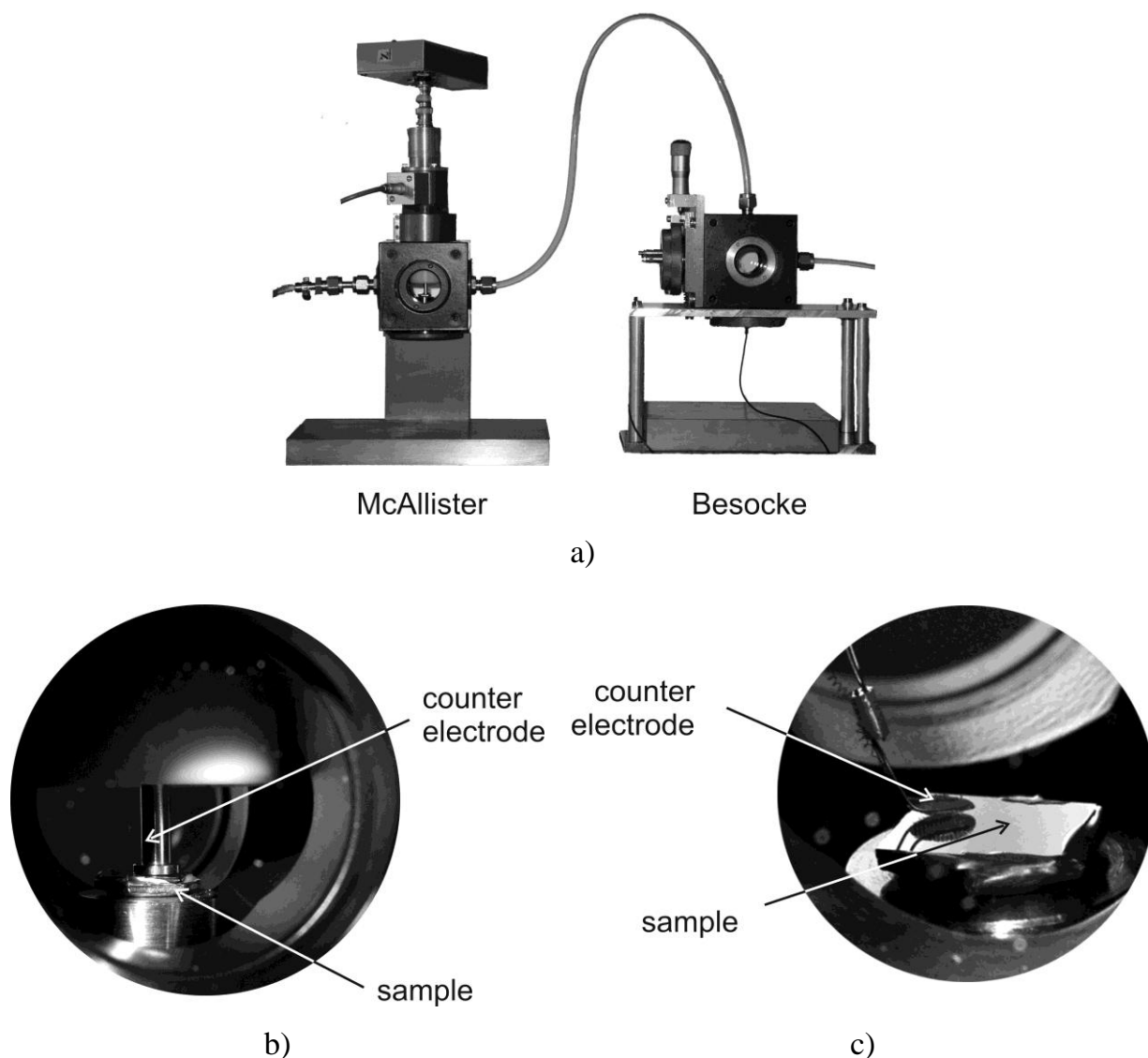

Figure 3.6: In series connected McAllister and Besocke Kelvin Probes for work function change measurements. A magnified picture of the samples and the counter electrodes is given in b) for the McAllister set-up and in c) for the Besocke set-up.

The pure substrates and the polymer covered samples were exposed to steps of 1, 3, 10 and 25 ppm ammonia separated by one and a half hours without ammonia as shown in

Figure 3.7. The measurements were performed in dry air and against a background of 50% r.h., additionally the response of the uncovered sample was studied in 90% r.h.
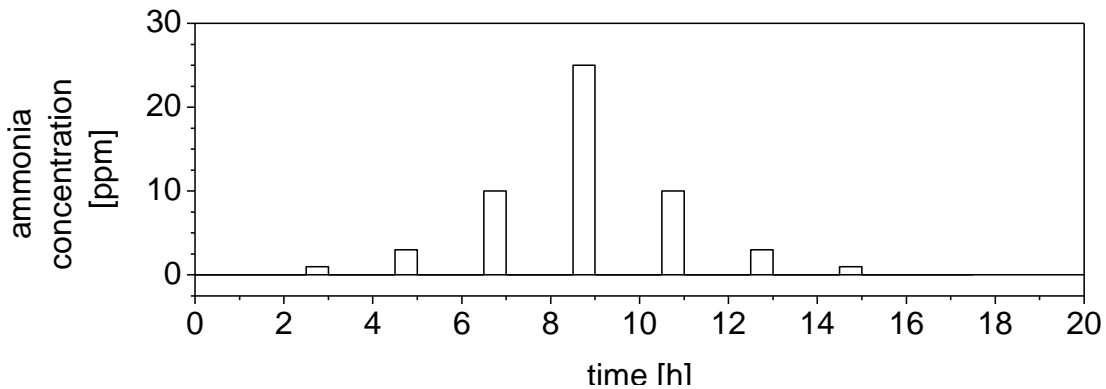

Figure 3.7: Measurement scheme applied in Kelvin Probe measurements. The sample was exposed to ammonia concentration steps between 1 and 25 ppm for 30 min separated by 90 min of dry air without ammonia. The experiments were performed in dry air and in a background of 50% r.h., additionally the response of the uncovered sample was studied in 90% ambient humidity.

3.2.3.1 Besocke set-up

After the measuring principle of Kelvin Probes was published (see 2.3.1) several technical approaches of work function measurement devices were developed. The Besocke set-up used in this work (Kelvin Probe type S manufactured by Besocke-Delta Phi, Figure 3.8 b) is an improvement of a Kelvin Probe described by Besocke and Berger in 1976 [168]. Typical results obtained with the Besocke Kelvin Probe set-up are shown in Figure 4.24 a) in 4.4.

The probe material is a gold covered stainless steel grid of 3 mm diameter fixed with an insulator to steel wires. According to the manufacturer the optimal sample-probe distance is about 1 mm and the gold grid has to be mounted in a plane-parallel orientation to the sample (Figure 3.6 c). The gold grid vibrations are produced by a piezoceramics with a base resonance frequency of 160 Hz which is set by the dimensions of the probe and the piezoelectric constant of the piezoceramics. The amplitude of the vibration can be varied via the driving electronics of the Kelvin Probe.

The driving electronics (Kelvin Control 07) purchased from the same company has outputs for driving the piezoelectric actuator, for the raw signal visualised by an

oscilloscope (Hewlett Packard 54602B), and for the Kelvin Probe signal connected to the data acquisition system (KP6500 from McAllister). For the determination of the contact potential the raw signal is amplified with a lock-in amplifier and a DC counter voltage is applied as discussed in 2.3.1. In the automatic modus the counter voltage is adjusted by the circuitry to minimize the charging current of the gold-grid / sample capacitor so that the compensating voltage equals exactly the difference of the work functions.

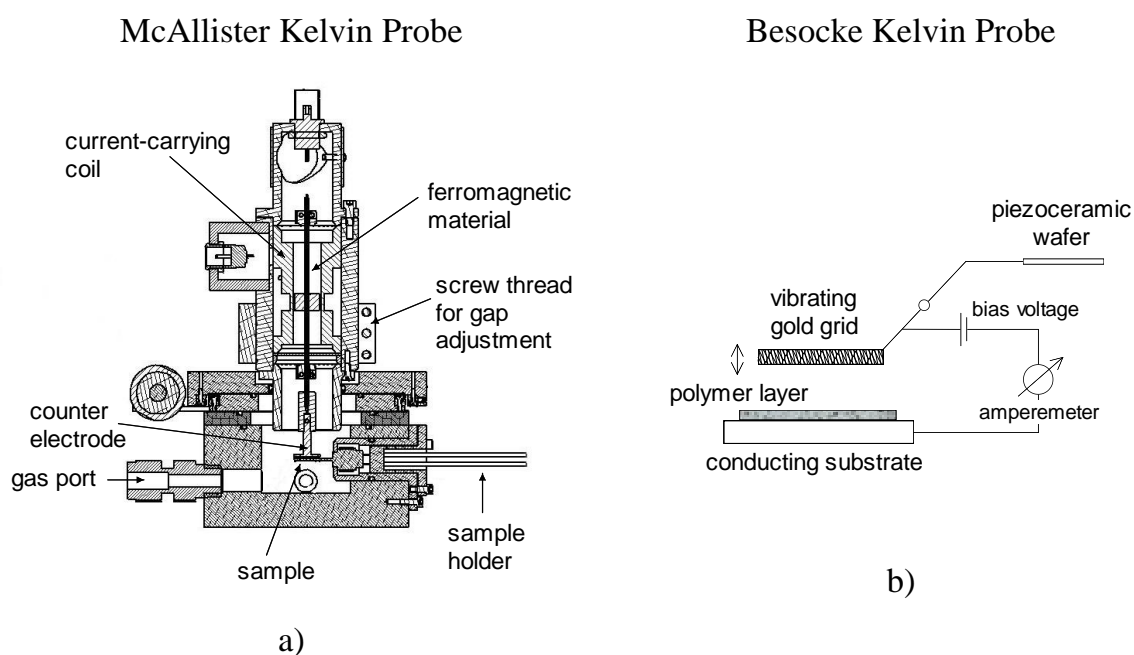McAllister Kelvin Probe

Besocke Kelvin Probe

Figure 3.8:   Schematic set-ups of the Kelvin Probes used in this work. a) McAllister set-up with an alternating current-carrying coil inducing an alternating magnetic field in which a ferromagnetic material connected with the counter electrode periodically moves [169]. b) Besocke set-up with a piezoceramic wafer inducing the gold grid vibrations. Additionally the electric circuit used for the determination of work function changes is sketched. In 3.2.3.1 and 3.2.3.2 the set-ups and their differences are discussed in more detail.

3.2.3.2 McAllister set-up

The McAllister Kelvin Probe KP6500 uses another procedure to determine the contact potential avoiding the unfavourable signal to noise ratio at the zero point which is the weak spot of the Besocke set-up:

Far away form the zero point the current is measured at several potential differences (V_{total}); in this region the signal to noise ratio is significantly improved. According

equation (2.26) a linear relationship exists between the potential difference and the measured current at constant capacitor plate distance and hence, the resulting current / potential difference plot shows a straight line whose slope is called "gradient". The counter voltage required for the zero point condition can be obtained by interpolation from the experimental data. In this work three potential differences between 4.95 and -4.95 V were applied to the sample and the response current was measured resulting in a straight line with a gradient of -0.254.
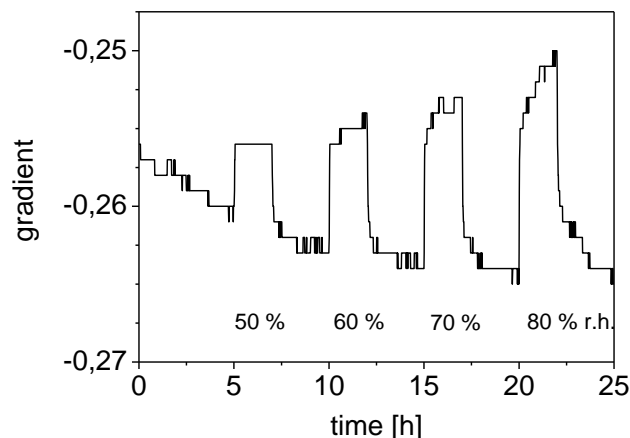

Figure 3.9: Humidity induced gradient changes observed in experiments performed without tracking mode. The 700 nm PAA covered substrate was exposed to 50, 60, 70, and 80% r.h. for 2 hours separated by 3 hours of dry air and measured in the McAllister Kelvin Probe set-up.

This method ensures a high accuracy but has the disadvantage to be very sensitive to gradient changes. Therefore measurements can only be compared with each other if they are performed with the same gradient which is basically determined by the distance of the capacitor plates. Due to outside influences, accidental variations of the distance may occur altering the Kelvin Probe response. To avoid this, the tracking mode provided by the software can be used adjusting the gradient by restoring the initial distance. An additional problem occurs if measurements in different ambient humidities are performed: Due to water sorption into the polymer the sample capacitance changes (2.2.2.1) and with it the gradient measured as followed from equation (2.26). Figure 3.9 shows an example of the humidity induced gradient change of a PAA sample which was recorded without tracking mode. If such measurements are performed in tracking mode the software alters the capacitor plate distance to keep

the gradient constant. This adulterates the measured contact potential difference because the gradient change was originally not induced by distance variations. Therefore it is not possible to obtain reliable CPD changes with the McAllister method if the capacitance of the sample depends on the ambient. Under these conditions the Besocke Kelvin Probe is preferable because it works under biased voltage and with it zero current conditions where the capacitance is not relevant.

In the McAllister set-up (Figure 3.8 a) the gold covered stainless steel counter electrode with a diameter of 5 mm is placed directly above the sample at a distance of about 0.1 mm or even less (Figure 3.6 b). To obtain low-noise signals and the aimed gradient the gap between the capacitor plates must be optimised with the screw thread shown in the figure and fine tuned with the tracking mode. An ac excitation coil induces an oscillation of a ferromagnetic material which is directly connected with the counter electrode resulting in a periodical movement which is required for the work function difference measurements as discussed in 2.3.1.

The McAllister Kelvin Probe is computer driven and controlled with the software KP6500 from McAllister. This software acquires the measurement data and allows the setting of several parameters for the Kelvin Probe; important examples are the frequency of the counter electrode vibration which was preset to 217 Hz, the number of measurements used for averaging (usually 128) and the gradient control with the tracking mode already mentioned above. Typical results obtained with the McAllister Kelvin Probe set-up are shown in Figure 4.24 b) in 4.4.

3.2.4 Infrared measurements

Infrared transmission spectroscopy performed with a Bruker Equinox 55 FT-IR spectrometer is the fourth experimental method used in this work. 2 µm thick polymer films are spray deposited from a solution of a 0.5 mg/ml PAA and the corresponding amount of the PAA salts in acetone and water (80% to 20%) directly on the 1 mm thick Germanium optical windows of the measurement chamber. The measurement chamber is made of stainless steel, inside and outside covered with black Teflon providing an inert ambient for the infrared measurements. The chamber illustrated in Figure 3.10 has two gas ports connecting it with the gas mixing station. Just as the

electrochemical measurements the infrared experiments were performed under equilibrium conditions in dry air and humidities up to 80% r.h. and ammonia concentrations between 1 and 30 ppm in dry and humid air.
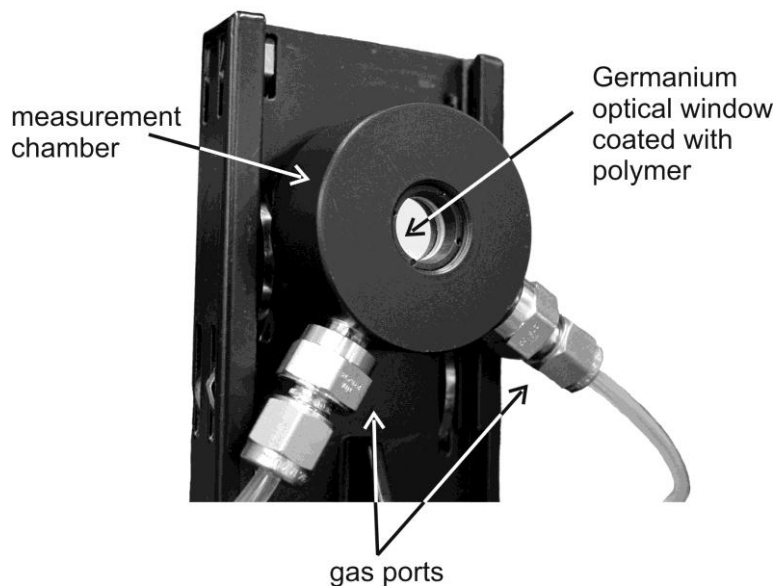

Figure 3.10: Black Teflon coated stainless steel measurement chamber for infrared measurements. The polymer to be measured is directly deposited on the Germanium optical window. Through the gas ports the desired gas composition is supplied.

The infrared spectra were taken in transmission with a resolution of 2 cm^{-1} in the range of 400 to 4000 cm^{-1} with 1024 scans per measurement in order to get a good signal to noise ratio. The accompanying software package OPUS 4 (Bruker Optik GmbH) controlled the spectrometer and was used to calculate the absorbance spectra using a reference spectrum taken without a polymer film in the measurement chamber. Additionally the spectra in dry air were used as reference to study analyte induced changes of the polymer materials. The spectra obtained are given in chapter 4.5.

4 Measurement results and interpretation

Results obtained with the previously described experimental methods are presented in the following sections. After a short discussion of the polymer layer morphology (in 4.1) the results of the gravimetric measurements are given (in 4.2). The interpretation of the QMB experiments provides information about mass changes upon water sorption, ammonia sorption and water sorption in a background of ammonia. Additionally, the influence of water sorption on the glass transition temperature is discussed. This information is supplemented by an insight into the polymer bulk processes and at the polymer electrode interface obtained from electrochemical measurements presented in 4.3. Kelvin Probe experiments were performed with McAllister as well as Besocke set-ups; the results of the different methods and of uncovered and polymer covered samples are compared with each other in 4.4. Detailed discussions of the interactions between water and ammonia molecules and the polymers, studied additionally based on the interpretation of infrared spectra, are presented in 4.5.

4.1 Characterisation of the polymer layer morphology

Depending on the counterion of the polyacrylate the deposition of the same amount of polymer with the spray-deposition method results in two different film types easily distinguishable by their optical microscope images (Figure 4.1 a) and by their roughness to thickness ratio (Figure 4.1 c) determined from the surface profile, which is given in Figure 4.1 b).

The materials with a large roughness to thickness ratio PAA (0.7) and NH_4PA (0.9) grow in islands on the substrate with the space between the islands covered by a very thin layer. The resultant layers are porous films with similar structured surfaces but different layer thicknesses: While the PAA layer has a thickness of 0.4 μm the one of the ammonium derivate is with 1.5 μm almost four times larger. The thickness of the NaPA film lies with 0.7 μm in between the thickness of the other layers but the roughness to thickness ratio is significant smaller (0.3). This is also reflected in the much smoother surface of this material.

PAA   NH$_4$PA   NaPA

a) Optical microscope images

b) Profile of the polymer layers

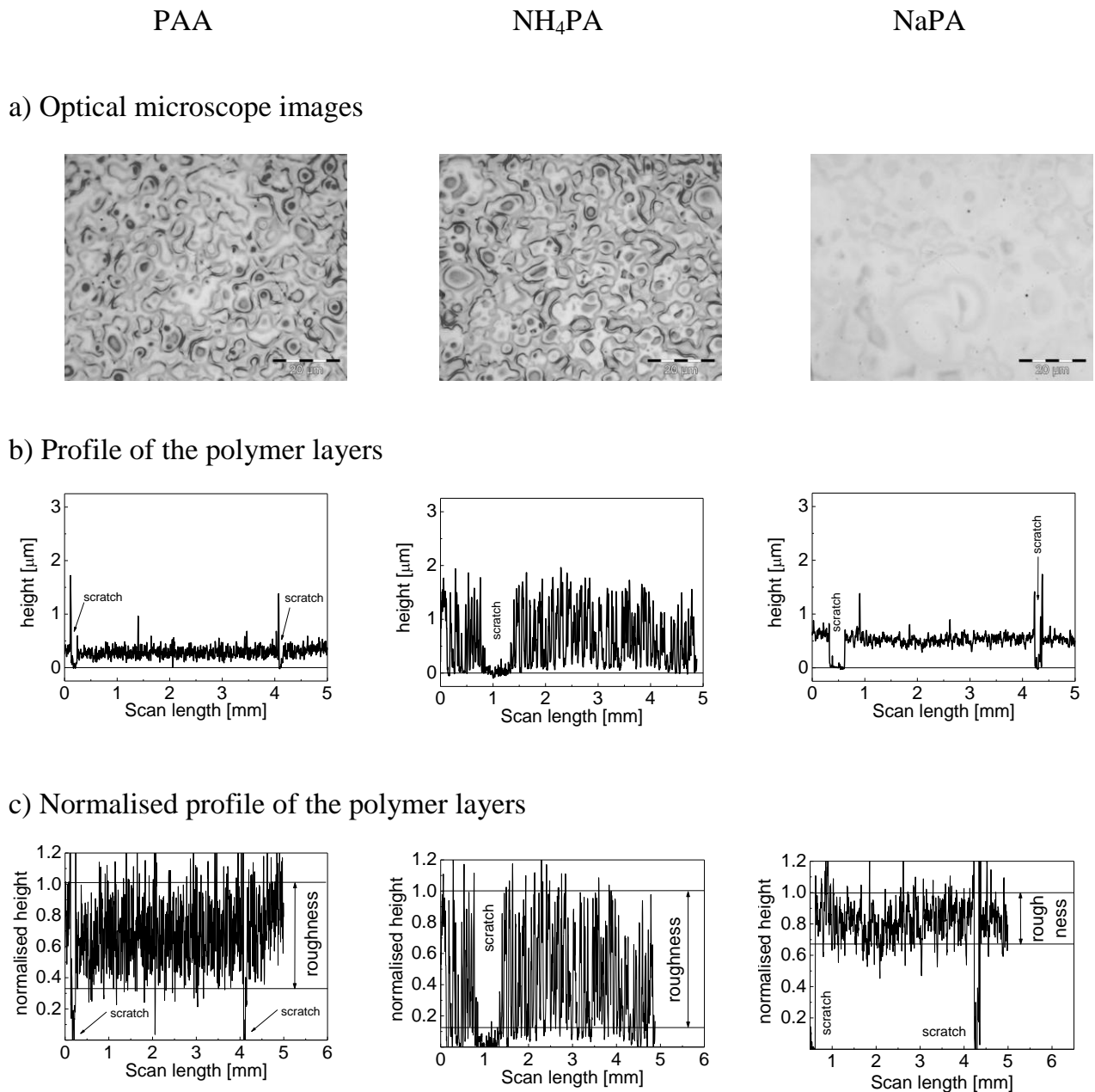c) Normalised profile of the polymer layers

Figure 4.1: Morphology studies of PAA and the same amount of its derivates spray deposited onto gold substrates. a) Optical microscope pictures with a scale bar representing 20 μm for all materials. While PAA and NH$_4$PA have an island like structure the surface of NaPA is much smoother. b) Stylus profiler scans show the surface roughness and the different thicknesses of the materials: 0.4 μm for PAA, 1.5 μm for NH$_4$PA, and 0.7 μm for NaPA. c) Normalised profiles of the surface are presented to compare the roughness to thickness ratio of the produced polymer films. The normalisation was made taking the polymer thickness as 1. The roughness to thickness ratios resulting from the normalized profiles were found to be: 0.7 for PAA, 0.9 for NH4PA and 0.3 for NaPA.

If the studied layers are prepared by using the drop-coating method, all produced films are transparent and very smooth with a surface roughness of about 20 nm. The thickness of the layers depends on the concentration of the polymer solution, which is used to prepare the films (see 3.1.1).

4.2 Gravimetric measurements

For the gravimetric measurements, the QMBs were covered with thin PAA, NH_4PA and NaPA layers, respectively. The raw experimental results are obtained as resonance frequency shifts of the polymer coated QMBs depending on humidity and ammonia concentration; an example of QMB raw data is given in Figure 4.2. From them the corresponding frequency shifts due water vapour and ammonia gas sorption are deduced, described in detail in the following chapters.
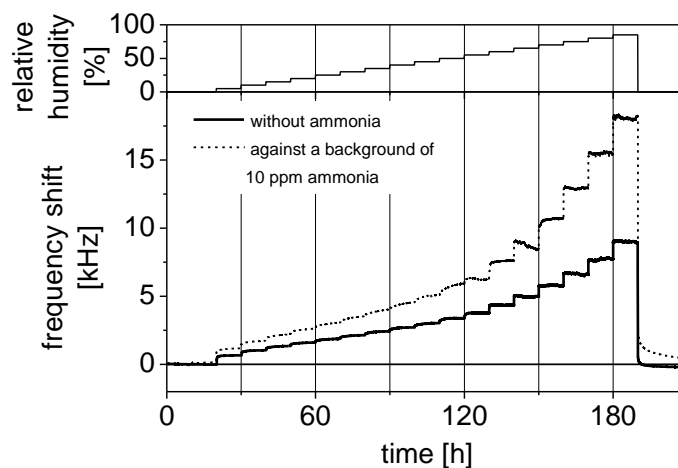

Figure 4.2: Resonance frequency shifts dependence on humidity and humidity in a background of 10 ppm ammonia for a 360 nm coated QMB. The measurement scheme is additionally given in the upper part of the figure.

4.2.1 Water sorption

According to the measurement scheme shown in the upper part of Figure 4.2 the polymer samples were dried and afterwards the humidity was increased by 5% each 10 hours. In a subsequent run the scheme was changed in such a way that the humidity pulses are separated by 5 hours dry gas exposure periods. The obtained frequency shifts are the same in both cases.

For PAA the QMB response was simultaneously determined for three different layer thicknesses; the sorption isotherms, that are the frequency shift dependencies on the humidity, are shown in Figure 4.3 a). The shapes of the sorption isotherms are characteristic for amorphous solids with two deviations from linearity: one at high humidities and the other one usually appearing as a "shoulder" at low relative humidities. It has not been well understood what gives rise to the initial shoulder but the increase at higher humidities is due to the formation of liquid water in the polymer and the glassy to rubbery transition of the material [86]. After exposure to humidity, the frequency shift disappears when the ambient atmosphere is switched to dry air; this fact indicates that the interaction between water molecules and the polymer is reversible. As shown in Figure 4.3 a) the sorption isotherm can successfully be fitted with the BET equation discussed in 2.1.4.1.
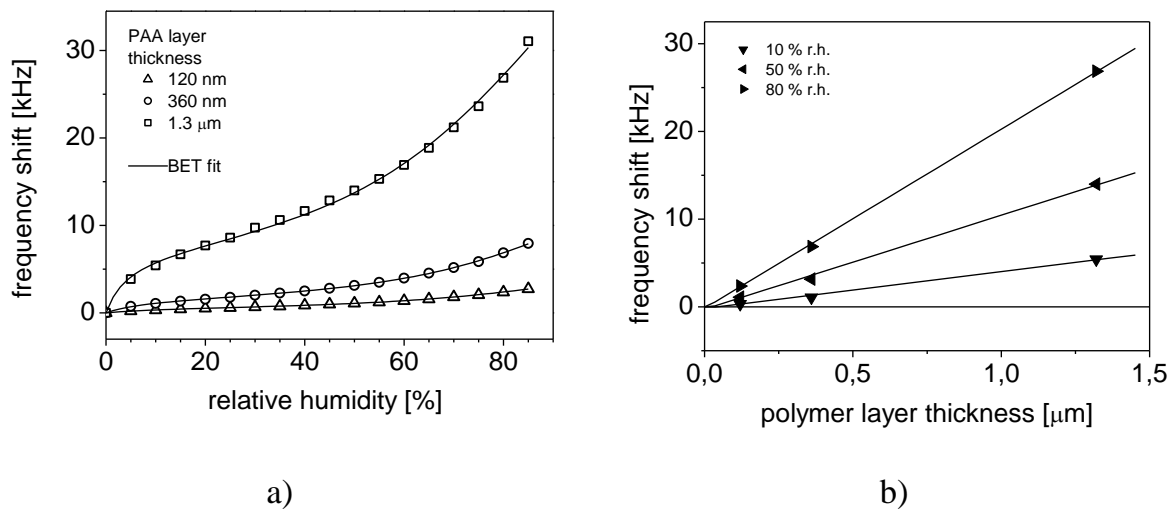

a)   b)

Figure 4.3: Frequency shift response of QMBs coated with 0.12, 0.36 and 1.3 μm PAA layers respectively. a) Frequency shifts plotted against the relative humidity can be described with BET isotherms (solid lines). b) The QMB response linearly increases with increasing polymer layer thickness as shown for three humidity examples.

During the sorption process water is taken up into the bulk of the PAA and therefore the amount of water sorbed at a given humidity, depends on the volume and, through it, on the thickness of the polymer layer covering the QMBs. The linear correlation between the QMB responses of layers with varying thickness is presented in Figure 4.3 b) for a low, a medium and a high humidity. It proofs that water sorption is a volume effect and gives evidence of the absence of changes in viscoelasticity during water

sorption and/or rigid behaviour (see 2.1.3). In the chosen range PAA films are "acoustically thin" and hence QMBs covered with PAA layers are really mass sensors and suited to study the sorption induced mass changes.

The non-linear increase of the sorption isotherm at high ambient humidities suggests that the static glass transition temperature of the sample is sufficiently lowered and the polymer undergoes a glassy to rubbery transition. To estimate the static glass transition temperature at different humidity levels the Flory-Fox equation (equation (2.9)) is used with the glass transition temperatures of dry PAA (106°C [163]) and of water (-135°C [170]) taken from literature and the weight fraction of polymer and of water calculated according to equation (2.10) from the QMB measurements. In Figure 4.4 the estimated glass transition temperatures calculated from the measurements of the 360 nm PAA layer, are plotted against the relative humidities causing the respective values. The temperature, which is required to observe the glassy to rubbery transition decreases with increasing humidity and at about 78% r.h. the glass transition temperature is lowered to room temperature and the polymer changes from its glassy to its rubbery state.
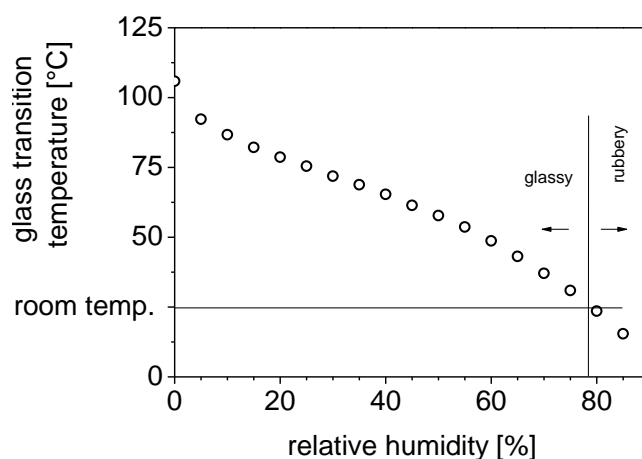

Figure 4.4: Glass transition temperature dependence on the relative humidity. The glass transition temperatures were estimated with the Flory-Fox equation (see 2.1.4.2) using data obtained from QMB measurements of substrates covered with 360 nm PAA. At room temperature the glassy to rubbery transition occurs at almost 80% r.h.

4.2.2 Ammonia sorption

Compared with the water sorption induced mass uptake, the effect due to ammonia is rather small but shows a similar dependence on the materials: While the response of

QMBs covered with PAA and NH$_4$PA are quite similar, the one of QMBs covered with the sodium derivate differs greatly.
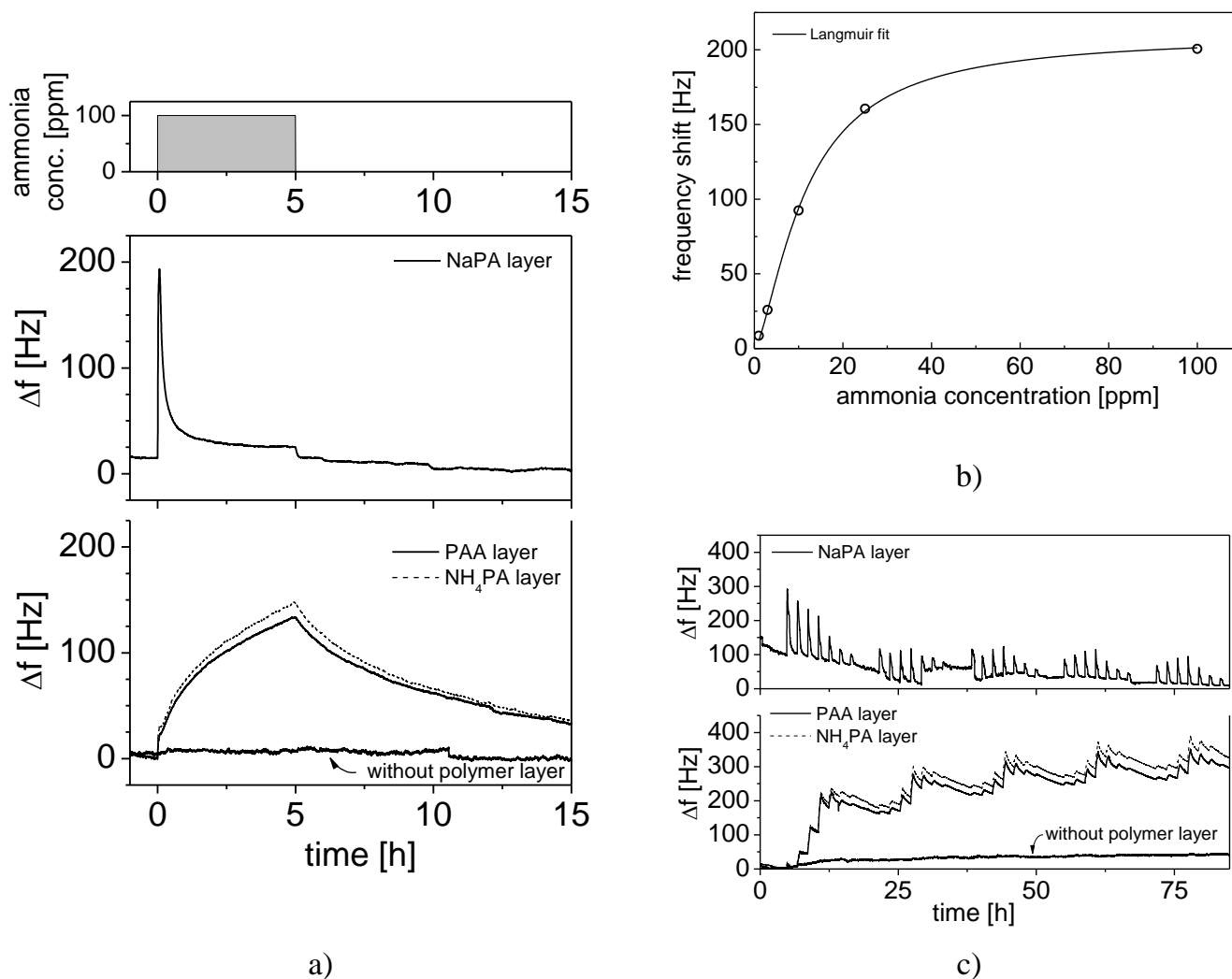

Figure 4.5: Response of QMBs covered with 360 nm PAA layer or the same amount of the ammonium and sodium derivates to several ammonia concentrations in dry air. a) The shape of the frequency shift upon a 100 ppm ammonia step depends on the studied material being very similar for PAA and NH$_4$PA but quite different for NaPA. b) Plotted against the ammonia concentration the frequency shift of the former can be described with a Langmuir isotherm (solid line) while the response of NaPA coated QMBs cannot be fitted with any known sorption isotherm. The example shown in the figure was measured with a PAA coated QMB. c) Frequency changes upon several exposure cycles for all materials studied. The measurement scheme was chosen according to Figure 3.3 in chapter 3.2.1.

In the case of PAA and NH$_4$PA in dry air the diffusion of ammonia into the polymer matrix is very slow and desorption after ammonia exposure is even slower and partly irreversible as presented in Figure 4.5 a). Even if the ammonia exposure time is extended to 10 hours the system is far away from equilibrium, which can only be estimated. The obtained sorption isotherm of a dry PAA sample is given in Figure 4.5 b) and well fitted with a Langmuir equation discussed in 2.1.4.1. As shown in Figure 4.5 c) the mass of the sample increases over several runs of ammonia exposure for these materials. If the ammonia measurements are performed in a background of humidity the response time decreases and the frequency shifts are much larger than in dry air. At all humidities, the sorption isotherms can be fitted with Langmuir equations.

The NaPA covered QMBs exhibit a completely different behaviour in dry air showing a very fast response time, an overshot for about 20 min, which is followed by a constant frequency shift until ammonia is removed from the ambient and a fast decay of the QMB response is observed. Unlike the other materials, the mass does not increase but does perhaps even decrease over several measurement runs. Both in dry air and in humid air none of the typical known sorption isotherms [83] is observed.

4.2.3 Water sorption in a background of ammonia

The water sorption measurements were repeated in a background of several ammonia concentrations. Due to the presence of ammonia the mass uptake of the sample during the water sorption process is strongly enhanced but the typical shape of the sorption isotherms remain and they still can be fitted with the BET equation as shown in Figure 4.6 a). From the measured data and with the assumption that at a given ammonia concentration the further frequency change of the QMBs is due to absorbed water molecules only, it is possible to calculate the polymer and water weight fraction again with equation (2.10) if the frequency shift due to the added polymer in dry air ($\Delta f_{PAA\,layer}$) is replaced with the frequency shift $\Delta f_{PAA\,layer\,with\,ammonia}$ considering mass changes due to absorbed ammonia in dry air. Infrared measurements show that this assumption is valid and that the mass uptake is due to an additional water uptake induced by the presence of water (Figure 4.28 in 4.5.1). With the calculated weight

fraction the static glass transition temperature of the system can be estimated. When the obtained values are plotted in the same manner as in Figure 4.4, the relative humidity required for the glassy to rubbery transition at room temperature can be determined. The dependence of this relative humidity on the ambient ammonia concentration is given in Figure 4.6 b). The higher the ammonia concentration the lower is the water concentration needed for the glass transition at a given temperature and the other way around.

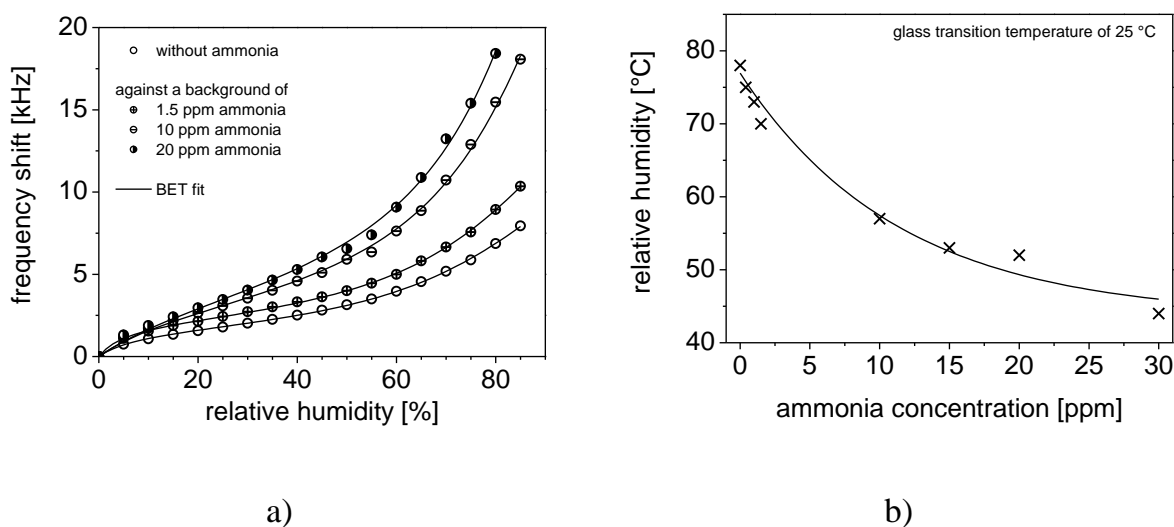a)   b)

Figure 4.6:   a) Gravimetric measurements with 360 nm PAA covered QMBs without ammonia (open circles) and in a constant background of ammonia. The QMB response upon an increase of humidity increases in the presence of ammonia while the plot against the humidity can always be fitted with BET isotherms (solid lines). b) Glass to rubber phase transition diagram estimated form the QMB responses by means of the Flory-Fox equation. It shows the ambient conditions (relative humidity and ammonia concentration) required for the glassy to rubbery transition of PAA at room temperature.

The relative frequency shifts due to interaction with ammonia (arrows in Figure 4.7 a) compared to the frequency shift without ammonia have been further derived to study the interaction mechanism between water and ammonia molecules in the PAA layer. The effects in a background of 10, 20 and 30 ppm ammonia are presented in Figure 4.7 b). The results are showing that as long as the relative humidity is low, the relative increase of the frequency shift due to interaction with ammonia is independent of the humidity. At higher humidity levels, however, the frequency linearly depends on it but with a slope almost independent on the ammonia concentration.

The humidity at which the switch between the humidity independent region and the dependent one takes place, is in agreement with the values required for the glassy to rubbery transition at room temperature; it also decreases with increasing ammonia concentration.

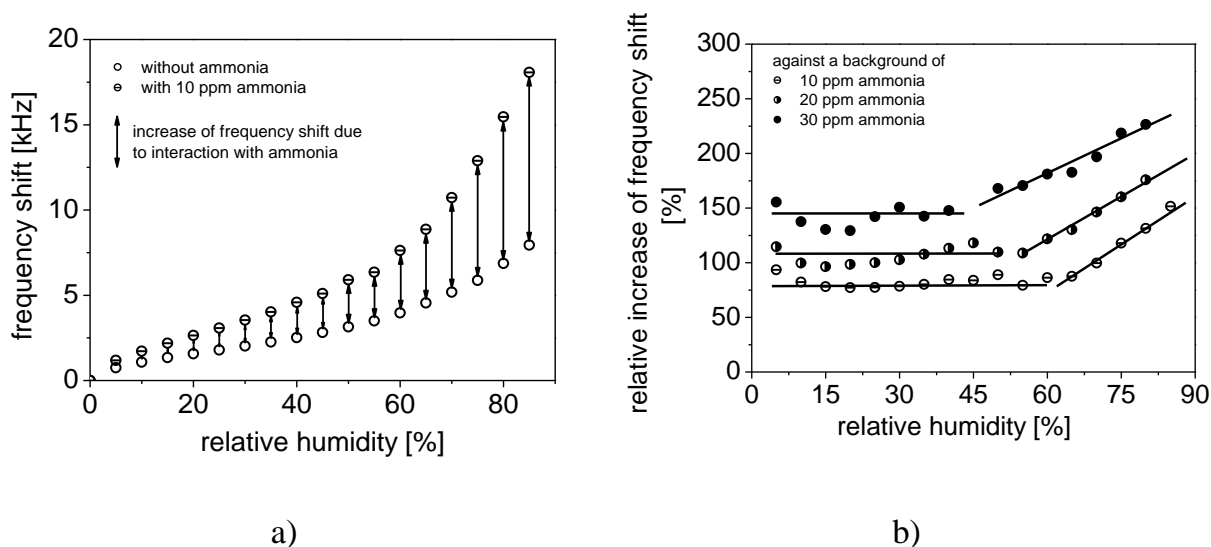a)   b)

Figure 4.7: a) Response of a QMB with 360 nm PAA layer to several levels of relative humidity without and with a background of 10 ppm ammonia. The arrows indicate the increase of frequency shift due to interaction with ammonia at a given humidity. b) Relative increase of the frequency shift in dependence on humidity for three different ammonia exposure levels. The frequency shift without ammonia at each humidity was taken as reference. The sample was a 360 nm PAA coated QMB.

To get a full picture of the water sorption process in PAA the sorption properties of the ammonium and the sodium derivates were also studied. The obtained sorption isotherms are shown in Figure 4.8 and it is obvious that the two derivates of the same acid show quite different responses: If the ammonia salt of the PAA is used, the system still responds with the same mass increase to several levels of relative humidity and ammonia concentrations (Figure 4.8 a) as the PAA film does, if the amount of polymer is the same in both cases. The response of the NaPA covered QMB to humidity (Figure 4.8 b) is much higher than the one of the other materials; almost 40 kHz frequency shift are observed in humid air even without ammonia. At low humidity levels the response vary from one measurement run to the next one but, unlike for PAA and NH_4PA, it is independent of the ammonia concentration. With

increasing humidity some influence of ammonia seems to be present, but the poor reproducibility of the NaPA film response does not allow for a clear conclusion.

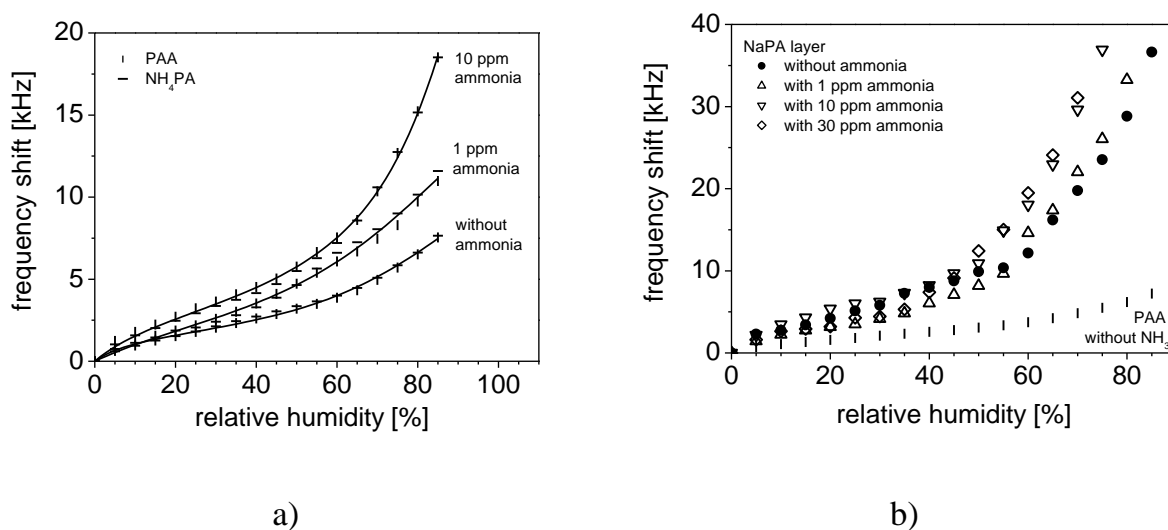a)   b)

Figure 4.8: Response of QMBs covered with 360 nm PAA and the same amount of the ammonium and sodium salts respectively. a) PAA coated QMB response in comparison with NH_4PA coated QMB to several levels of relative humidity without and with 1 and 10 ppm ammonia. The data are fitted with BET isotherms (solid lines). b) Response of NaPA coated QMBs to several levels of relative humidity without and with 1, 10, and 30 ppm ammonia. For comparison the frequency shift of a PAA coated QMB upon humidity exposure without ammonia is given in the same figure.

4.3 Electrochemical measurements

Systematic impedance measurements were performed to study the electrochemical properties of a system consisting of metal comb electrodes covered with a polymer layer. To supplement the obtained information, cyclo-voltammetric and voltage step measurements were added.

4.3.1 Impedance measurements

The main experimental results are the dependencies of the electrical parameters as revealed by the impedance spectrograms in the 1 mHz − 1 MHz range. In controlled atmosphere containing different levels of humidity the raw data (real and imaginary components of the impedance) are spanning over more than eight orders of magnitude; their direct comparison being impossible, scaled representations have been derived that give a feeling for the samples' behaviour (see for example the impedance of a

PAA layer in Figure 4.9). The Nyquist plot for different humidity values shifts from a vertical line in dry air over "one-semicircle" and the "two-semicircles" type (one of them very large, only partially shown in the picture; plotted with squares in Figure 4.9) to the "three-semicircles" type (plotted with circles and triangles in Figure 4.9; again, one semicircle is very large and only partially shown in the picture), indicating the onset of further electrochemical processes. At higher humidities, this semicircle is partially or completely overlapped by the large lower frequencies semicircle. After drying the sample, the initial impedance spectra are obtained again showing that the effect of humidity on the electrical properties of PAA is reversible. This is in agreement with the gravimetric measurements which are also indicating the reversibility of the water sorption (see 4.2.1).
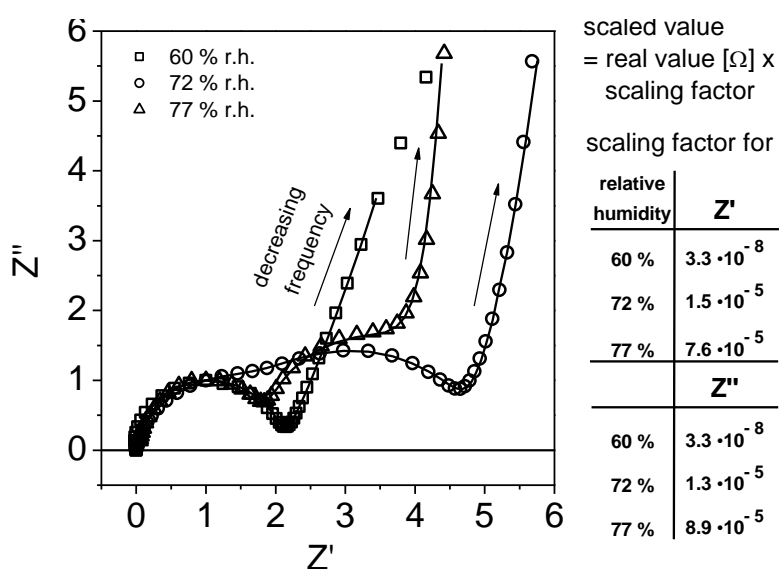

scaled value
= real value $[\Omega]$ x
scaling factor

scaling factor for

relative humidity	Z'
60 %	$3.3 \cdot 10^{-8}$
72 %	$1.5 \cdot 10^{-5}$
77 %	$7.6 \cdot 10^{-5}$
	Z"
60 %	$3.3 \cdot 10^{-8}$
72 %	$1.3 \cdot 10^{-5}$
77 %	$8.9 \cdot 10^{-5}$

Figure 4.9: Scaled Nyquist plot for a sample covered with a 2 μm PAA layer at different humidity levels. The radius of the first circle is scaled to 1.

In dry air gaseous ammonia does not influence the electrochemical properties of PAA and NH_4PA (see Figure 4.10 a) but the impedance of the comb structure covered with NaPA changes a bit if ammonia is present in the ambient; it does not, however, display a clear dependence on the ammonia concentration. The great difference between the impedance of PAA and NH_4PA and in contrast NaPA is notable.

PAA
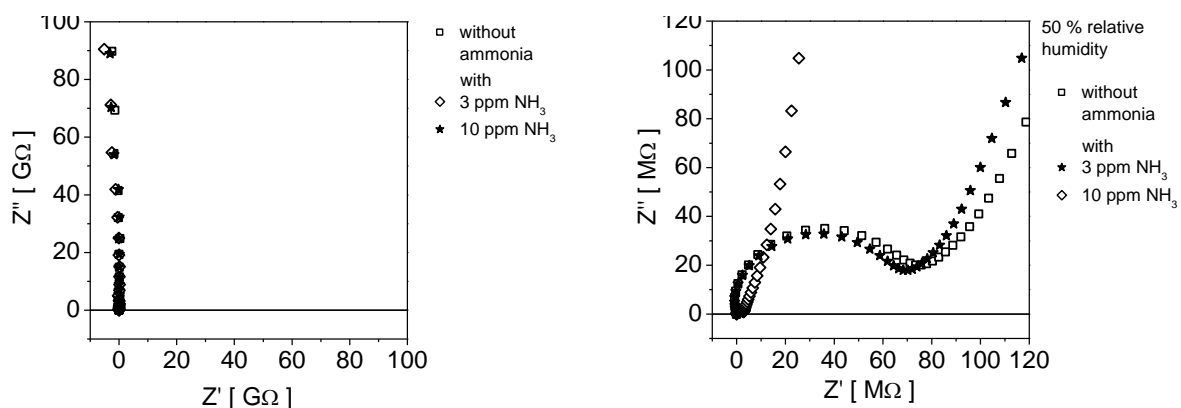
NH$_4$PA
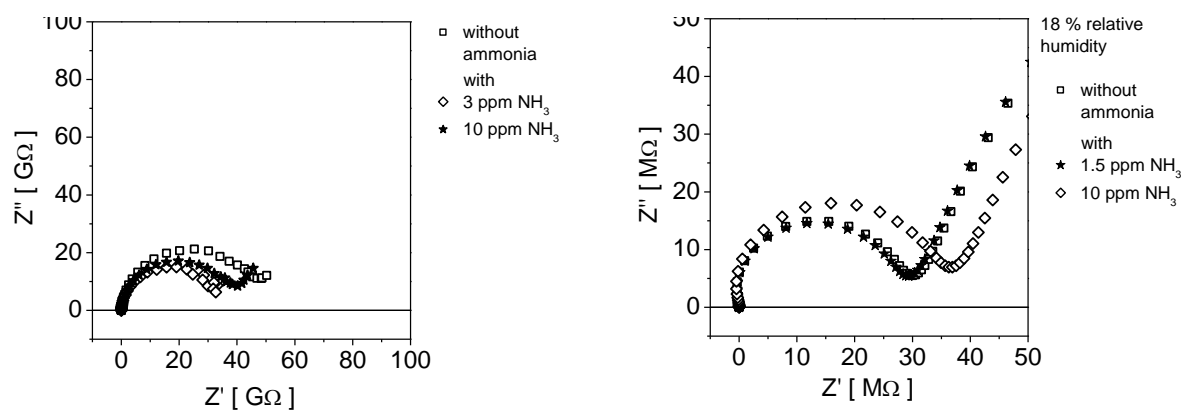
NaPA

a) Dry air   b) Humid air

Figure 4.10: Influence of ammonia on the impedance of the measured sample in a) dry and b) humid air presented as Nyquist plot. The substrates were covered with 2 μm PAA, NH$_4$PA and NaPA films respectively.

The behaviour of PAA and NH$_4$PA completely changes if the ambient atmosphere contains some humidity. Then the presence of ammonia is dramatically enhancing the

water effect in this materials and a strong impedance decrease of the polymer layer is observed. For example in the non-scaled Figure 4.10 b) for PAA it is no more possible to see the semicircle describing the high frequency response of the layer at 10 ppm ammonia and the one for NH_4PA is also very small. The response of NaPA covered samples is almost unchanged by the presence of ammonia. Only a slight increase of the impedance with increasing ammonia concentration is observed.
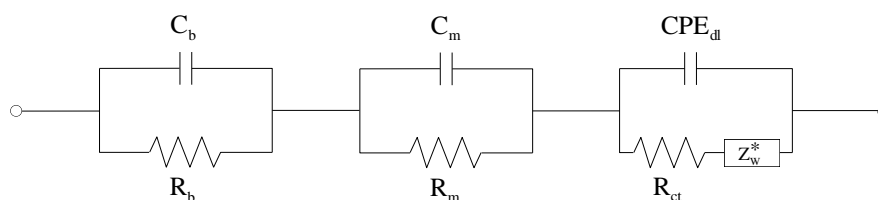

Figure 4.11: Equivalent circuit representing the electrochemical system studied in this work: C_b and R_b are the capacitance and the resistance describing the bulk properties of the polymers; CPE_{dl} represents the double layer capacitance parallel to the charge transfer resistance of processes at the electrode surface R_{ct} probably supplemented with a Warburg impedance Z_W^*. The elements C_m and R_m describe the properties of a third semicircle appearing in the Nyquist plot between the bulk and the electrode elements. Further work is required to explain the meaning of this semicircle.

For the interpretation of the AC impedance spectroscopy results the equivalent circuit sketched in Figure 4.11 is used. Depending on the ambient conditions one to three $R\parallel C$ circuits are necessary to fit the measured data. The semicircle at the highest frequencies is due to the impedance of the polymer layer and can be fitted with R_b representing the resistance of the bulk and C_b the capacitance of the electrode structure covered with polymer as dielectric material in parallel (see 2.2.2.1). Here one has to point out the relative meaning of the term "high frequency", which, depending on the ambient conditions, is addressing the whole measurement range but always refers to the outermost left element presented in the Nyquist plot. According to the discussion below (see 4.3.1.2) the large semicircle at the lowest frequencies is caused by the redox reaction at the electrodes and can be fitted with the charge transfer resistance R_{ct} for the electrode reaction in parallel to the double layer capacitance CPE_{dl}. Additionally, if the electroactive species has to diffuse to the electrodes a complex Warburg impedance element Z_W^* may be used in the equivalent circuit to model the

observed behaviour in a certain humidity range. The third semicircle which, depending on the studied polymer for the first time appears at about 60% r.h. (PAA and NH$_4$PA) and 30% r.h. (NaPA), respectively, in between the other elements may be related to the polymer / electrode interfaces [124] and is fitted with the parallel R$_m \parallel$ C$_m$ circuit.

4.3.1.1 Polymer bulk properties

The humidity dependence of the polymer bulk resistance, R$_b$, and the capacitance of the electrode structure covered with polymer, C$_b$, is shown in Figure 4.12 (open squares) for a PAA layer deposited on metal electrodes. R$_b$ decreases with increasing humidity but has a kink at about 40% r.h. so that one can observe two regions with two different slopes in the logarithmic scale. The capacitance increases with increasing humidity showing a kink at about the same humidity as the resistance curve. When the impedance measurements at the same humidity levels are repeated after the sample was kept in dry air for at least 3 days the run of the resistance and capacitance curve is unchanged as long as the sample has never been exposed to ammonia before. If the impedance measurements are performed with several PAA samples the bulk properties differ not more than 10% from each other and are independent of the layer thickness in the measured range (1 to 30 µm) as expected for humidity measurements [171]. However, the thicker the polymer layer the longer is the time required to equilibrate the system with the ambient.

In a background of ammonia the plots of resistance and capacitance values against the relative humidity keep the shape but shift with about 20% r.h. to lower humidities (open circles in Figure 4.12). If the gaseous ammonia is removed from the ambient and, additionally, the sample is dried for at least 3 days a rerun of the impedance measurement does not yield the results obtained before ammonia exposure (filled squares in Figure 4.12): the resistance is much smaller at low humidities and the kink is shifted to higher humidities. Above 60% r.h. the bulk resistance before and after ammonia exposure converges. The capacitance shows no clear trend at low humidities but similar to the results obtained before ammonia exposure strongly increases at higher ones.

a)   b)
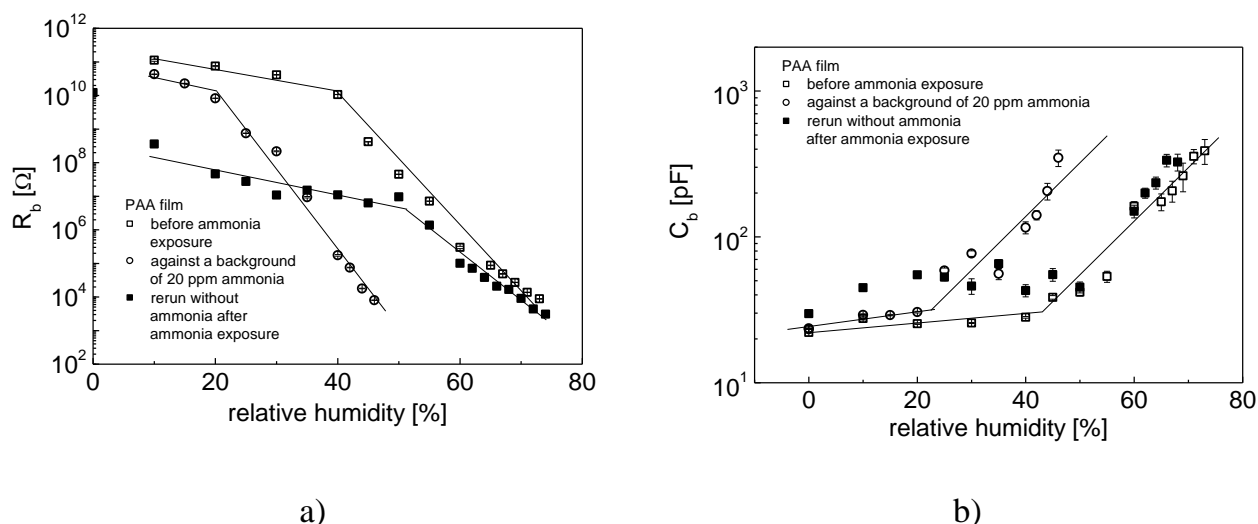
Figure 4.12: a) Bulk resistance and b) capacitance of the electrode structure covered with PAA as dielectric material depending on the humidity and ammonia concentration of the ambient. The humidity measurements were performed before the sample was ever exposed to ammonia (open squares), in a background of 20 ppm ammonia (open circles) and in a rerun without ammonia after ammonia exposure (filled squares).

The ammonium and sodium derivates differ in their electrochemical response to water vapour in the atmosphere (Figure 4.13). At low humidity levels both materials exhibit a lower resistance than the polyacrylic acid and NH_4PA shows a kink at about 50% r.h. approaching the bulk resistance of PAA above this humidity. This shape and especially the position where the kink of the bulk resistance occurs is in agreement with the observations made for PAA measured after previous ammonia exposure but without ammonia in the ambient (see Figure 4.12 a). The curve of NaPA shows no kink and over the whole humidity range the slope is similar to the slopes of the other materials above their kink humidity.

The capacitance of all samples increases with increasing humidity and a kink is observed. While for NaPA the kink appears already at about 30% r.h. followed by a strong increase of the capacitance, the curve for PAA is much lower until the kink occurrence at about 45% r.h. and the capacitance rises. At higher humidities above 50% r.h., the capacitance data obtained for NH_4PA is similar to those of PAA but at lower humidities it is in between the capacitances observed for the acid and the sodium salt.

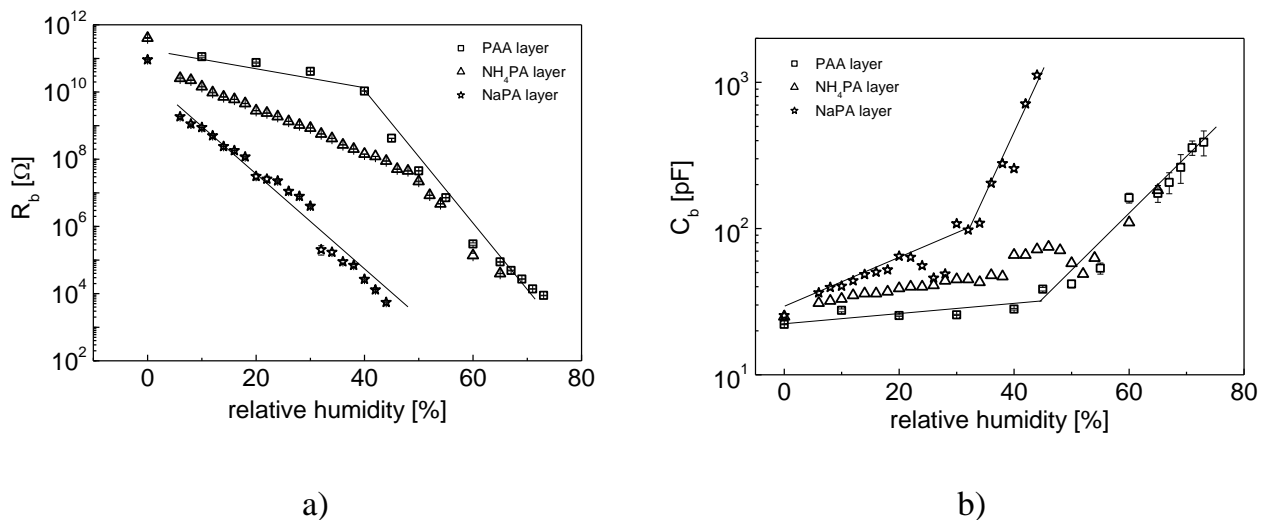a)   b)

Figure 4.13: a) Bulk resistance and b) capacitance of the electrode structure covered with polymers as dielectric material depending on the humidity of the ambient. The results obtained for PAA (squares), NH_4PA (triangles), and NaPA (stars) are compared.

With the Brasher-Kingsbury equation (equation (2.17)) the volume fraction of water in the polymer layer can be obtained from the capacitance data at several levels of relative humidity. For PAA and its derivates this equation gives only a rough estimation because rigid behaviour and negligible swelling, which are the assumptions made in the derivation of the Brasher-Kingsbury equation, cannot be assumed, especially at higher humidities. However, the obtained values presented in Figure 4.14 are still helpful: They show, in accordance with the QMB measurements discussed in 4.2.1, that the water sorption into the polymers is similar for PAA and NH_4PA and quite different for NaPA. This is notably valid for the point at which a strong increase of the volume fraction starts and for the values at high humidities.

As shown in Figure 4.12 humid ammonia pre-exposure strongly influences the humidity dependent bulk parameters for PAA and NH_4PA. In contrast, a previous ammonia exposure has no influence of the resistance and capacitance of NaPA: The bold filled stars in Figure 4.15, deduced from the rerun of the measurements after ammonia exposure, coincide with the data obtained before ammonia exposure (open stars). A similar behaviour is observed for NH_4PA at higher levels of relative humidity but at lower humidities the responses differ and the data taken form the rerun after ammonia exposure do not display a clear dependence on the humidity.
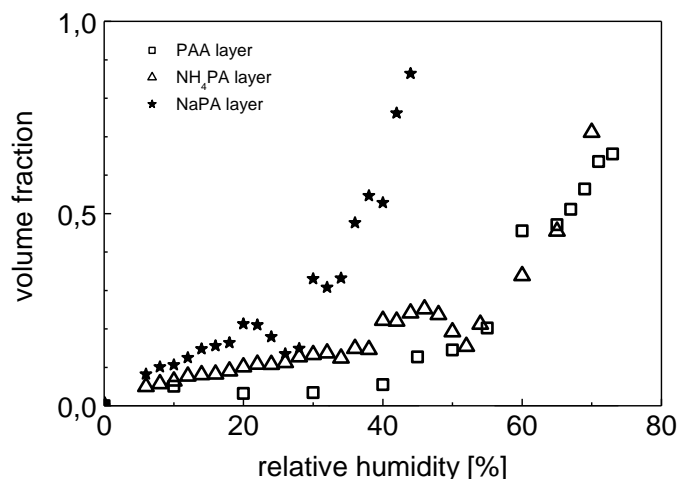
Figure 4.14: Water volume fraction in the polymers depending on the ambient humidity. According to the Brasher Kingsbury equation (2.17) the water volume fraction was estimated from the bulk capacitance data shown above (Figure 4.13 b).
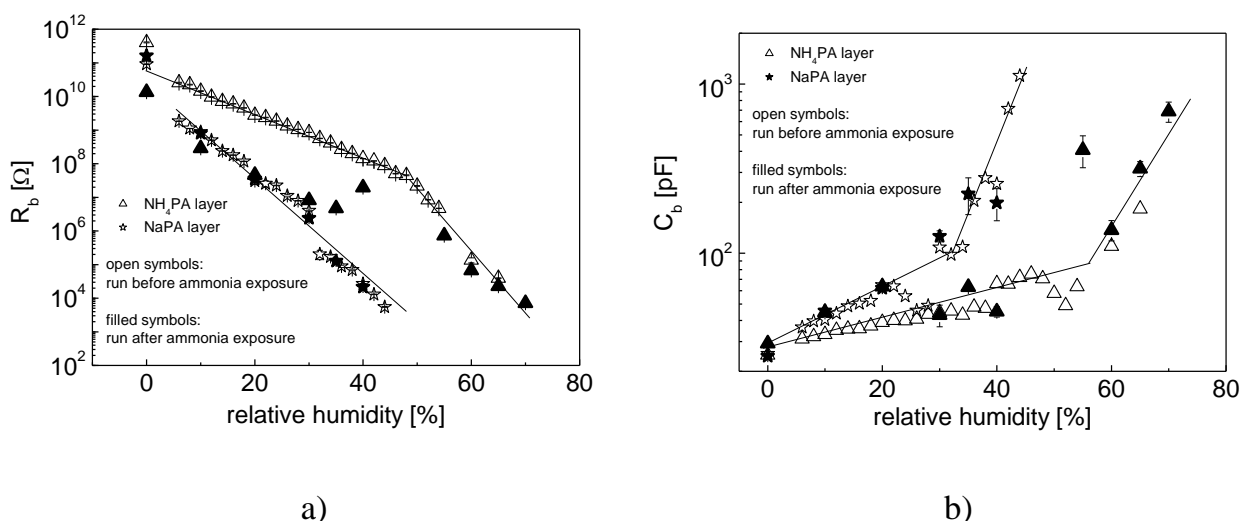

a)   b)

Figure 4.15: a) Bulk resistance and b) capacitance of the electrode structure covered with NH_4PA (triangles) and NaPA (stars) respectively depending on the humidity of the ambient before (open symbols) and after (filled symbols) ammonia exposure. In between this measurement runs the samples were kept in 50% r.h. with 20 ppm ammonia for three days and subsequently dried for one week in dry air.

4.3.1.2 Electrode processes

At low humidity levels the semicircle at high AC frequencies is the only element in the Nyquist plot but with increasing humidity a second element appears to lower frequencies. At the onset humidity of the new element a straight line becomes visible (with an angle of about 55° in respect to the x-axis (Figure 4.16 a). This angle deviates

79

from the expected 45° degree for a Warburg impedance but the linear slope still suggests diffusion, probably overlapping with other processes.

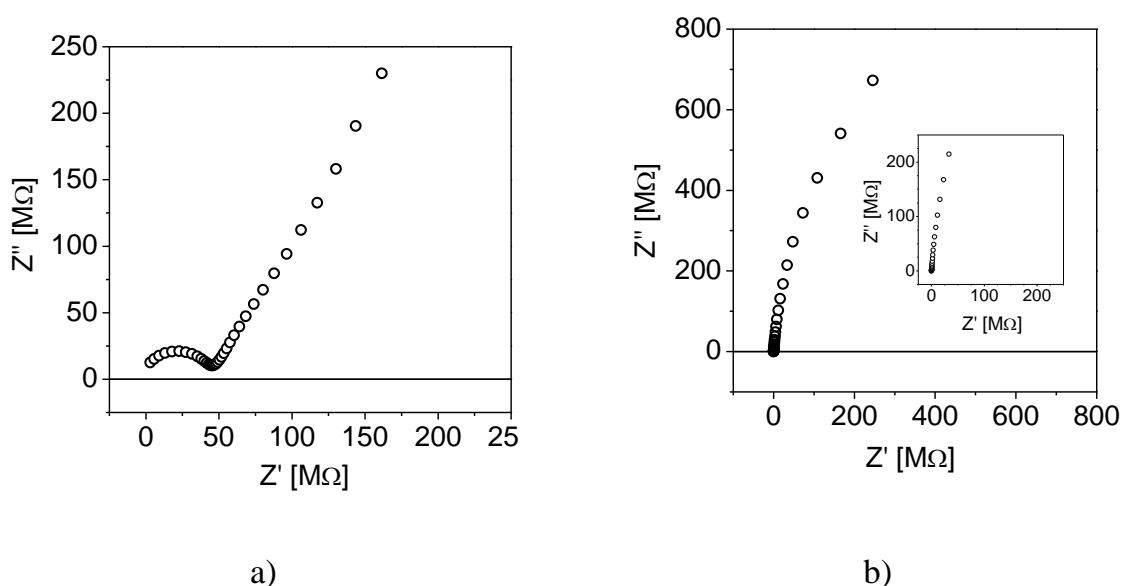a)   b)

Figure 4.16: Low frequency elements in the Nyquist plot. At low ambient humidities, for example 20% r.h. (a), the impedance linearly increases showing a Warburg impedance like behaviour in the low frequency range. With increasing humidity, for example at 60% r.h. (b) the element changes from a straight line to an arc indicating the onset of a new electrochemical process. The inlet shows the behaviour in the 0 to 250 MHz range. The measurements were performed with a PAA coated substrate but the results obtained with NH$_4$PA are very similar.

At higher humidities the element changes from a straight line to an arc indicating the onset of a new electrochemical process (Figure 4.16 b). This process is observed in PAA as well as in the other studied polymers. To investigate this process, bias voltages were applied and the impedance measurements repeated. An example of such measurements performed with an NH$_4$PA sample at 60% r.h. is given in Figure 4.17 a) where the strong effect of the applied voltage on the low frequency element is observable in the impedance spectra. The data can be interpreted with an equivalent circuit containing a resistance and a constant phase element in parallel and a Warburg impedance to account for the straight line at small humidities (Figure 4.17 b). The constant phase element cannot be replaced by a capacitance because the parameter n is with 0.88 far away from 1 indicating that a distribution of relaxation times occurs possibly caused by the roughness of the electrode. Above 1 V bias voltage, the

equivalent resistance obtained form the measurements, strongly decreases with increasing bias voltage (Figure 4.17 c) suggesting that the resistance is caused by charge transfer reactions at the electrode surface (see 2.2.2.2). In contrast, the CPE is almost independent of the applied voltage – a characteristic feature of the double layer capacitance (Figure 4.17 d).
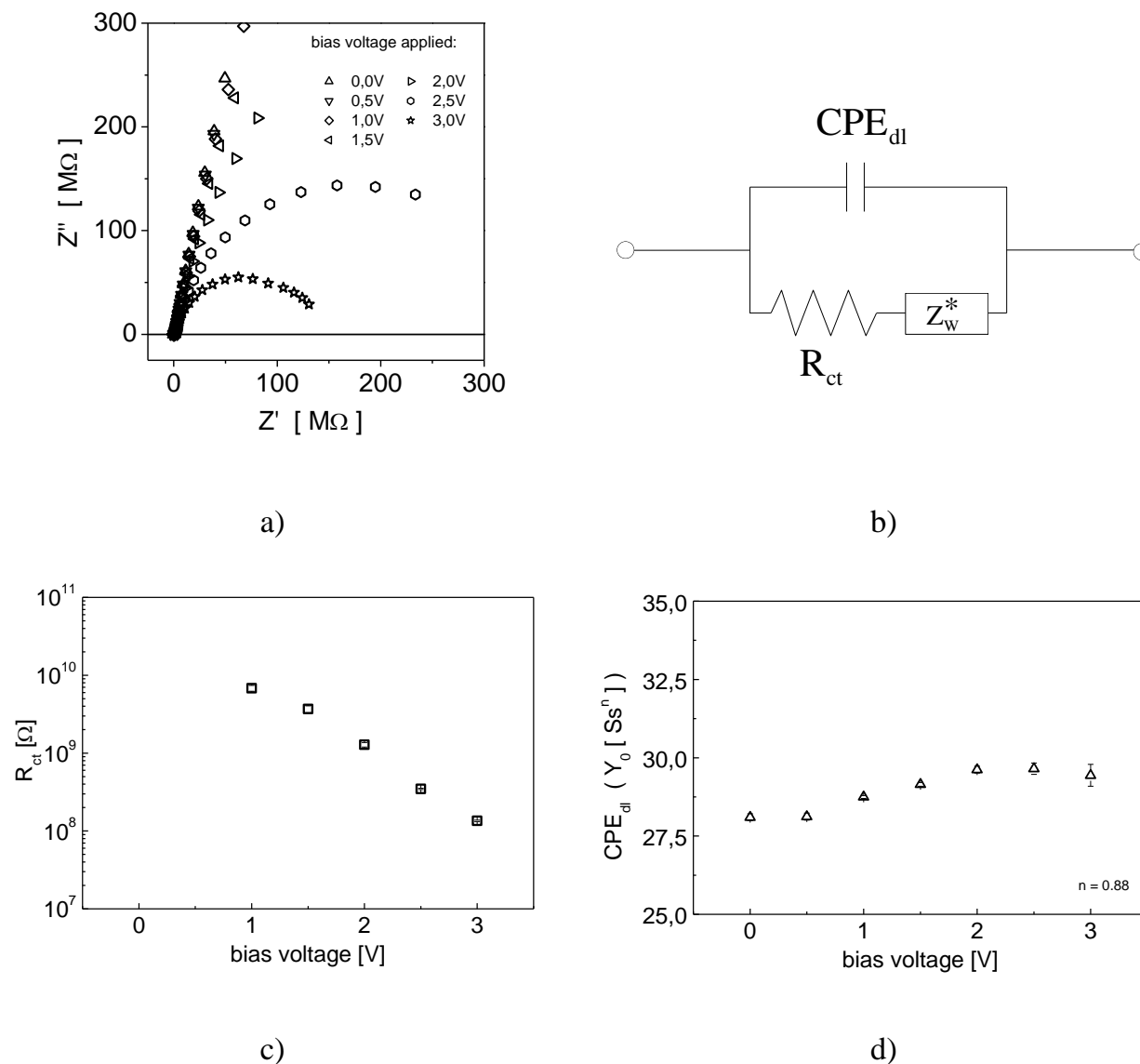

a)

b)

c)

d)

Figure 4.17: Dependence of the low frequency response on an applied bias voltage: a) The Nyquist plot shows the strong influence of a direct voltage on the impedance of the sample. The voltage was varied between 0 and 3 V in 0.5 V steps. b) The obtained arcs can be fitted with an equivalent circuit containing the charge transfer resistance (R_{ct}), the double layer capacitance (C_{dl}) and especially at low ambient humidities the Warburg impedance element. The charge transfer resistance and the double layer capacitance obtained form the impedance measurements are represented in (c) and (d) respectively. The measurements were performed at 60% r.h. with a NH_4PA coated substrate.

For the study of the charge transfer reactions at the electrode in detail, the usefulness of the impedance technique is limited because only a small part of a huge semicircle can be fitted resulting in large errors. In contrast, the dependence of the constant phase element on the relative humidity can be fitted more precisely and is shown in Figure 4.18 for PAA and its ammonium and sodium salts. While for PAA and NH$_4$PA the same results were obtained, NaPA differs significantly showing a large increase of the CPE already at low humidities. Bias voltages applied to a PAA sample exposed to dry ammonia do not change the impedance spectra of the sensor indicating that ammonia is not involved in any charge transfer reactions (Figure 4.18). In humid air the presence of ammonia induces a decrease of the impedance, probably due to an increase of the water content in the polymer and with it at the polymer electrode interface (compare with Figure 4.7 in 4.2.3).
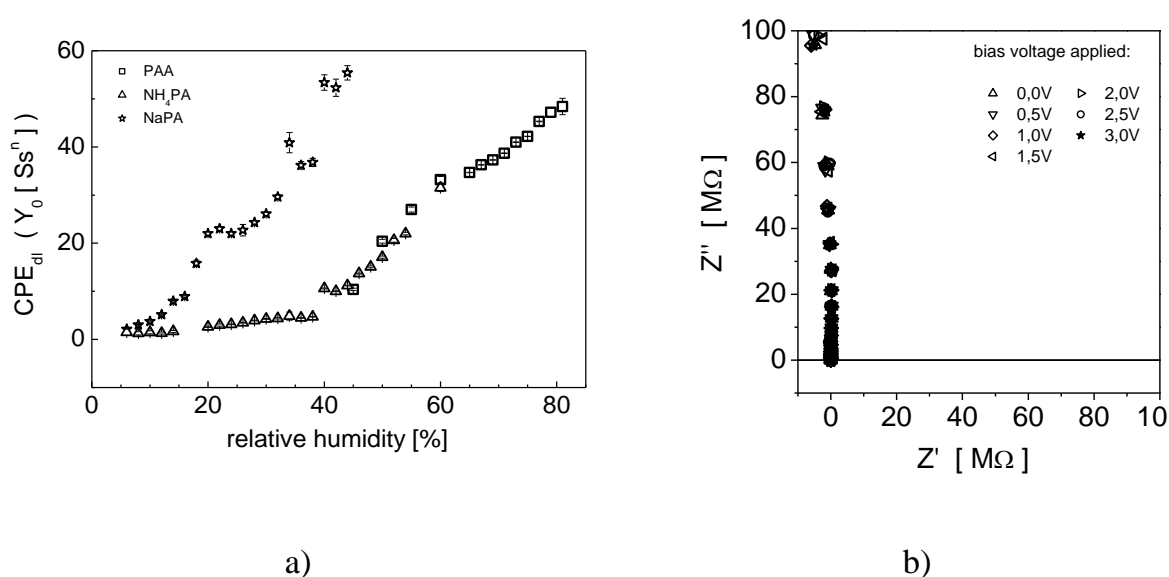

a)   b)

Figure 4.18: a) Dependence of the double layer capacitance on the relative humidity measured for PAA and its derivates. b) Negligible influence of a bias voltage on the impedance of a PAA sample in the presence of 10 ppm ammonia in dry air.

These observations suggest that the water content of the polymers determines the processes at the electrodes because the water content of PAA and NH$_4$PA is the same while the one of NaPA is much higher as demonstrated by gravimetric measurements (see Figure 4.8 in 4.2.3). To study the processes at the electrodes in more detail the impedance spectra must be supplemented by other electrochemical techniques because

several elements possibly overlapping each other in the sharp increase of the arc cannot be separated. Therefore voltage step and cyclic voltammetry measurements were, additionally, performed (see 4.3.2).

4.3.1.3 Electrochemical properties represented by the $R_m \| C_m$ circuit

In a certain humidity range an additional semicircle appears between the one at high frequencies caused by the bulk processes and the one at low frequencies due to electrode processes: this intermediate semicircle can be observed in a small humidity range only; it does not appear at humidities below 60% (PAA and NH_4PA) and 30% (NaPa) respectively, and at higher humidities it is partially or completely overlapped by the large semicircle at lowest frequencies (see Figure 4.9). An example of this semicircle is given in Figure 4.19 (semicircle marked with an arrow) for NH_4PA.

The impedance measurements were performed with several applied bias voltages and the results are shown in Figure 4.19. The shape of the middle semicircle does not change with the applied voltage and this indicates that the middle semicircle is not caused by a process involving charge transfer at the electrodes (see 2.2.2.2).
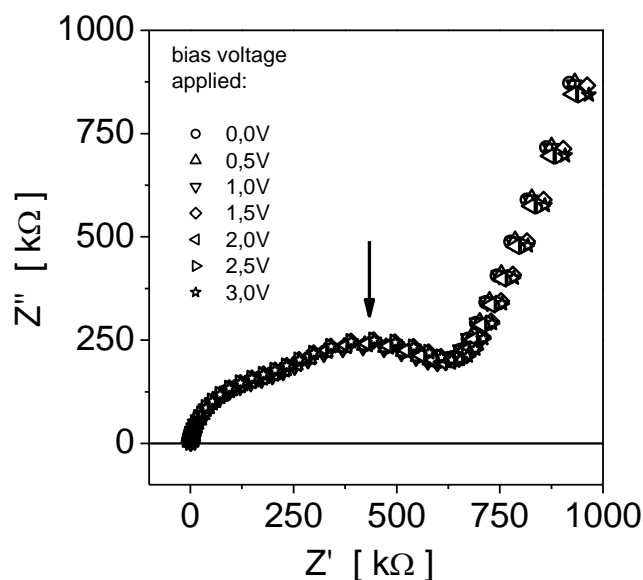

Figure 4.19: The middle semicircle appearing in the Nyquist plot is independent on an applied bias voltage. These measurements were performed with a NH_4PA sample in 60% relative humidity; experiments with PAA and NaPA show the same Nyquist plot at other humidities.

The equivalent circuit resistance which is fitted from the impedance data decreases with increasing humidity forming a straight line in the semi logarithmic representation. The resistance curves of the different materials are parallel and the one of PAA and NH$_4$PA are very similar while the one of NaPA is shifted to lower humidities. The capacitance C$_m$ increases with increasing humidity showing the same material dependence as the one observed for R$_m$: The results for PAA and NH$_4$PA are quite similar and observed at higher humidities. The capacitance obtained for the sodium derivate is shifted to lower humidities (Figure 4.20).
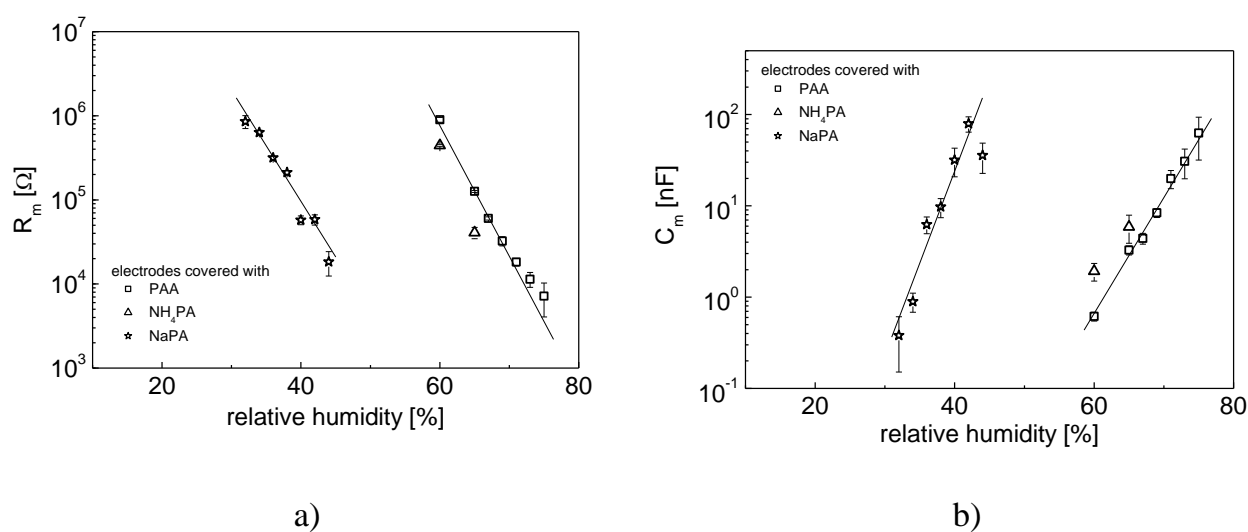

a)   b)

Figure 4.20: a) Equivalent resistance and b) capacitance describing the dependence of the impedance parameters of the middle semicircle on the relative humidity. The response for PAA and NH$_4$PA is almost the same but the one for NaPA significantly differs.

4.3.2 Voltage step and cyclic voltammetry measurements

Voltage step and cyclic voltammetry measurements were additionally performed to study the processes at the electrode polymer interface. As discussed in 2.2.3 the electroactive species can be determined due to the dependence of the diffusion current on the composition of the ambient atmosphere. In Figure 4.21 a) the current decay is plotted against the square root of time showing the current several seconds after the potential step was applied to the sample. After 30 s the current reaches a quasi-steady state condition and remains almost unchanged; this is the diffusion current which is plotted against the relative humidity in Figure 4.21 b). Without ammonia the diffusion current increases linearly with the humidity until a kink appears at about 73% r.h. and

the slope becomes stiffer still showing a straight line in the semi-logarithmic representation. The linear relation between the relative humidity and the logarithmic representation of the diffusion current suggests that the electroactive species is water; this is consistent with the impedance spectroscopy results (see Figure 4.18 in 4.3.1.2). The kink appears in a humidity region where the polymer switches over from the glassy to the rubbery state as estimated from the gravimetric measurements with the Flory-Fox equation (see 2.1.4.2 and Figure 4.4 in 4.2.1). The correlation between the kink of the diffusion current and the glassy to rubbery transition is confirmed by humidity measurements in a background of 20 ppm ammonia as shown with open circles in Figure 4.21 b). Under these last conditions the kink appears at lower humidities: a shift at about 30% r.h. is observed for the kink of the diffusion current as well as for the estimation with the Flory-Fox equation (see Figure 4.6 b) in 4.2.3).

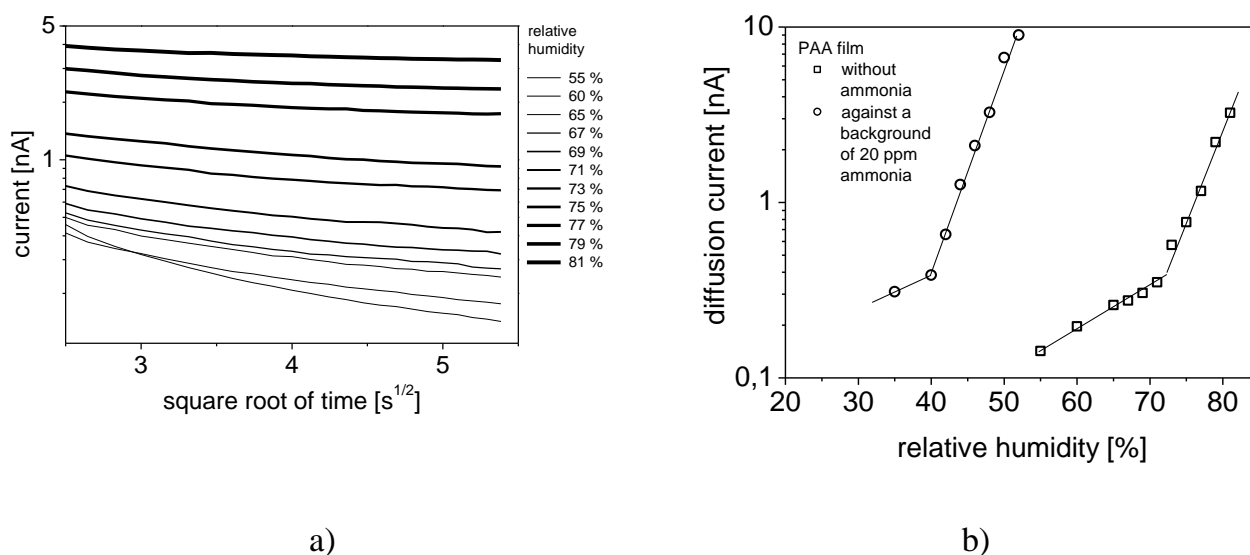a)   b)

Figure 4.21: a) Current decay induced voltage step plotted against the square root of time. The measurement was performed with a PAA coated sample at relative humidities between 55 and 81% r.h. without ammonia. b) If the diffusion current obtained from the voltage step experiment is plotted against the relative humidity two straight lines with a kink in between are observed (squares). In the presence of 20 ppm ammonia the same shape appears but shifted to lower humiditites (circles).

The electroactive species, water, diffuses to the electrodes and forms the double layer at the electrode surface. Charge transfer reactions do not occur at low humidity levels and therefore no peaks appear in the range of -1 to 1 V as shown in Figure 4.22 a). With increasing humidity (for example bold line in Figure 4.22 a) the cyclic

voltammogram tilts indicating the onset of a charge transfer reaction which will occur at higher applied voltages.

In the absence of water the response under ammonia exposure is very small and independent of the ammonia concentration as shown in Figure 4.22 b). Likewise, in the presence of humidity no charge transfer reactions induced by ammonia are observed in the studied electrical potential range (dashed line in Figure 4.22 a). The obtained cyclic voltammogram is very similar to the one without ammonia at higher humidities because ammonia increases the amount of water in the polymer (see Figure 4.30 in 4.5.1)
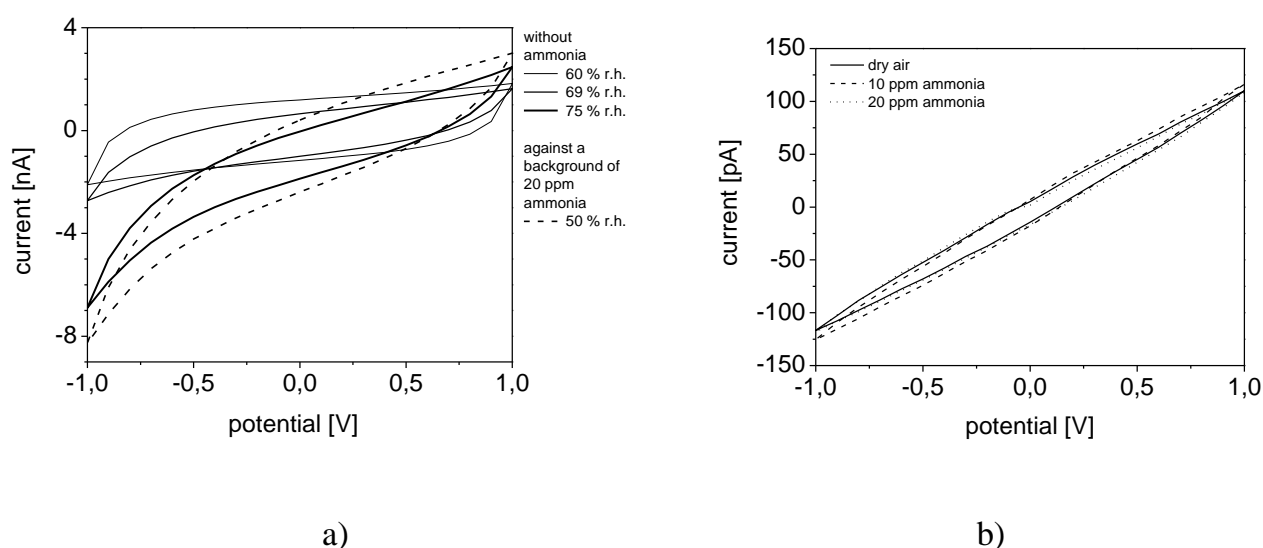

a)   b)

Figure 4.22: a) Cyclic voltammetry diagram dependence on the humidity and ammonia content of the ambient. In the presence of ammonia (dashed line) the diagram is similar to the one in humid air at higher levels of humidity. b) In dry air, ammonia has almost no influence on the cyclic voltammetry diagram (dashed and dotted lines in comparison with the solid line). The measurements were performed with a PAA coated sample.

To study the formation of the double layer at the electrode surface the cyclic voltammetry measurements were performed at given ambient conditions with different scan rates (Figure 4.23 a) as discussed in 2.2.3. If the scan rates match the frequency range in which the electrode processes are observed in the impedance spectroscopy (see 4.3.1.2) the results can be compared with each other. While the impedance measurements show a straight line or an arc only, the CV measurements reveal that the electrode processes are more complex. The straight lines with two different slopes appearing if the current at any chosen point is plotted against the scan rate indicates

that the double layer has to be described with two different capacitances (Figure 4.23 b). Further studies are necessary to complete the understanding of the processes at the electrodes.

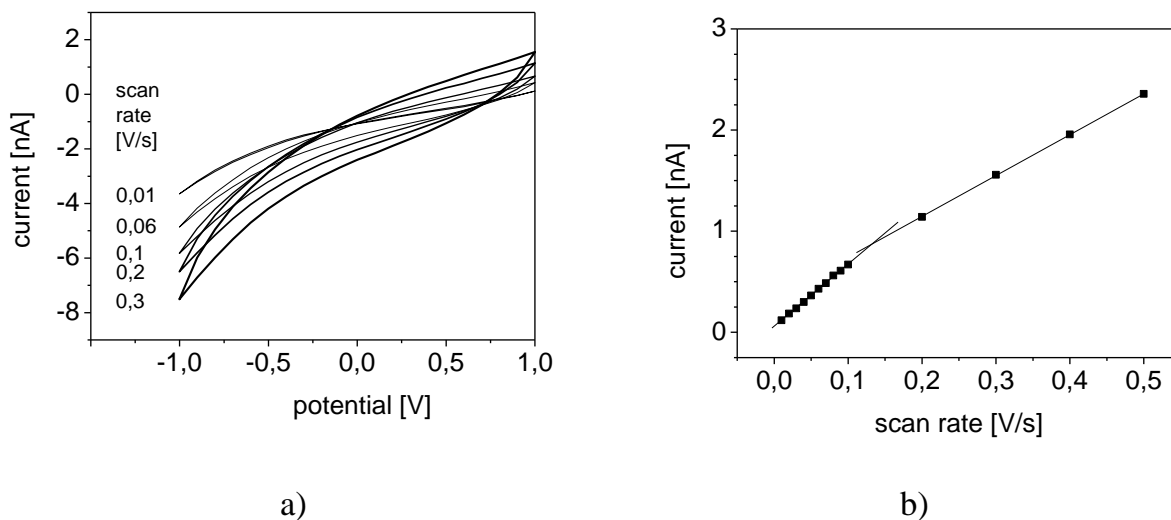a)   b)

Figure 4.23: CV measurements of a PAA sample in 85% r.h. performed with several scan rates between 0.5 and 0.01 V/s. a) Some examples for the obtained cyclic voltammetry diagrams. b) Current dependence on the scan rate taken from the CV measurement at 1 V.

4.4 Kelvin Probe measurements

Kelvin Probe measurements were performed in Besocke and McAllister setups, both described in 3.2.3. The pure gold substrate as well as the gold substrate spray deposited with PAA, NH_4PA or NaPA layers where studied upon exposure to several ammonia concentrations in dry air or in a background of 50% r.h. An example of the Kelvin Probe raw data is given in Figure 4.24 for PAA covered gold substrates exposed to ammonia in dry air. The Kelvin Probe signals observed in the two different setups slightly vary in shape but the data interpretation (see Figure 4.27) shows that both setups yield the same contact potential difference (CPD) changes. The variation in shape is probably determined by the properties of the experimental setups as, for example, the measurement routine, the distance between the sample and the reference electrode and the geometry of the measurement chamber.
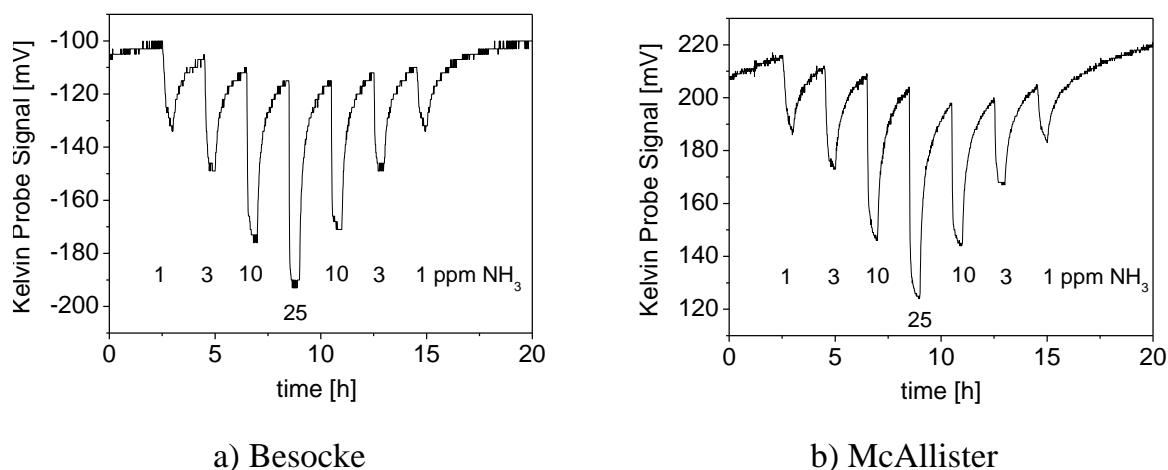
a) Besocke   b) McAllister

Figure 4.24: Kelvin Probe raw response to ammonia exposure between 1 and 25 ppm NH_3 in dry air obtained with a Besocke (a) and a McAllister (b) set-up.

4.4.1 Work function changes of the uncovered gold substrate

As discussed in 2.3.2.1 and 2.3.2.2 both gaseous ammonia and water vapour sorption changes the work function of gold in the same direction. In this work the sorption of the two species was combined, i.e. in a background of several humidity levels the effect of ammonia sorption on the Kelvin Probe signal was studied. It is observed that the response under ammonia exposure is more complex in the presence of humidity as shown in Figure 4.25. In dry air, negative changes of the Kelvin Probe signals are observed, which decrease with increasing humidity. At about 50% r.h. the changes are very small and if the humidity is further increased the sign of the CPD change upon ammonia exposure is switched. In a background of 90% r.h., remarkable large positive changes are measured. The interpretation of the data is included in Figure 4.27.

After the gold substrate has been once exposed to higher humidities, the initial properties cannot be obtained due to a drying process under a stream of dry air at room temperature: When the sample was kept in 90% r.h. and subsequently dried for at least one week, ammonia sorption measurements show positive CPD changes also in dry air. This is in agreement with the studies of other authors showing that water vapour are chemisorbed at the gold surface with bounds strong enough to resist desorption at

room temperature [148, 149, 152]. If the sample is washed with acetone and afterward dried the initial ammonia sorption properties recover and in dry air negative CPD changes are observed again.
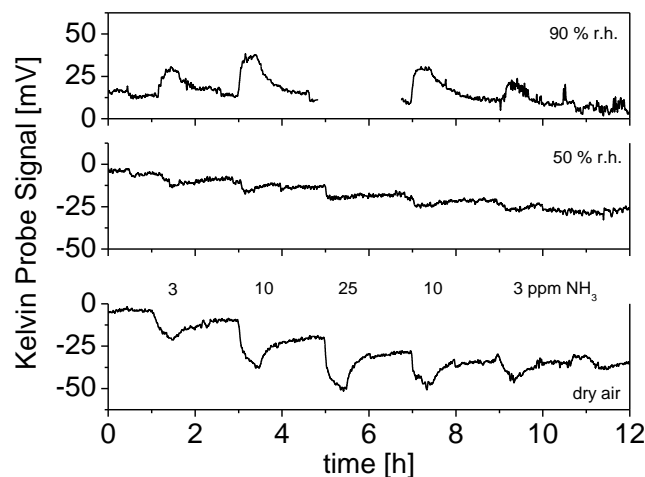

Figure 4.25: Response of an uncoated gold substrate to ammonia pulses in dry air, 50% and 90% relative humidity. The measurements were performed with the McAllister set-up and due to experimental limitations the 25 ppm NH_3 pulse is not measured in 90% r.h.

4.4.2 Work function changes of the polymer coated gold substrates

The Kelvin Probe signal of the PAA and NH_4PA sample decreases when it is exposed to ammonia in dry air while the gold substrate covered with NaPA respond with a positive CPD change (Figure 4.26). The response time corresponding to 70% of the equilibrium value is in all materials well below 5 min and the great difference to the response time in QMB measurements is striking attention. While the QMB response of PAA and NH_4PA samples reflects the very slow ammonia sorption into the bulk of the polymer, the different time dependent trends of the Kelvin Probe signal indicate that the contact potential difference measured upon ammonia exposure is not caused by an effect associated with the bulk sorption process. This observation is also valid for NaPA sample even if the shape of the QMB and Kelvin Probe signals is quite different in this case.

The CPD changes of the uncovered gold substrate and of the PAA and NH_4PA samples show the same sign upon ammonia and water sorption. This behaviour is not observed for NaPA where a positive CPD change due to ammonia sorption but a negative CPD change due to interaction with water molecules is found.
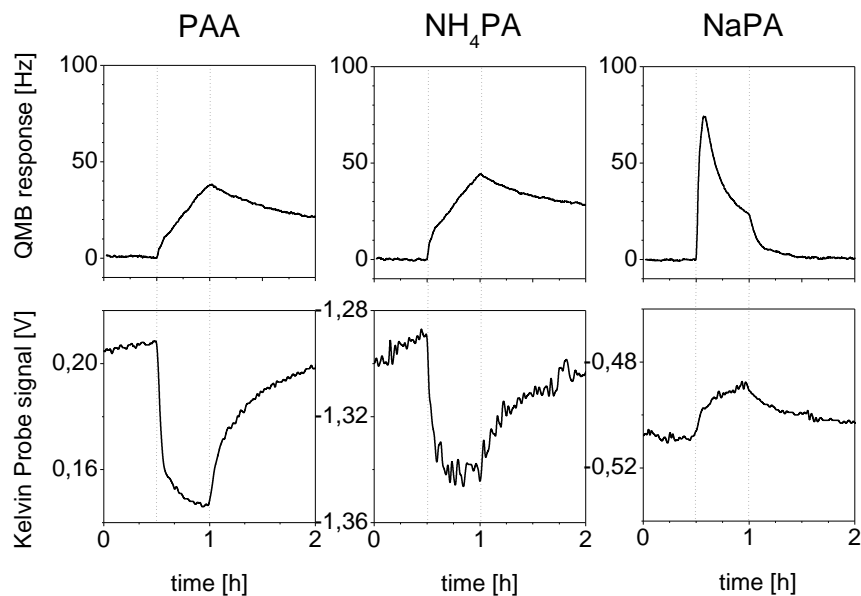
Figure 4.26: Comparison of the time constant observed in gravimetric (QMB) and Kelvin Probe measurements upon a 10 ppm ammonia pulse in dry air measured with the McAllister set-up for all materials studied.

a) dry air   b) humid air (50 % r.h.)
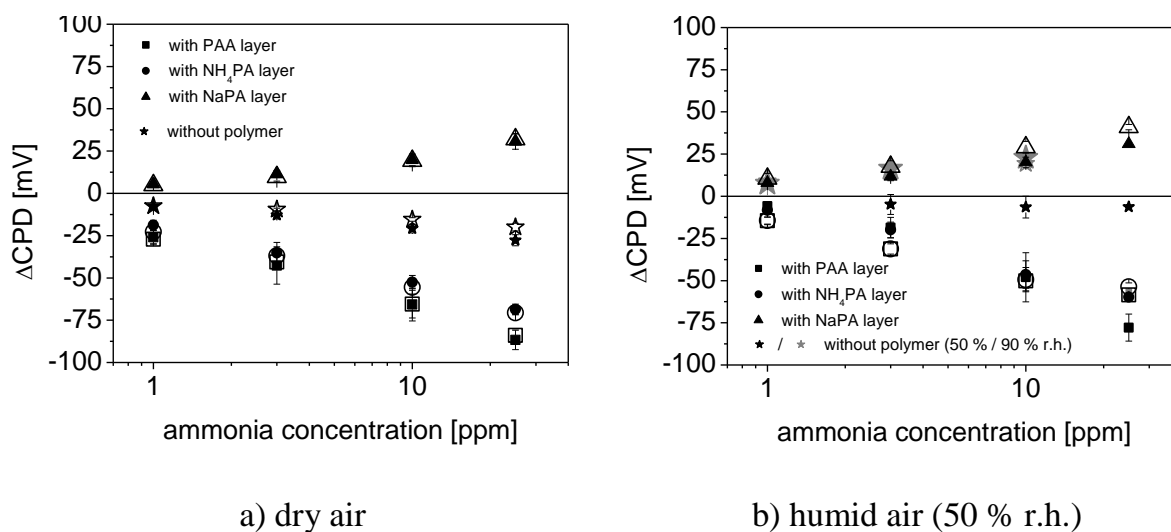
Figure 4.27: CPD changes induced by interaction of ammonia with the PAA, NH_4PA and NaPA covered gold substrates in dry air (a) and 50% r.h. (b). The data obtained for the uncovered sample in 90% r.h. are also included in b). Values obtained with the Besocke set-up are marked with open symbols while the filled symbols represent McAllister measurements.

The interpretation of the Kelvin Probe data in dry and humid air is shown in Figure 4.27. The filled and the open symbols representing the CPD changes obtained with the

McAllister and the Besocke setup, respectively, match very well providing evidence that the different measurement setups are not inducing differences.

In dry air the CPD changes induced by ammonia interaction with the PAA and NH_4PA coated gold substrates are negative and almost identical (squares and circles in Figure 4.27). They are significantly larger than the response of the uncovered gold (stars in Figure 4.27) that, as already discussed, also has a negative sign in dry ambient (see 2.3.2.1). In a background of 50% r.h. the ammonia induced CPD change of the gold substrate both uncovered and covered with PAA and NH_4PA decreases. If the ambient contains a relative humidity of 90% r.h., ammonia induces a positive CPD change for the gold (grey filled stars in Figure 4.27 b). Also, in the positive ΔCPD range the response of the NaPA sample to ammonia exposure is observed in dry air as well as in humid air.

4.5 Spectroscopic studies

The transmittance spectra of the studied polymers is already described in literature and presented in 2.4.1. In this chapter changes upon water vapour and ammonia gas sorption are discussed. For this purpose a reference spectrum taken with the polymers in dry air is used; the resulting absorbance spectra show the bands that change their intensity and position under analyte gas or humidity exposure. A decrease in concentration of a species results in a negative band and an increase in a positive band. In the following chapters, the absorbance spectra of three different wave number regions are discussed in detail. Afterwards, irreversible changes of PAA induced by the interaction with gaseous ammonia in humid air are presented.

4.5.1 Hydrogen bonded water and CH_2 stretching vibrations (3750 to 2500 cm^{-1})

Water sorption into the polymer layer causes several changes in the infrared spectrum of polyacrylic acid. In the 3750 to 2500 cm^{-1} wave number region a band appearing at about 3500 cm^{-1} is most noticeable (solid lines in Figure 4.28 a). Studies performed with similar materials [172] suggest that this band is caused by symmetric stretching vibration of hydrogen bonded water molecules and therefore can be used to study the

water sorption into the polymer. According to Lambert-Beer's law, the absorbance is proportional to the concentration of the IR absorbing species in the material and hence the signal height in the absorbance spectra is a measure for the concentration of water in the PAA layer. The signal height increases with increasing humidity and the dependence on the humidity can be described with a BET isotherm (Figure 4.28 b). This is in agreement with the QMB measurements described in 4.2.1 suggesting that the mass increase of PAA layers upon water sorption is mainly caused by hydrogen bonded water species. The asymmetric stretching vibration of hydrogen bonded water molecules appears at higher wave numbers; it is usually much weaker and often cannot be observed in the spectra.

a)   b)
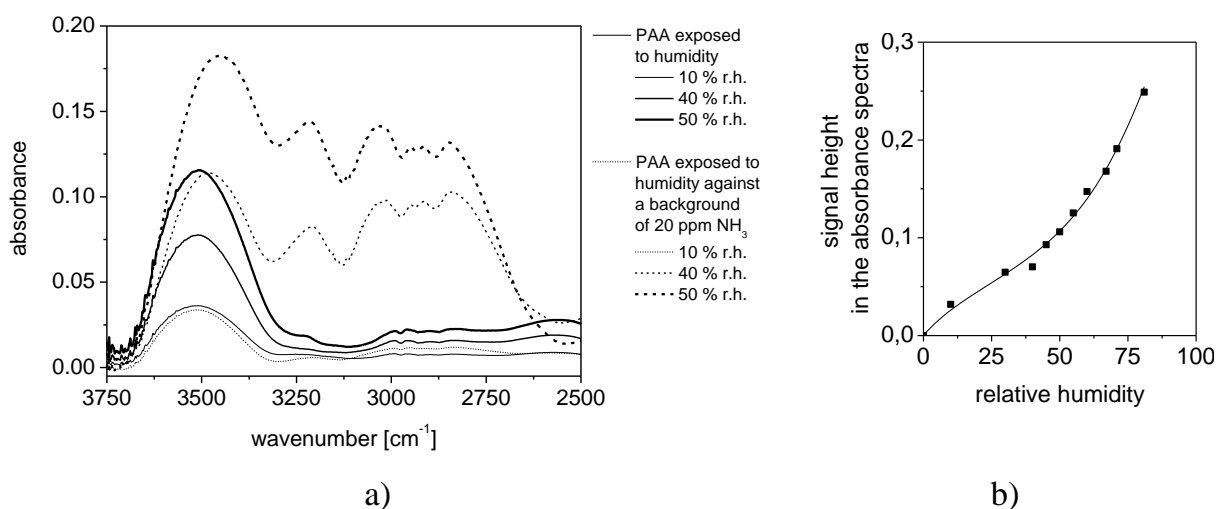
Figure 4.28: a) Comparison of PAA infrared absorbance spectra at several humidities without ammonia (solid lines) and in a background of 20 ppm NH_3 (dashed lines) in the 3750 to 2500 cm^{-1} wave number range. b) Dependence of the 3500 cm^{-1} band signal height in the infrared spectra on the relative humidity without ammonia. The data can be described with a BET isotherm (solid line in figure b).

From 40% r.h. on a shoulder appears to lower wave numbers (at about 3200 cm^{-1}, marked with an arrow in Figure 4.30 a), which increases with increasing humidity. According to calculations performed for similar polymers [172] in this region a band due to water clusters bound to the polymer via hydrogen bonds is expected. If the infrared spectra are compared with the impedance measurements it is striking that the humidity at which this band appears for the first time corresponds to the humidity at which the kink is observed for the resistance of the polymer bulk (see 4.3.1.1). This

observation is also valid if the measurements are repeated in a background of 20 ppm ammonia: The kink shifts to 20% r.h. and also the band in the infrared spectra is visible already at this humidity (at about 3200 cm^{-1}, marked with an arrow in Figure 4.30 b). Therefore, the water species causing this shoulder are probably responsible for the bulk conduction above the kink humidity. This conclusion is confirmed by measurements of the sodium derivate of PAA with both techniques (Figure 4.29). The interpretation of the impedance data show that the bulk resistance of this material has no kink and over the whole humidity range the slope is similar to the slopes of the other materials above their kink humidity. Accordingly, in the impedance spectra the band at about 3200 cm^{-1} appears at all humidities. The same correlation between the peak at about 3200 cm^{-1} and the onset of the vehicle type conduction mechanism is observed for NH_4PA. In this material the switch between the conduction mechanisms occur at higher humidities than in the other polymers and in the humidity range below this switch the peak at about 3200 cm^{-1} is not manifesting itself in the impedance spectra.
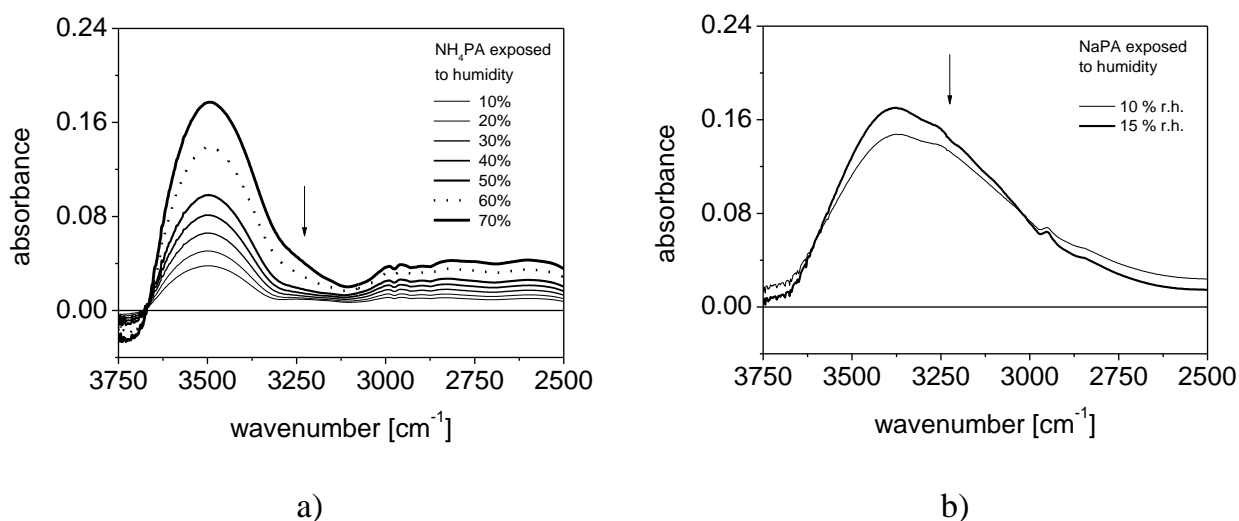
Figure 4.29: Appearance of a shoulder or band at about 3200 cm^{-1} (marked with an arrow). a) For NH_4PA, this shoulder can be observed at humidities 60% r.h. and above. b) In NaPA this peak is very strong and already present at very low humidity levels.

In a background of ammonia changes of the spectra are observed if the humidity exceeds a certain level as shown in Figure 4.28 a). Up to 10% r.h. the absorbance does almost not change compared to the measurement of the same humidity without ammonia in the atmosphere. At higher humidities, the bands of the water species at

about 3500 and 3200 cm^{-1} increase due to the presence of ammonia. For the band corresponding to water clusters, the increase already occurs at lower humidities and the increase of this band is also more distinct than for the one due to single water molecules hydrogen bonded to the polymer. Additionally, between 3100 and 2750 cm^{-1} further bands appear: They are caused by N-H stretching vibrations of the ammonium radical formed by the reaction of PAA with the gaseous ammonia [162] and changes of the polymer conformation during gas sorption resulting in an increase of the absorption due to symmetric and asymmetric CH$_2$ stretching vibrations of the polymer backbone.

a)   b)
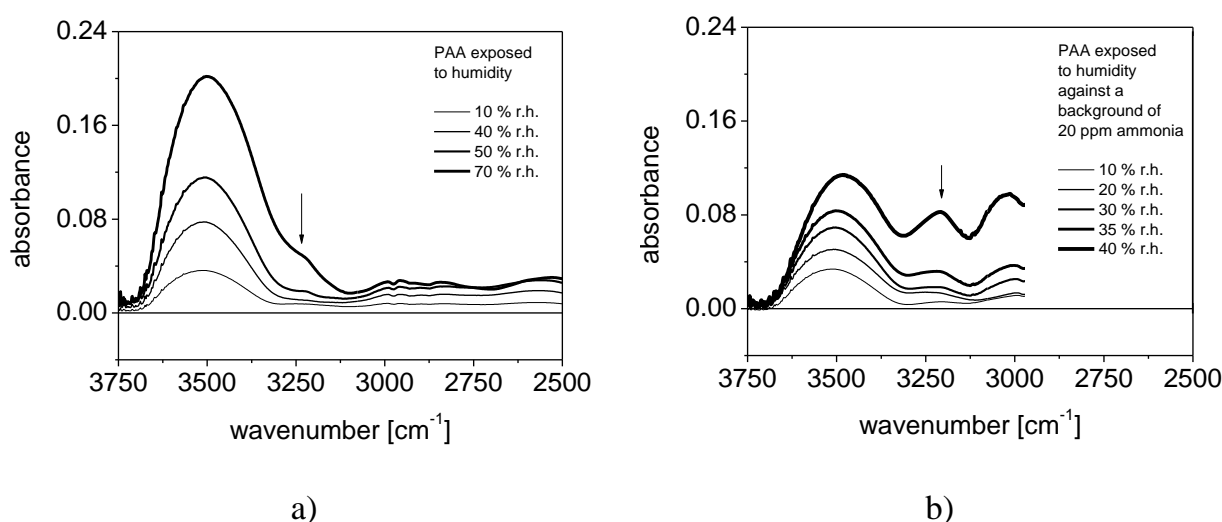
Figure 4.30: Appearance of a shoulder or band at about 3200 cm^{-1} (marked with an arrow) related to condensed water or water clusters. For PAA, this shoulder can be observed at 50% r.h. and above (a) or much earlier in the presence of ammonia (b). In a background of 20 ppm NH$_3$ the shoulder is already visible at 20% r.h. and becomes a distinctive band at higher humidities.

4.5.2 Range of C=O stretching vibrations (1800 to 1600 cm^{-1})

Valuable information about changes in the polymer upon water and ammonia sorption can be gained if variations in the range of the C=O stretching vibrations are studied. As discussed in 2.4.1.1 the band at about 1700 cm^{-1} is composed of four bands, which have different dependences on the presence of water vapour and ammonia gas in the ambient as shown in Figure 4.31.

Even at very small humidities the water molecules form hydrogen bonds to unassociated carboxyl groups; the decrease of carboxyl groups causes a negative band

at 1737 cm^{-1}. Some of these originally unassociated groups, form carboxylate anions with protons as counter ions, as discussed in the following chapter; others form species connected via hydrogen bonds. The interaction of water molecules with single hydroxyl radicals causes a positive band at 1730 to 1720 cm^{-1}. Another possibility is the incorporation of water into cyclic dimers or into three-dimensional structures, open dimers or oligomers as sketched in Figure 2.15 in 2.4.1.1. The formation of these species leads to an increase of the absorbance in the range of 1700 to 1690 cm^{-1}. At 1708 cm^{-1} the main band is slightly negative due to interaction with water. Even if some of the carboxyl groups, originally forming cyclic dimers, react with water towards the species already discussed above the majority of the interchain hydrogen bonds and with them the structure of the polymer remains unchanged. The band at about 1625 cm^{-1} is due to the HOH water bending vibration in the polymer.
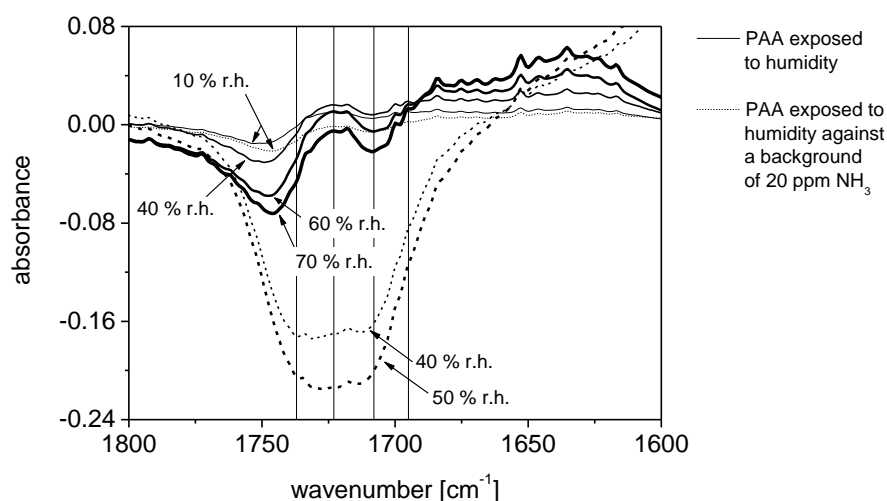
Figure 4.31: Different changes of the bands in the C=O stretching region upon humidity exposure without (solid line) and in a background of 20 ppm ammonia (dashed line). The vertical lines give the wave numbers of the bands discussed in 2.4.1.1.

The presence of ammonia does hardly affect the infrared spectra as long as the humidity is very low but with increasing humidity this is no more the case: Negative bands are observed at 1730 to 1720 cm^{-1} and 1708 cm^{-1} indicating that cyclic dimers and chain structures are destroyed, due to the presence of ammonia, and the carboxylate ion is formed (see 4.5.3). The destruction of the interchain hydrogen bonds increases the flexibility of the polymer chains and, with it, lowers the static glass transition temperature. This is in agreement with the ammonia dependence of the

static T_g deduced from the QMB measurements (Figure 4.6 b) in 4.2.1). Additionally, the amount of unassociated carboxyl groups decreases due to the interaction with ammonia and water molecules and a negative band appears at 1737 cm^{-1}. Due to the presence of ammonia the carboxyl groups form carboxylate anions and water incorporation into cyclic or chain structures possibly does not occur, as suggested by the missing positive band in the 1700 to 1690 cm^{-1} region. The band associated with water bending vibrations is overlapped by the strong positive signal of the carboxylate anion and, therefore, cannot be identified in the spectra.

4.5.3 Stretching modes of the carboxylate anion (1600 to 1000 cm^{-1})

Figure 4.32 a) shows the absorbance spectra below 1600 cm^{-1}. At high humidities a weak positive band at 1557 cm^{-1} indicates the formation of carboxylate anions in the polymer. In accordance with the interpretation of the C=O group this peak strongly increases in the presence of ammonia if the relative humidity is high enough. Associated with asymmetric C-O stretching modes of the acid anion, this band is strong and constant in wave number while the one caused by symmetric C-O stretching modes has many other skeletal vibrations occurring in the same range. For the identification of the latter one, the intensity of the bands was compared (Figure 4.32 b): With a intensity ratio of 7.8 : 1 the bands marked with (A) and (B) are very close to the value given in literature (see 2.4.1.2) showing that (B) is associated with the symmetric C-O stretching modes. The band (C) in Figure 4.32 a) appears only in the presence of ammonia and is allocated to N-H deformation modes of the NH_4 radical. Scissors and bending vibration changes of CH_2 and CHCO groups due to the increased flexibility of the polymer backbone upon the destruction of the hydrogen bonds causes the positive bands between 1500 and 1425 cm^{-1}. Additionally, the destruction of hydrogen bonds shows itself in the negative band between 1300 and 1130 cm^{-1}, the wave number range at which combinations of the C-O stretching and O-H bending vibrations are observed.
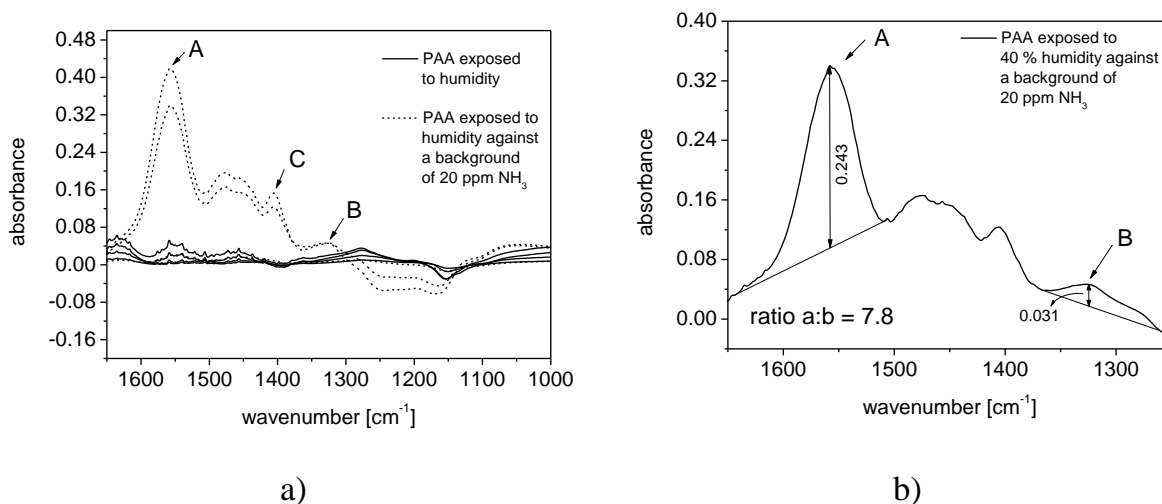
a)   b)

Figure 4.32: a) Absorbance spectra of PAA in the 1650 to 1000 cm^{-1} wave number range measured at several humidities without ammonia and in the presence of 20 ppm NH_3. The indicated bands are associated with the asymmetric CO_2 stretching vibration (A) and the symmetric one (B) and the N-H deformation of the NH_4 radical (C). b) The height ratio of band (A) and (B) for the example of 40% r.h. in the presence of 20 ppm ammonia result in 7.8 suggesting that (B) really is caused by the symmetric CO2 stretching vibration as discussed in chapter 2.4.1.2.

4.5.4 Irreversible changes of PAA due to interaction with gaseous ammonia

After removal of ammonia from the ambient, the sample was dried and subsequently exposed to the same humidity without ammonia (Figure 4.33). From the infrared spectra it is obvious that ammonia molecules in humid air irreversibly change the polymer:

In the region marked with (A) in Figure 4.33, bands caused by N-H stretching vibrations remain in the spectra when ammonia is removed from the ambient (point-dashed line in the figure). This observation is confirmed by the band marked with (B) in the figure, which is allocated to N-H deformation modes of the NH_4 radical. Beside the detection of ammonium ions in the polymer matrix, the infrared spectra show several permanent changes of the polymer matrix due to the incorporation of NH_4 ions during ammonia exposure, as for example reflected in the bands caused by symmetric and asymmetric CH_2 stretching vibrations observed in the wave number region marked with (A). Additionally the environment of the carboxylic groups changes irreversibly:

97

The C=O stretching vibrations (marked with (C) in the figure), observed after ammonia exposure, are weaker than in a newly prepared PAA layer, which has never been exposed to ammonia before. This indicates the permanent destruction of some interchain hydrogen bonds in the polymer as discussed in chapter 4.5.2., which is also reflected by an absorbance increase of the asymmetric and symmetric C-O stretching vibrations bands of the formed carboxylates which are marked with (D) in Figure 4.33. These results are in accordance with impedance measurements presented in Figure 4.12 and discussed in chapter 4.3.1.1.

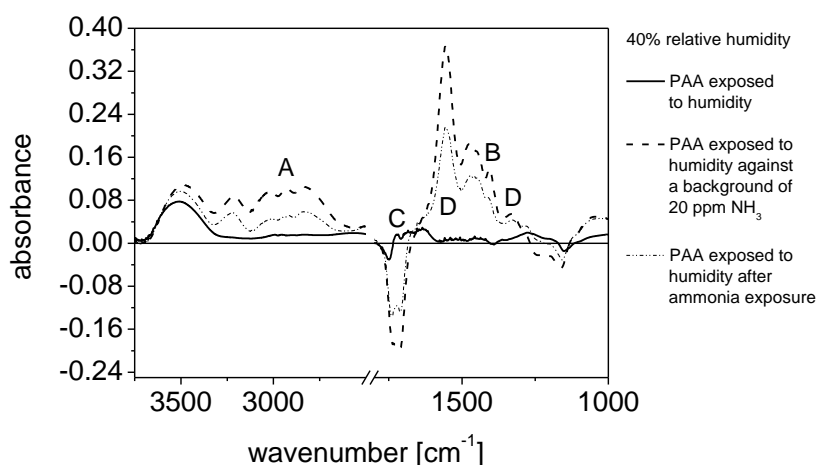Figure 4.33: Infrared spectra taken at 40% r.h. before the sample was ever exposed to ammonia (solid line), in a background of 20 ppm ammonia (dashed line) and in a rerun without ammonia after ammonia exposure (point-dashed line). The wave number regions marked with letters are discussed in the text; the region between 2500 and 1800 cm^{-1} is omitted because no relevant information can be gained there.

5 Discussion and modelling

Based on the measurement results presented in the previous chapter, a phenomenological model is developed that describes the interaction of PAA and its derivates with water vapour and ammonia gas. Beside the sorption process itself, the model explains the influence of the gaseous species on the physical properties of the polymers: Changes of glass transition temperature, resistance and capacitance are discussed and the origin of Kelvin-Probe signals due to ammonia exposure is clarified.

The infrared spectra of the studied polymers (Figure 2.12 in 2.4.1) show that the chains of PAA and NH_4PA are connected via hydrogen bonds and that such hydrogen bonds do not appear in the sodium derivate. The presence or absence of hydrogen bonds causes different structures of the materials, sketched in Figure 5.1. PAA and NH_4PA form three-dimensional networks while the polymer chains of NaPA are connected to each other either by strong ionic interactions or much weaker Van-der-Waals forces. The high glass transition temperature of NaPA (see chapter 3.1) suggests that ionic forces determine the properties of the sodium salt.

This influences the structure of the polymer layers produced in a spray deposition process (Figure 4.1 in 4.1). If the material is able to form strong hydrogen bonds, it prefers to grow on the already deposited polymer instead of the gold surface of the substrate. This gives rise to the island-like structure and the high porosity and thickness of the PAA and NH_4PA layers. The difference in the thicknesses of the two films made of the same amount of polymer is due to the much larger size of the ammonium ion compared to the proton and by that the increased distance between the chains. The developed polymer structure also explains why the carboxylate group in the ammonium salt of PAA causes a weak band in the infrared spectra only: In contrast to the interpretation published by Lee et al. (see 2.4.1.2) the data obtained in this work suggest that this band is weak even if the most COO^- groups bond to ammonium ions. Due to the formation of hydrogen bonds between ammonium and C=O groups the delocalisation of the carboxylate negative charge is hindered and the characteristic mesomerism stabilisation of the structure does not occur. Therefore, the formed carboxylate anions appear in the infrared spectra at wave numbers at which

usually the carboxyl groups are observed. The weak carboxylate band is caused by few COO^- groups that are not hydrogen bonded to other groups.

Polymer chains connected via hydrogen bonds in PAA and NH_4PA
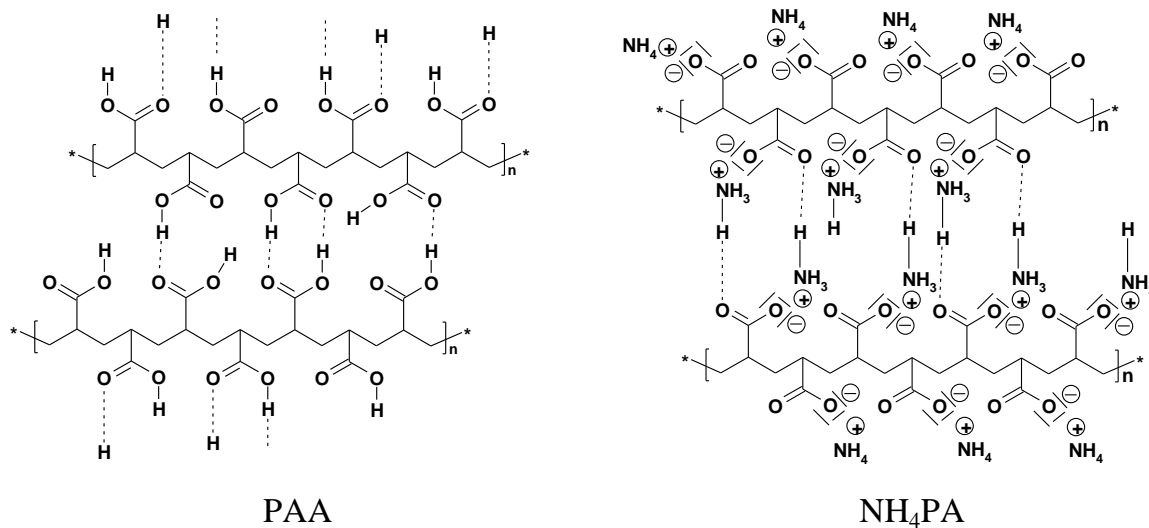
PAA NH_4PA

Unconnected polymer chains in NaPA
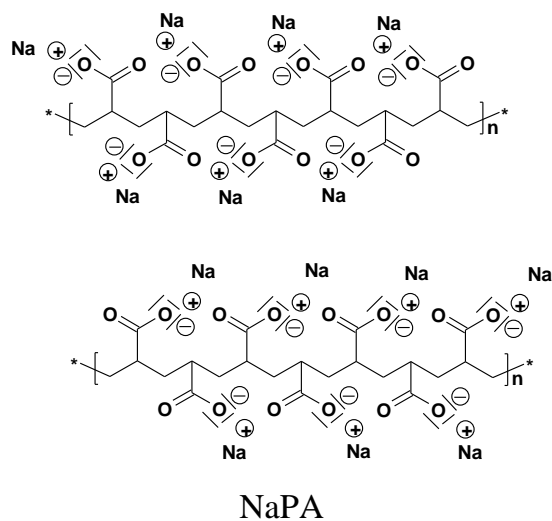
NaPA

Figure 5.1: Steric structure of the hydrogen bonded polymers PAA and NH_4PA and in contrast to these materials NaPA which is not able to form hydrogen bonds.

On NaPA almost the same attraction forces are exerted by the already deposited polymer and the gold substrate; therefore, no deposition location is preferred and the sodium salt grows in a thin and compact layer on the gold substrate, similar to an ionic crystal.

5.1 Processes in the polymer bulk

The ability to form hydrogen bonds does not only influence the structure of the polymers but also the sorption properties of the materials. While the pure acid and the ammonium salt sorb the same mass percentage of water vapour (Figure 4.8 a) in 4.2.3) and ammonia gas in dry air (Figure 4.5 c) in 4.2.2) respectively, NaPA sorbs much more water (Figure 4.8 b) in 4.2.3) and shows a complicated response to an ammonia pulse in dry air (Figure 4.5 c) in 4.2.2). For the water sorption process, the difference between the two types of material structures is confirmed by the estimation of the water volume percentage in the polymer from the bulk capacitance data (Figure 4.14 in 4.3.1).

5.1.1 Water sorption

In this chapter the water sorption processes into PAA and its ammonium and sodium salts are discussed. Beside the already mentioned dependence on the presence or absence of hydrogen bonds, the sorption process and the properties of the water in the polymers depend on the level of ambient humidity resulting in a BET isotherm. A model describing the water uptake and the electrochemical properties of the water containing polymers is developed in the following sections.

5.1.1.1 Mass changes due to water sorption

At low humidities, the hydrogen bonds forming a three-dimensional network of PAA and NH_4PA are strong enough to resist water-induced breaking. Hence, water can only be sorbed in the limited free volume between the interconnected polymer chains (marked A in Figure 5.2)[173]. Beside unspecific interaction processes due to weak Van-der-Waals forces, the water molecules form hydrogen bonds with free polymer sides (marked B in Figure 5.2) or become incorporated into cyclic dimers (marked C in Figure 5.2) or into three-dimensional structures, open dimers or oligomers (see Figure 4.31 and interpretation in 4.5.2). Additionally (see Figure 4.32 and interpretation in 4.5.3), some of the water molecules destroy interchain hydrogen bonds and react with acid sides of the polymer forming hydroxonium cations and carboxylate anions (marked D in Figure 5.2). With increasing water content more and

more interchain hydrogen bonds are destroyed and the polymer matrix becomes more flexible until the glass transition temperature is lowered to room temperature and the ability of the chains to move is hardly restricted by hydrogen bonds any more. Due to this process, the free volume in the polymer increases and allows more water being sorbed into the bulk of the polymer. This happens for both materials at about 78% r.h. (Figure 4.4 in 4.2.1) and explains the significant increase of water uptake at higher humidity levels (Figure 4.8 a) in 4.2.3).

In NaPA, a hygroscopic material without hydrogen bonds, water penetrates more easily into the polymer, the chains can move and the material swells even at low humidities (Figure 4.8 b) in 4.2.3), sorbing much more water than the other polymers, as sketched in Figure 5.2.

a)   b)
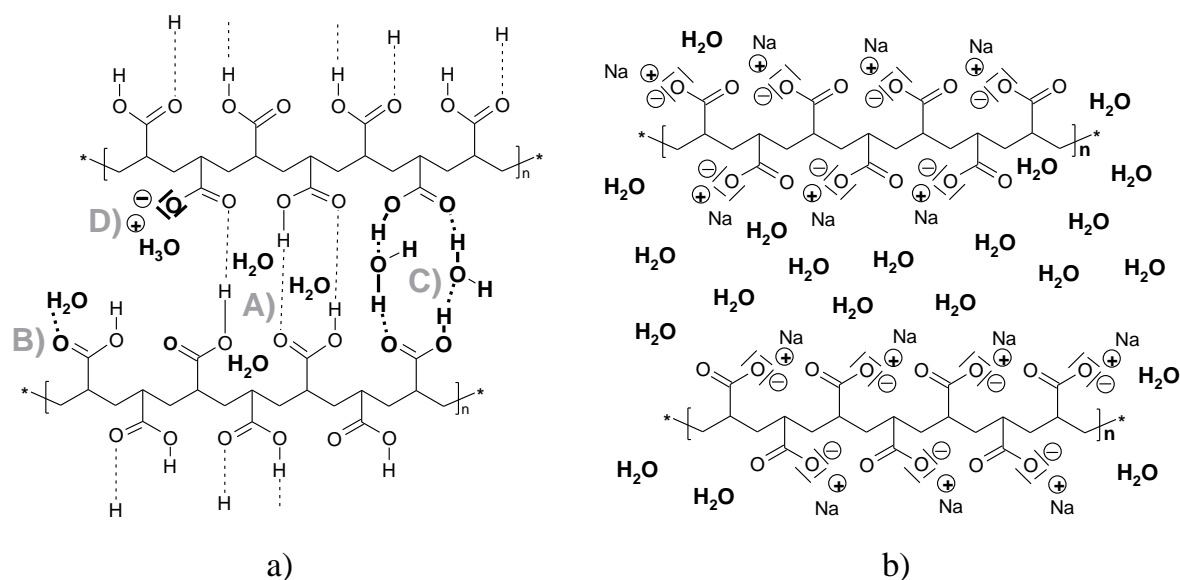
Figure 5.2: Interaction of the polymers with sorbed water molecules: a) PAA and NH₄PA: At low humidity levels the hydrogen bonds are strong enough to resist breakage by water and therefore water is sorbed into the limited free volume of the polymer (A) or hydrogen bonds to free C=O groups not engaged in the interchain hydrogen bonding (B). To a much smaller extent water will react with interchain hydrogen bonds and incorporate into cyclic dimers (C) or form hydroxonium and carboxylate ions (D). b) NaPA: Water sorption is not restricted by hydrogen bonds and therefore water penetrates more easily into the polymer.

5.1.1.2 Electrochemical property changes due to water sorption

As discussed in 2.2.2.1 sorbed water influences the electrochemical properties of the sorbing material. The capacitance change is mainly caused by the water uptake into the

polymer because added water molecules increase the permittivity of the coating material due to the high relative dielectric constant of water. While the capacitance increases with the water content, the resistance is reduced due to conduction processes involving either water molecules or liquid water. In the semi-logarithmic scale the resistance of PAA decreases linearly with increasing ambient humidity showing a kink at about 40% r.h. between two regions of different slope (open squares in Figure 4.12 in 4.3.1.1). The two regions indicate two distinct conduction processes which are governed by the Grotthuss type and the vehicle type mechanism, respectively (see Figure 2.6 in 2.2.2.1):

At low humidities most of the carboxylate groups of the polymer are engaged in interchain hydrogen bonds forming a stiff three-dimensional network. Water molecules which are sorbed into the network are able to, as well, accept and donate hydrogen bonds to free the acid groups of the polymer and, therefore, two sorption processes are possible. H_2O either hydrogen bond to a free carboxyl group (marked A in Figure 5.3 a), not involved in the interchain bonding, or accept a hydrogen bond from a free acid OH-group (marked B in Figure 5.3 a). In the infrared spectra a band allocated to hydrogen bonded water molecules appears at about 3500 cm^{-1} (solid lines in Figure 4.28 a). Additional water molecules diffusing into the polymer will form hydrogen bonds with the already sorbed molecules (marked C in Figure 5.3 a) until a chain of water molecules grows throughout the polymer allowing a Grotthuss type conduction process (Figure 5.3). While this type of polymer / water interaction is responsible for the conductivity at low levels of humidity and probably most important for the mass uptake due to water sorption into PAA (see 4.5.1), another type of water species governs the electrochemical properties at high humidities.

In 40% r.h. a shoulder appears in the infrared absorbance spectra (Figure 4.30 a) in 4.5.1) of PAA in humid air indicating the formation of a new species. According to the discussion in 4.5.1 this band is probably caused by the formation of water clusters and liquid water in the polymer layer, which acts as a plasticizing agent decreasing the polymer network stiffness. The combination between the presence of liquid water and a more flexible polymer matrix, favours the vehicle type conduction mechanism against the Grotthuss type: The charge is carried by an ion drift through the polymer

that can be described as a concentrated solution with very big poly-anions and smaller cations; the latter are able to move throughout the solution (Figure 5.3 b).

a)   b)
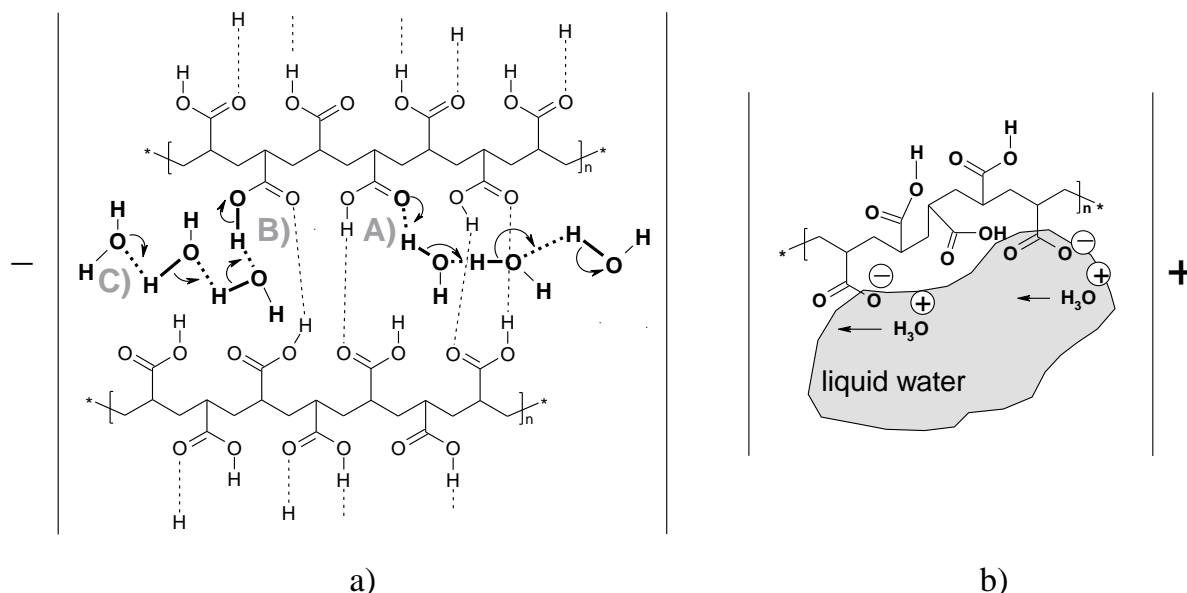
Figure 5.3: a) At low humidity levels water sorbed into the polymer can act as hydrogen bond donor (A) or acceptor (B). Additional water molecules sorbed into the polymer will hydrogen bond to the ones already present until a chain of water molecules grows throughout the polymer (C) allowing a Grotthuss like conduction process. b) At high humidities liquid water is present in the polymer allowing the conduction due to ion drift according to a vehicle type mechanism.

The humidity dependent resistance of NH_4PA shows a similar run in the semi logarithmic representation as the resistance of the acid but the resistance values are significantly lowered (Figure 4.13 in 4.3.1.1). Similarly to PAA, the shape of the plot suggests that the conduction mechanism is a Grotthuss type at low humidities and a vehicle type at high humidities, respectively, which is confirmed by the two different water species appearing in the infrared spectra (see Figure 4.30 in 4.5.1). As discussed above, the water uptake of both materials is identical, as proved by the QMB measurements (Figure 4.8 b) in 4.2.3) but an agreement between the PAA and NH_4PA capacitance data is not observed (Figure 4.13 b) in 4.3.1.1). This can be explained by two different effects: 1) different swelling processes may occur even though the same amount of water is sorbed into the polymer and 2) some water traces from the production process may be left in the polymer: Due to interactions between water

molecules and the ammonium ions in the polymer, water may be kept in the NH_4PA while, in contrast, PAA is not able to retain water molecules if it is exposed to dry air for several days. This suggestion cannot be proved with gravimetric measurements because the mass uptake relative to the mass in dry air is measured and so it is not possible to determine water that also remains in the polymer in dry air.

At low humidities, the lower resistance, when compared to the data obtained for PAA, may be caused by water traces from the production process, because already a small amount of water strongly influences the resistance. Additionally, ammonium ions can donate and possibly accept hydrogen bonds to and from water molecules. If this happens, ammonium ions can take part in the Grotthuss mechanism allowing the formation of an uninterrupted path throughout the polymer at lower water concentrations than required in PAA. Probably, both effects contribute to the reduced resistance of NH_4PA.

The materials differ also in the humidity at which the switch from one conduction process to the other one and, with it, the kink in the resistance plot is observed: In the ammonium salt this kink obviously appears at higher humidities than for the acid because, due to the large ammonium ions, the volume of the polymer is increased (Figure 4.1 b) in 4.1) and water molecules sorbed at the oxygen atoms of the polymer are far away from each other. Therefore, the water molecules poorly interact with each other and the formation of water clusters and, subsequently, liquid water is hindered. This explanation of the kink shift is confirmed by the infrared measurements showing that the band associated with water clusters does not appear until humidities as high as 60% r.h. (Figure 4.29 in 4.5.1).

In the presence of liquid water much more charge carriers are available, compared to PAA, because the polyacrylic acid is a weak acid and, therefore, only very few acid sides dissociate in water; on the opposite, the cations of the ammonium salt easily solve in water. The higher amount of charge carriers in NH_4PA and, on the other hand, the higher conductivity of solved protons from the carboxylic groups of the polymer as available in PAA, almost balances each other, so, that the resistance of the ammonium salt is just a little lower than the one of the acid.

The resistance of NaPA is small if compared to the other polymers at all humidity levels and over the whole measured humidity range a vehicle type mechanism occurs. This results from the impedance data (Figure 4.13 a) in 4.3.1.1) and infrared measurements (Figure 4.29 in 4.5.1): The resistance curve resulting from the impedance measurements shows no kink and a slope similar to the one of the other materials above their kink humidity; in the infrared spectra, the band allocated to water clusters appears already at humidities as low as 10% r.h. The sodium salt easily dissociates in poly-anions and sodium cations forming many charge carriers in the concentrated solution, which are responsible for the high conductance of this material in humid air. While the slope of the resistance plot is humidity independent, the capacitance dependence strongly increases above 30% r.h. In contrast to the other materials, where the kink in the resistance plot is in agreement with the onset of the strong capacitance increase, the slope of the NaPA resistance does not change. This is due to the fact that water clusters are already present in the polymer and that the increased water uptake is not associated with the onset of a new conduction process.

The dried polymers are not expected to conduct electricity because the glass transition temperature of the studied polymers is much higher than room temperature and, therefore, the polymer chains cannot move (see 2.2.2.1). Contrary to these expectations, the salts of PAA show some electrical conductance even if the sample was kept for several days under dry air (Figure 4.5 in 4.2.2). This conductance is caused by some water traces that cannot be removed from the polymer by just keeping the sample under a stream of dry air, as shown in the infrared spectrum of NaPA where a weak and broad band allocated to water species above 3250 cm^{-1} is present. In the spectrum of NH_4PA, water traces cannot be observed because the vibrations of polymer interchain hydrogen bonds overlap any water bands that would appear in the same wave number region; still, it is likely that also in this material water traces are responsible for the conductance in the "dried" polymer.

5.1.2 Ammonia sorption

If the polymers in dry ambient are exposed to ammonia the three-dimensional network of polymer chains and hydrogen bonds in PAA and NH_4PA hinder the gaseous species

to penetrate into the polymers giving rise to a very slow sorption process as shown in Figure 4.5 a) in 4.2.2). Ammonia molecules, which enter the polymer matrix, are possibly hydrogen bonded to free carboxylic or carboxylate sides via hydrogen bonds and a condensation of the gaseous species does not occur; this is indicated by the sorption behaviour that can be fitted with a Langmuir sorption isotherm (Figure 4.5 b) in 4.2.2) describing processes where the monolayer coverage is not exceeded. If the gaseous ammonia is removed from the ambient, the desorption process is even slower and partially irreversible (Figure 4.5 c) in 4.2.2).

In the material without interchain hydrogen bonds, the sorption behaviour is quite different. The ammonia gas rapidly enters the polymer resulting in a strong mass increase upon ammonia exposure (Figure 4.5 a) in 4.2.2). As discussed above even in the dried NaPA some water is present (marked A in Figure 5.4) occupying carboxylate sorption sites. Ammonia interacts with such water molecules forming ammonia-water complexes (marked B in Figure 5.4). The formed species diffuse out of the polymer (marked C in Figure 5.4) while ammonia enters, resulting in a mass lowering of the sample due to the water evacuation from the polymer; this is reflected in the mass decrease during the ammonia exposure, which starts about 20 min after the beginning of exposure time. After a sufficient amount of water molecules is removed from the sorption sites of the polymer, the ammonia prefers the interaction with the polymer (marked D in Figure 5.4) and an equilibrium is reached. Over several runs the water content of the polymer is lowered and a mass decrease is observed (Figure 4.5 c) in 4.2.2). Water evacuation does not occur in PAA and NH_4PA because, if water is present in these polymers, it is incorporated into the three-dimensional network and cannot easily be removed.

For all materials in dry air these changes are very small and with impedance measurements no systematic dependencies on the ammonia concentration are obtained. In dry air and at low humidity levels, the influence of ammonia on the infrared spectra is negligible (see for example the spectra for 10% r.h. in Figure 4.28 in 4.5.1) but this dramatically changes at higher humidities because the presence of ammonia induces an increased water uptake (see the spectra at 40 and 50% r.h. in the same figure). This phenomenon is discussed in the following chapter.
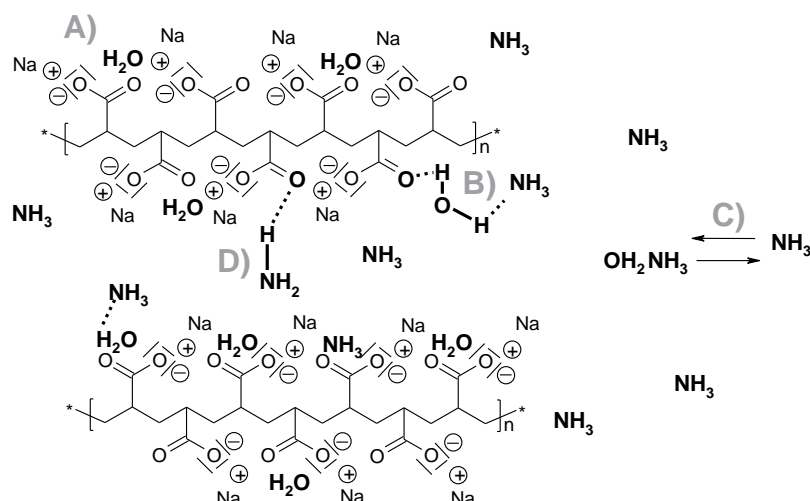
Figure 5.4: Ammonia sorption of NaPA kept in dry air. It is not possible to completely remove water from the sodium salt of polyacrylic acid (A) and therefore sorbed ammonia molecules react with preadsorbed water molecules (B). The water ammonia interaction leads to the formation of ammonia water complexes which may diffuse out of the polymer (C). Further ammonia molecules can interact with the sorption site of the polymer (D) being not longer occupied by water molecules.

5.1.3 Water sorption in a background of ammonia

In a background of ammonia water sorption leads to an increased mass gain for PAA (Figure 4.6 a) in 4.2.3) and NH$_4$PA (Figure 4.8 a) in 4.2.3) while the mass gain of NaPA is unaffected (Figure 4.8 b) in 4.2.3); the glassy to rubbery transition of PAA occurs at lower humidities (Figure 4.6 b) in 4.2.3); the bulk resistance of PAA decreases and the switch between the conduction mechanisms is shifted to lower humidities (Figure 4.12 a) in 4.3.1.1), the bulk capacitance is varied accordingly (Figure 4.12 b) in 4.3.1.1) and new bands appear in the infrared spectra (see 4.5). A model considering these observations is presented in the following sections.

In the presence of water, ammonia, as a strong hydrogen bond acceptor [174], interacts with the acid groups of PAA and NH$_4$PA not only occupying the free carboxylate groups but also destroying hydrogen bonds of chain structures and cyclic dimers (A) in Figure 5.5 much more distinctively than without ammonia (see 4.5.2); these interactions lead to the formation of ammonium cations and polyacrylate anions in the layer (see 4.5.3). Due to the break up of the hydrogen bonds, the polymer chains become more flexible and this lowers the glass transition temperature: the higher the

ammonia concentration is the lower is the required humidity to observe glass transition at room temperature (Figure 4.6 b) in 4.2.3).
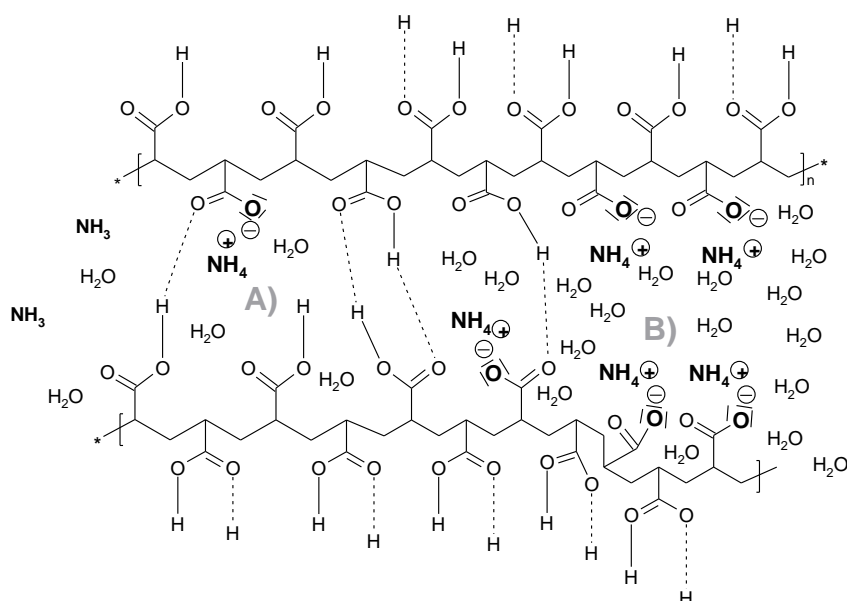
Figure 5.5:   Interaction of ammonia in the presence of water with interchain hydrogen bonded PAA: Ammonia strongly interacts with the acid sites of the polymer destroying the hydrogen bonds (A). Therefore the polymer matrix becomes more flexible and much more water can be sorbed into the polymer (B).

In the glassy state the interaction of ammonia with interchain hydrogen bonds modifies the polymer matrix so that the free volume of the polymer increases and more water can be sorbed (marked B in Figure 5.5). In this humidity range, the relative additional mass uptake is independent on the humidity and only determined by the ammonia background concentration (Figure 4.7 in 4.2.3). This behaviour is observed for PAA as well as for NH$_4$PA, because the water sorption properties of both materials depend on the chain-linking via hydrogen bonds. In contrast, if the polymer chains do not form a three dimensional network via hydrogen bonds, gaseous ammonia cannot modify the polymer matrix and, therefore, the presence of ammonia does not influence the water sorption properties. This is observed in the gravimetric studies of NaPA layers exposed to different levels of humidity with and without ammonia in the ambient (Figure 4.8 b) in 4.2.3). The decreased resistance and the increased capacitance of the hydrogen bonded polymers are mainly caused by the increased polymer water content. The latter promotes the formation of water clusters and liquid water, as confirmed by

IR measurements (Figure 4.28 in 4.5.1) and as a result of this process the vehicle type conduction mechanism replaces the Grotthuss one already at lower humidities (Figure 4.12 in 4.3.1.1).

In the presence of ammonia, the formation of water clusters is favoured if compared to the sorption of water molecules to the polymer, probably, because ammonia itself occupies the sorption sites at the polymer chains. The liquid water, in turn, influences the ammonia uptake because ammonia likes to dissolve in water due to its very high solubility (89.9 g per 100 cm^3 water [175]) and, thus, the weight of the sample additionally increases. This process does not only depend on the inter-chain hydrogen bonds and, therefore, even the NaPA layer response to ammonia at higher humidity levels (Figure 4.8 b) in 4.2.3). Above the glass transition in the rubbery state, these complex interdependent sorption processes of water and ammonia causes the linear rise of the relative mass increase.

After removing ammonia from the ambient atmosphere, the IR spectra does not recover completely because the ionic bond between the ammonium cation and the polyacrylate anion is very strong, so that the ammonium ion remains in the polymer. And, even if the polymer is after a drying procedure exposed to the same humidity without ammonia (point-dashed line in Figure 4.33 in 4.5.4), several changes of the infrared spectra, if compared to the spectra of a newly prepared PAA layer, can be observed, confirming that, once in contact with humid ammonia gas, PAA irreversibly forms the ammonium polyacrylate at some acid sites of the polymer; this is a reaction well known in literature [176] as a typical interaction of solid organic acids with gaseous ammonia. This explains the irreversible change of the electrical properties due to ammonia exposure (Figure 4.12 in 4.3.1.1) and the fact that the equivalent resistance and the capacitance of the ammonia exposed PAA approach the values obtained for ammonium polyacrylate (Figure 4.12 and Figure 4.13 in 4.3.1.1). It also explains the difference between the gravimetric and the electrochemical experiment results: While PAA and NH$_4$PA show the same dependence on humidity in gravimetric measurements (both materials have inter-chain hydrogen bonds which govern the mass uptake from the ambient), the electrochemical properties of the two materials strongly differ. Accordingly, if PAA partly reacts with NH$_3$ toward NH$_4$PA

this has no effect on the gravimetric response but strongly influences the electrochemical properties of the material.

5.2 Processes at the electrode

After the bulk processes induced by water and ammonia sorption are discussed in the previous chapter, the following sections deal with the processes at the polymer / electrode interface. In the first chapter, the electrochemical properties are discussed and, in the second one, a model is deduced describing the influence of the sorption processes on the gold electrode work function.

5.2.1 Electrochemical processes at the electrode

The electrochemical processes at the electrode, mirrored by the low frequency part of the impedance spectra, probably depend on the water content of the polymer only (see Figure 4.18 in 4.3.1.2). Differences between PAA and its derivates are caused by the different water contents of these materials at the same ambient humidities possibly varied by the presence of ammonia. Therefore, the charge transfer reaction, diffusion processes and the double layer charging are basically the same for all studied polymers and described for all materials at once.

Under the usual conditions applied in this work, at humidities between 0 and 90% and ammonia concentrations in the range of 0 to 100 ppm almost no charge transfer reactions are observed at the electrodes. This is proven by the absence of a full semicircle in the low frequency part of the Nyquist impedance plot and by the absence of peaks in the CV diagram in all measurement conditions (Figure 4.22 in 4.3.2). It changes only if a voltage of several volts is applied to the electrode comb structure of the sample: Peaks in the CV diagram and the appearance of a full semicircle in the low frequency part of the impedance spectra (Figure 4.17 a) in 4.3.1.2) indicate the presence of an electrochemical reaction at the electrodes. As discussed in 2.2.2.2 the electrochemical process is probably the decomposition of water into gaseous hydrogen and oxygen (equations (2.19) and (2.20)). This suggestion is confirmed by the observation that, even if high voltages are applied, no electrochemical reactions are

observed in the dry polymer and if the sample is exposed to dry ammonia (Figure 4.18 b) in 4.3.1.2 and Figure 4.22 b) in 4.3.2).

Without an additionally applied voltage, the onset of this charge transfer reaction happens at high water contents in the polymer when a very large charge transfer resistance can be estimated from the impedance measurements (Figure 4.16 b) in 4.3.1.2). At lower humidities, other processes, such as the diffusion of the electroactive species to the electrodes and the charging of the double layer at the electrode surface, determine the electrochemical properties as discussed in the following section.

At low water contents, electrode processes do not occur because the concentration of the electroactive species at the electrode is too small. With increasing water in the polymer, some electrode processes may happen but the rate determining process is still the water diffusion to the electrodes. Therefore, in the Nyquist plot, a straight line inclining with an angle to the x-axis close to 45° caused by Warburg impedance appears in the spectra. The diffusion depends on the availability of water in the polymer, as reflected by the linear relationship between the diffusion current and the humidity in the semi-logarithmic representation (Figure 4.21 b) in 4.3.2). Additionally, the state of the polymer matrix determines the diffusion properties of the system: In the glassy state the water molecules cannot easily move through the polymer because they are hindered by interchain hydrogen bonds. If these hydrogen bonds are broken up and the polymer becomes glassy, the water diffusion is less restricted resulting in a larger slope of the diffusion current dependence of the humidity (Figure 4.21 b) in 4.3.2). In the rubbery state, the diffusion is usually fast and the charging of the double layer at the electrode surface becomes rate determining. CV measurements indicate that the double layer charging, even in the absence of ammonia, is not a simple process but is caused by at least two different processes depending on the frequency of the applied AC voltage (Figure 4.23 in 4.3.2). For a full understanding of the double layer charging further experiments will have to be performed.

5.2.2 Kelvin Probe signal of polymer coated gold electrodes

Kelvin Probe signals observed for polymer coated electrodes are not caused by the interaction of PAA or its derivates with ammonia at the polymer surface exposed to

the gases. Even if this is the standard explanation for work function changes of sensitive layers (see 2.3.2.3), it cannot be applied for the samples prepared with PAA and its salts, because the conductance of the polymers, especially in dry air, is to low to allow the reaching the equilibrium between the polymer surface and the electrodes. Furthermore, sorption processes into the bulk and charge transfer reactions at the polymer / gold interface are not responsible for the observed signals. The first one can be excluded because the time constants of the bulk processes determined with gravimetric measurements are completely different from the time constants observed from Kelvin Probe measurements (Figure 4.26 in 4.4.2). Charge transfer reactions would lead to peaks in CV diagrams that are not observed, as discussed in the previous chapter.

Therefore, as no charge is transferred at the electrodes, the Kelvin Probe signals must be caused by sorption or desorption processes at the electrode surface. In the following chapters, a model describing these mechanisms is developed.

5.2.2.1 Kelvin Probe signals in dry air

As described in 2.3.2.1 the sorption of ammonia onto the gold surface leads to a decrease of the work function. With PAA or NH_4PA covering the metal the effect is intensified and the negative Kelvin signal increases (squares and circles in Figure 4.27 in 4.4.2). This can be explained by two different mechanisms: The first one is a simple concentration of the ammonia in the polymer if compared to the ammonia concentration in the ambient. Due to the resultant higher amount of ammonia at the polymer / electrode interface, the Kelvin Probe signal is increased. The mechanism inducing the Kelvin Probe signal is the same as the one for the uncovered gold substrate, discussed in 2.3.2.1 and illustrated in Figure 5.6 a). The second mechanism considers the interaction between ammonia molecules at the gold surface and the carboxyl or carboxylic groups of the polymer. In the gas phase, ammonia vigorously accepts hydrogen bonds but does not act as a hydrogen bond acceptor [174]. This may change in the presence of a metal surface because, due to dispersion effects between ammonia and the gold, the free electron pair of ammonia is attracted. The gold / ammonia complex is not such a strong Lewis base as gaseous ammonia and, therefore,

it is able to donate hydrogen bonds to an oxygen atom in the polymer. As shown in Figure 5.6 b), such interactions increase the charge density at the nitrogen atom aligned to the gold surface. The intensified negative partial charge of the nitrogen atom causes an increased downward charge flow on the gold surface. This causes an enhanced dipole moment in the metal and, with it, the negative Kelvin Probe signal increases.

Probably both mechanisms contribute to the Kelvin Probe signal changes observed for polyacrylic acid or ammonium polyacrylate coated gold samples. The response of the sodium polyacrylate (see the triangles in Figure 4.27 in 4.4.2) cannot satisfactorily be described with this model. For understanding of work function changes at the sodium polyacrylate / gold interface it is necessary to clarify the processes at a gold surface exposed to ammonia in humid ambient. This is discussed in the following chapter.
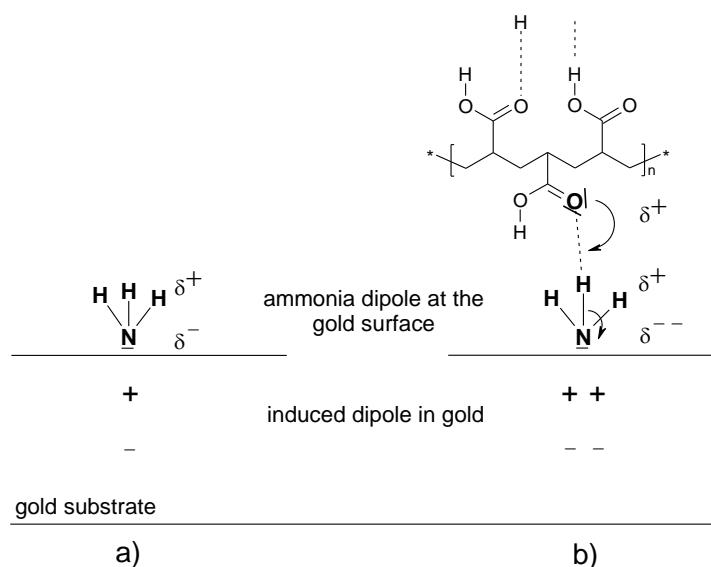
Figure 5.6: Interaction of ammonia with an uncoated gold surface (a) and the interaction change if the ammonia additionally forms hydrogen bonds to a polymer as PAA and NH$_4$PA coating the gold surface (b).

5.2.2.2 Kelvin Probe signals in humid air

Depending on the humidity level, water molecules will partly or completely cover the surface of the gold layer. If such a modified surface is exposed to ammonia, the ammonia molecules interact with water molecules present at the surface (marked A in Figure 5.7), forming hydrogen bonds with each other (marked B in Figure 5.7) and, eventually, leave the gold surface as a ammonia-water complex (marked C in Figure

5.7). This process leads to an increase of the gold work function: As shown in 2.3.2.2 bonding of water molecules to the metal surface causes a negative work function change. If the water molecules are removed from the surface through interaction with ammonia, the initial work function change is reversed and a positive response of the Kelvin Probe set-up is recorded.

The direct interaction of ammonia with the metal (marked D in Figure 5.7) takes place in parallel if the gold surface is not completely covered with water molecules. This is observed at intermediate humidities (for example at 50% r.h. as shown in Figure 4.25 in 4.4.1): The negative work function change due to ammonia / gold interaction is almost balanced by the positive work function changes caused by the displacement of water molecules. Therefore, the observed Kelvin Probe signals are remarkably small but still negative.

If the water content in the ambient is increased, the displacement of water molecules outweighs by far the other effect and, therefore, a positive Kelvin Probe signal is observed (for example in 90% r.h. presented in Figure 4.25 in 4.4.1).

Figure 5.7: In humid air the gold surface is covered with adsorbed water molecules (A). Ammonia interacts with these water molecules forming ammonia water complexes via hydrogen bonds (B) which may desorb from the gold surface (C). Afterwards, the free sorption sites can be occupied by ammonia molecules (D).

In NaPA, water from the preparation process cannot completely be removed from the sample by just keeping it under a stream of dry air as described above (see 5.1.1.2). These water molecules are also sorbed onto the gold substrate so that, even in a dry ambient, the metal surface under a sodium polyacrylate layer is wetted. If such a sample is exposed to ammonia, the Kelvin Probe response is a positive signal as in the case of uncovered gold exposed to ammonia in a background of high humidity. Due to

the permanent presence of water molecules, the signal is almost unchanged by variations of the ambient humidity (see the triangles in Figure 4.27 in 4.4.2).

Water sorbed into PAA or NH_4PA layers does not wet the surface of the gold substrate because the water molecules prefer to remain in the polymer bulk, where they are able to form hydrogen bonds with PAA or its ammonium salt. Therefore, gold substrates covered with these materials show negative Kelvin Probe signals even if they are exposed to humidity. However, some water molecules will also be sorbed by the gold and therefore the signal slightly decreases compared to the measurements in dry air (see the squares and circles in Figure 4.27 in 4.4.2).

After discussion of the observed phenomenon in detail the important results are summed up in the following chapter and an outlook for possible applications of the knowledge gained in this work is given.

6 Summary and outlook

The main achievement of this work is the setting up of a phenomenological model describing water vapour and ammonia gas sorption into PAA and the associated changes of the latter's chemical and electrochemical properties. Based on gravimetric, electrochemical, Kelvin Probe and infrared measurement the developed model supports the improvement of PAA as base sensing material for applications and allows a deeper understanding of the sensing mechanism, of the measurements performed and of already published results.

From experiments with PAA and its ammonium and sodium salts, the importance of the presence or absence of hydrogen bonds connecting the polymer chains was uncovered. The interaction of water vapour and gaseous ammonia with hydrogen bonds, explains the sensitivity to those analytes and their cross sensitivity. In contrast to previous published suggestions [38, 47], the presence of water does not increase the number of sorption sites for ammonia molecules but, due to few ammonia molecules, the hydrogen bonds get destroyed and much more water can be sorbed into the polymer. Due to these interactions, gravimetric measurements for ammonia detection are unambiguous only if the measurements are performed in dry air or at a constant humidity. For sensor applications, a constant humidity should be preferred because the additionally sorbed water molecules cause a stronger increase of the measurement device response and, with it, the signal to noise ratio decreases. However, as soon as humidity variations occur, gravimetric measurements are not suitable to determine the ammonia content in the ambient.

If humidity is the target analyte, chemical modifications of PAA can prevent the cross sensitivity to ammonia: In the absence of hydrogen bonds, as for example in NaPA, the gravimetric response is independent on the ammonia concentration but the disadvantage of this material is the poor reproducibility of the sensor response. To combine the ammonia independence of NaPA with the good reproducibility of the PAA response, the hydrogen bonds in the acid should be partly transferred to the sodium salt and partly replaced by chemical bonds which can be obtained due to cross linking reactions; such chemical bonds cannot be destroyed by ammonia molecules. Further studies are required to determine the optimal ratio of sodium carboxylate sites

to cross linked sites resulting in a humidity sensing material with low cross sensitivity and high stability and, with it, good reproducibility of the sensor signals.

As published in literature, cross linked polyacrylic acid was already used for humidity sensing with electrochemical devices [20]. The observed resistance switch can be explained by using the phenomenological model obtained in this work: Depending on the water content of the polymer films, the conduction proceeds according to two distinctive mechanisms. At low humidities non condensing water molecules build up networks over hydrogen bonds in the free space between the PAA chains providing a path for proton transfer. Under the action of an externally applied field, a hopping process along an uninterrupted "route", in average oriented in the field direction, occurs; the charge is carried through the polymer film according to a Grotthuss mechanism. With increasing water content, more and more water clusters and liquid water are formed, which enable the free migration of ammonium and hydroxonium ions via a vehicle type mechanism; that is the onset of a convection drift current. Both mechanisms occur in the cross linked PAA as well as in the pure PAA and the ammonium salt. In strongly hygroscopic materials, as for example the sodium salt of PAA, the vehicle type conduction mechanism determines the conductance over the whole humidity range.

While ammonia in dry air does not influence the electrochemical properties of polyacrylic acid, in humid air a strong resistance decrease and capacitance increase are induced by the presence of ammonia. The observation is in agreement with the gravimetric measurements and is caused by the increased water uptake in the presence of ammonia. To avoid that, further development of the sensing material is required, similar to the one described for gravimetric measurements. Directly, the ammonia molecules seem to have a limited influence on the conduction process only and, therefore, a sensor principle which is based on electrochemical methods is not useful for the detection of gaseous ammonia in the ambient.

For ammonia detection with PAA sensitive layers, it is more suitable to use Kelvin Probe or field effect transducer measurements. It is known in literature that these devices allow the determination of ammonia with a small cross sensitivity to humidity [21, 46] and it was suggested that the sensing process occurs at the polymer electrode

interface [47]. Kelvin Probe and impedance measurements combined with voltage step and cyclic voltammetry experiments were performed in this work leading to a deeper understanding of the processes at the electrode. The gained knowledge can be used to develop an improved polymer layer: The optimal material allows ammonia to diffuse to the electrodes but hinders the contact between water and the electrodes.

This is an example of the usefulness of the phenomenological model for the purposeful preparation of sensing materials. Future work is required to transfer the information gained for the model system, the water vapour and ammonia gas sorption process into PAA, to a more general level. With the study of NaPA, a polar material without the ability to form hydrogen bonds, first steps in this direction were done but to get a full picture of the potentials of chemically modified sensitive layers further studies have to be performed for other polymer types for example non-polar or basic materials and other modifications, especially cross linked polymers.

When such studies are available, selective and sensitive materials can purposefully be prepared for the desired application and the measurement technique applied.

Bibliography

[1]   K. Arshak, E. Moore, G. M. Lyons, J. Harris and S. Clifford, A review of gas sensors employed in electronic nose applications, *Sensor Review* 24 (2), **2004**, 181-198.

[2]   H. T. Nagle, R. Gutierrez-Osuna and S. S. Schiffman, The how and why of electronic noses, *IEEE Spectrum* 35 (9), **1998**, 22-31.

[3]   www.appliedsensor.com.

[4]   www.airsense.com.

[5]   A. J. Ricco, Surface Acoustic Wave Sensors and Potential Uses, *The Electrochemical Society Interface* 3 (4, Winter), **1994**, 38-44.

[6]   V. E. Henrich and P. A. Cox, The surface science of metal oxides, Cambridge University Press, Cambridge, **1994**.

[7]   W. Göpel, Chemical imaging: I. Concepts and visions for electronic and bioelectronic noses, *Sensors and Actuators B: Chemical* 52 (1-2), **1998**, 125-142.

[8]   U. Weimar and W. Gopel, Chemical imaging: II. Trends in practical multiparameter sensor systems, *Sensors and Actuators B: Chemical* 52 (1-2), **1998**, 143-161.

[9]   J. G. Brace, T. S. Sanfelippo and S. G. Joshi, A study of polymer/water interactions using surface acoustic waves, *Sensors and Actuators* 14 (1), **1988**, 47-68.

[10]   C. Brunner, Über die Bestimmung des Wassergehaltes der Atmosphäre, *Poggendorfs Annalen* 20, **1830**, 274.

[11]   M. V. Regnault, Études sur l'hygrométrie, *Annales de chimie et de physique* 3 (15), **1845**, 129-236.

[12]   C. Koppe, Über Feuchtigkeitsbestimmung, *Österreichische Zeitschrift für Meteorologie*, **1879**, 49.

[13]   T. Deneke, Über die Bestimmung der Luftfeuchtigkeit zu hygienischen Zwecken, *Medical Microbiology and Immunology* 1, **1886**, 47-75.

[14]   N. Yamazoe and Y. Shimizu, Humidity sensors: Principles and applications, *Sensors and Actuators* 10 (3-4), **1986**, 379-398.

[15]   H. Arai and T. Seiyama, Humidity Sensors, in eds. W. Göpel, J. Hesse and J. N. Zemel, *Sensors, A Comprehensive Survey*, VCH Verlagsgesellschaft, Weinheim, **1991**.

[16]   G. Scholz, Market analysis: sensors and instruments for gas humidity, *Technisches Messen* 59, **1992**, 88-109.

[17]   Z. M. Rittersma, Recent achievements in miniaturised humidity sensors--a review of transduction techniques, *Sensors and Actuators A: Physical* 96 (2-3), **2002**, 196-210.

[18]   C.-Y. Lee and G.-B. Lee, Humidity Sensors: A Review, *Sensor Letters* 3, **2005**, 1-15.

[19]   Z. Chen and C. Lu, Humidity Sensors: A Review of Materials and Mechanisms, *Sensor Letters* 3, **2005**, 274-295.

[20]   S. Wu, F. Li, Y. Zhu and J. Shen, The switch-type humidity sensing properties of polyacrylic acid and its copolymers, *Journal of Materials Science* 35 (8), **2000**, 2005-2008.

[21]   A. Oprea and U. Weimar, High sensitivity polyacrylic acid films for ammonia detection with field effect devices, *Sensors and Actuators B: Chemical* 111-112, **2005**, 572-576.

[22]   M. Harbeck, New Application of organic polymers in chemical gas sensors, *PhD*, University of Tübingen, Tübingen, **2005**.

[23]   K. B. Lehmann, Experimentelle Studien über den Einfluß technisch und hygienisch wichtiger Gase und Dämpfe auf den Organismus, *Archiv für Hygiene* 5, **1886**, 1-126.

[24]   M. Bendahan, P. Lauque, C. Lambert-Mauriat, H. Carchano and J.-L. Seguin, Sputtered thin films of CuBr for ammonia microsensors: morphology, composition and ageing, *Sensors and Actuators B: Chemical* 84 (1), **2002**, 6-11.

[25]   H. Sterzl-Eckert and H. Greim, Grenzwertfestsetzung durch die Senatskommission der Deutschen Forschungsgemeinschaft zur Prüfung gesundheitsschädlicher Arbeitsstoffe, in ed. H. d. g. Berufsgenossenschaften, *BIA-Report 4/98: Symposium: Grenzwerte für chemische Einwirkungen an Arbeitsplätzen*, St. Augustin, **1998**.

[26]   H. Greim, *Gesundheitsschädliche Arbeitsstoffe, toxikologisch-arbeitsmedizinische Begründungen von MAK-Werten*, Wiley-VCH, Weinheim, **1997**.

[27] http://www.baua.de/de/Themen-von-A-Z/Gefahrstoffe/TRGS/TRGS-900.html_nnn=true.

[28] http://ec.europa.eu/employment_social/health_safety/docs/oel_ammonia_en.pdf, **1992**.

[29] M. E. Meyerhoff, Polymer membrane electrode based potentiometric ammonia gas sensor, *Analytical Chemistry* 52 (9), **1980**, 1532-1534.

[30] Y. M. Fraticelli and M. E. Meyerhoff, Automated determination of ammonia with a potentiometric gas sensor and flowing internal electrolyte, *Analytical Chemistry* 53 (7), **1981**, 992-997.

[31] B. Ostrick, R. Pohle, M. Fleischer and H. Meixner, TiN in work function type sensors: a stable ammonia sensitive material for room temperature operation with low humidity cross sensitivity, *Sensors and Actuators B: Chemical* 68 (1-3), **2000**, 234-239.

[32] A. Galdikas, A. Mironas, V. Strazdiene, A. Setkus, I. Ancutiene and V. Janickis, Room-temperature-functioning ammonia sensor based on solid-state CuxS films, *Sensors and Actuators B: Chemical* 67 (1-2), **2000**, 76-83.

[33] V. V. Chabukswar, S. Pethkar and A. A. Athawale, Acrylic acid doped polyaniline as an ammonia sensor, *Sensors and Actuators B: Chemical* 77 (3), **2001**, 657-663.

[34] O. K. Varghese, D. Gong, W. R. Dreschel, K. G. Ong and C. A. Grimes, Ammonia detection using nanoporous alumina resistive and surface acoustic wave sensors, *Sensors and Actuators B: Chemical* 94 (1), **2003**, 27-35.

[35] S. Sen, K. P. Muthe, N. Joshi, S. C. Gadkari, S. K. Gupta, Jagannath, M. Roy, S. K. Deshpande and J. V. Yakhmi, Room temperature operating ammonia sensor based on tellurium thin films, *Sensors and Actuators B: Chemical* 98 (2-3), **2004**, 154-159.

[36] E. Milella and M. Penza, SAW gas detection using Langmuir-Blodgett polypyrrole films, *Thin Solid Films* 327-329, **1998**, 694-697.

[37] H. Nanto, Y. Hamaguchi, Y. Yokoi, S. Kurosawa, T. Oyabu, E. Kusano and A. Kinbara, A smart ammonia gas sensor using QCM with plasma-polymerized membrane, *Sensors and Materials* 13 (2), **2001**, 69-76.

[38] B. Ding, M. Yamazaki and S. Shiratori, Electrospun fibrous polyacrylic acid membrane-based gas sensors, *Sensors and Actuators B: Chemical* 106 (1), **2005**, 477-483.

[39] A. Karthigeyan, R. P. Gupta, K. Scharnagl, M. Burgmair, S. K. Sharma and I. Eisele, A room temperature HSGFET ammonia sensor based on iridium oxide thin film, *Sensors and Actuators B: Chemical* 85 (1-2), **2002**, 145-153.

[40] J. F. Giuliani, H. Wohltjen and N. L. Jarvis, Reversible optical waveguide sensor for ammonia vapors, *Optics Letters* 8, **1983**, 54-56.

[41] J. Redtenbacher, Ueber die Zerlegungsprodukte des Glyceryloxydes durch trockene Destillation, *Annalen der Chemie und Pharmacie* 47 (2), **1843**, 113-148.

[42] J. W. Nemec and W. Bauer, in ed. M. Grayson, *Kirk-Othmer Encyclopedia of Chemical Technology*, Wiley, New York, 3rd edition, **1978**.

[43] M. J. Durrani and P. A. Manji, Water-Swellable Polymers (Carbomer Resins), in ed. J. C. Salamone, *Polymer Materials Encyclopedia*, CRC Press, New York, **1996**.

[44] L.-Å. Lindén and J. F. Rabek, Dental Polymers (Hydrogels), in ed. J. C. Salamone, *Polymer Materials Encyclopedia*, CRC Press, New York, **1996**.

[45] V. Z. Annenkova, V. B. Kazmirovskaya, E. J. Zhdankovich and e. al., *Khim.-Farm. Zh.* 24, **1990**, 34.

[46] A. Oprea, E. Simon, M. Fleischer, H.-P. Frerichs, C. Wilbertz, M. Lehmann and U. Weimar, Flip-chip suspended gate field effect transistors for ammonia detection, *Sensors and Actuators B: Chemical* 111-112, **2005**, 582-586.

[47] A. Oprea, N. Barsan and U. Weimar, Ammonia detection mechanism with polyacrylic acid sensitive layers: Field effect transduction, *Sensors and Actuators B: Chemical* 111-112, **2005**, 577-581.

[48] S. J. Martin, A. J. Ricco, D. S. Ginley and T. E. Zipperian, Isothermal Measurements and Thermal Desorption of Organic Vapors Using SAW Devices, *IEEE Transactions UFFC* 34 (2), **1987**, 142-147.

[49] D. S. Ballantine, S. L. Rose, J. W. Grate and H. Wohltjen, Correlation of surface acoustic wave device coating responses with solubility properties and chemical structure using pattern recognition, *Anal. Chem.* 58 (14), **1986**, 3058-3066.

[50] G. n. Sauerbrey, Verwendung von Schwingquarzen zur Wägung dünner Schichten und zur Mikrowägung, *Zeitschrift für Physik A* 155 (2), **1959**, 206-222.

[51] J. Curie and P. Curie, ÉLECTRICITÉ. - Développement, par pression, de l'électricité polaire dans les cristaux hémièdres à faces inclinées, *Comptes*

rendus hebdomadaires des séances de l'Académie des sciences 91, **1880**, 294-297.

[52]   D. A. Buttry and M. D. Ward, Measurement of interfacial processes at electrode surfaces with the electrochemical quartz crystal microbalance, *Chemical Reviews* 92 (6), **1992**, 1355-1379.

[53]   D. S. Ballantine, R.M. White, S. J. Martin, A. J. Ricco, E. T. Zellers, G. C. Frye and H. Wohltjen, *Acoustic Wave Sensors: Theory, Design and Physico-Chemical Applications*, Academic Press, San Diego, CA, **1997**.

[54]   V. M. Mecea, Is quartz crystal microbalance really a mass sensor?, *Sensors and Actuators A: Physical* 128 (2), **2006**, 270-277.

[55]   J. W. Grate, S. J. Martin and R. M. White, Acoustic Wave Microsensors Part 1, *Analytical Chemistry* 65, **1993**, 940A-948A.

[56]   A. J. Ricco, S. J. Martin and T. E. Zipperian, Surface acoustic wave gas sensor based on film conductivity changes, *Sensors and Actuators* 8 (4), **1985**, 319-333.

[57]   K. B. Sundaram and A. Khan, Characterization and optimization of zinc oxide films by r.f. magnetron sputtering, *Thin Solid Films* 295 (1-2), **1997**, 87-91.

[58]   V. Mortet, O. Elmazria, M. Nesládek, M. Elhakiki, G. Vanhoyland, J. D'Haen, M. D'Olieslaeger and P. Alnot, Structural characterisations of AlN/diamond structures used for surface acoustic wave device applications, *physica status solidi (a)* 199 (1), **2003**, 145-150.

[59]   W. H. King, Piezoelectric Sorption Detector., *Analytical Chemistry* 36 (9), **1964**, 1735-1739.

[60]   H. Wohltjen and R. Dessy, Surface acoustic wave probe for chemical analysis. I. Introduction and instrument description, *Analytical Chemistry* 51 (9), **1979**, 1458-1464.

[61]   S. J. Martin, G. C. Frye and S. D. Senturia, Dynamics and Response of Polymer-Coated Surface Acoustic Wave Devices: Effect of Viscoelastic Properties and Film Resonance, *Analytical Chemistry* 66 (14), **1994**, 2201-2219.

[62]   K. Bodenhöfer, A. Hierlemann, G. Noetzel, U. Weimar and W. Gopel, Performances of Mass-Sensitive Devices for Gas Sensing: Thickness Shear Mode and Surface Acoustic Wave Transducers, *Analytical Chemistry* 68 (13), **1996**, 2210-2218.

[63]   D. S. Ballantine and H. Wohltjen, Surface acoustic wave devices for chemical analysis, *Analytical Chemistry* 61 (11), **1989**, 704A-715A.

[64]   J. W. Grate and M. Klusty, Surface acoustic wave vapor sensors based on resonator devices, *Analytical Chemistry* 63 (17), **1991**, 1719-1727.

[65]   D. C. Stone and M. Thompson, Interdigital capacitance and surface acoustic wave sensors, *Analytical Chemistry* 65 (4), **1993**, 352-362.

[66]   J. W. Grate, S. J. Martin and R. M. White, Acoustic Wave Microsensors Part 2, *Analytical Chemistry* 1993, **1993**, 987A-995A.

[67]   D. L. Bartley and D. D. Dominguez, Elastic effects of polymer coatings on surface acoustic waves, *Anal. Chem.* 62 (15), **1990**, 1649-1656.

[68]   R. A. Crane and G. Fischer, Analysis of a quartz crystal microbalance with coatings of finite viscosity, *Journal of Physics D: Applied Physics* 12 (12), **1979**, 2019-2026.

[69]   K. K. Kanazawa and J. G. Gordon, Frequency of a quartz microbalance in contact with liquid, *Analytical Chemistry* 57 (8), **1985**, 1770-1771.

[70]   M. Yang and M. Thompson, Perturbation of the electrified interface and the response of the thickness-shear mode acoustic wave sensor under conductive liquid loading, *Analytical Chemistry* 65 (24), **1993**, 3591-3597.

[71]   Z. A. Shana and F. Josse, Quartz Crystal Resonators as Sensors in Liquids Using the Acoustoelectric Effect, *Analytical Chemistry* 66 (13), **1994**, 1955-1964.

[72]   H. Levine and L. Slade, Glass transition in foods, in eds. H. G. Scwartzberg and R. W. Hartel, *Physical Chemistry of foods*, Marcel Decker, New York, **1992**.

[73]   I. Langmuir, THE ADSORPTION OF GASES ON PLANE SURFACES OF GLASS, MICA AND PLATINUM., *Journal of the American Chemical Society* 40 (9), **1918**, 1361-1403.

[74]   H. Freundlich, *Colloid and Capillary Chemistry*, Methuen, London, **1926**.

[75]   A. Frumkin and A. Slygin, Über die Platinelektrode, *Acta Physicochim. U.R.S.S.* 3, **1935**, 791-818.

[76]   S. Brunauer, K. S. Love and R. G. Keenan, Adsorption of Nitrogen and the Mechanism of Ammonia Decomposition Over Iron Catalysts, *Journal of the American Chemical Society* 64 (4), **1942**, 751-758.

[77]   H. B. Bull, Adsorption of Water Vapor by Proteins, *Journal of the American Chemical Society* 66 (9), **1944**, 1499-1507.

[78]   A. B. D. Cassie, Absorption of water by wool, *Transactions of the Faraday Society* 41, **1945**, 458 - 464.

[79]   A. J. Hailwood and S. Horrobin, Absorption of water by polymers: analysis in terms of a simple model, *Transactions of the Faraday Society* 42, **1946**, B084-B092.

[80]   S. Brunauer, P. H. Emmett and E. Teller, Adsorption of Gases in Multimolecular Layers, *Journal of the American Chemical Society* 60 (2), **1938**, 309-319.

[81]   R. S. Bradley, Polymolecular adsorbed films. Part I. The adsorption of argon on salt crystals at low temperatures, and the determination of surface fields, *Journal of the Chemical Society (Resumed)*, **1936**, 1467-1474.

[82]   R. L. D'Arcy and I. C. Watt, Analysis of sorption isotherms of non-homogeneous sorbents, *Transactions of the Faraday Society* 66, **1970**, 1236-1245.

[83]   A. W. Adamson and A. P. Gast, Physical Chemistry of surfaces, Wiley, Weinheim, 6th edition, **1997**.

[84]   K. T. Valsaraj and L. J. Thibodeaux, Equilibrium adsorption of chemical vapours onto surface soils: model predictions and experimental data, in ed. J. L. Schnoor, *Fate of pesticides and chemicals in the environment*, Wiley, New York, **1992**.

[85]   D. O. Hayward and B. M. W. Trapnell, Chemisorption, Butterworths, London, **1964**.

[86]   B. Hancock and G. Zografi, The Use of Solution Theories for Predicting Water Vapor Absorption by Amorphous Pharmaceutical Solids: A Test of the Floryâ€"Huggins and Vrentas Models, *Pharmaceutical Research* 10 (9), **1993**, 1262-1267.

[87]   J. A. Groetsch III and R. E. Dessy, A surface acoustic wave (SAW) probe for the thermomechanical characterization of selected polymers, *Journal of Applied Polymer Science* 28 (1), **1983**, 161-178.

[88]   S. J. Martin and G. C. Frye, Surface acoustic wave response to changes in viscoelastic film properties, *Applied Physics Letters* 57 (18), **1990**, 1867-1869.

[89]   J. W. Grate, S. W. Wenzel and R. M. White, Frequency-independent and frequency-dependent polymer transitions observed on flexural plate wave ultrasonic sensors, *Analytical Chemistry* 64 (4), **1992**, 413-423.

[90]   T. G. Fox, Influence of diluent and of copolymer composition on the glass transition temperature of a polymer system, *Bulletin of the American Physical Society* 1, **1956**, 123.

[91]   B. C. Hancock and G. Zografi, The Relationship Between the Glass Transition Temperature and the Water Content of Amorphous Pharmaceutical Solids, *Pharmaceutical Research* 11 (4), **1994**, 471-477.

[92]   M. Gordon and J. S. Taylor, Ideal copolymers and the second-order transitions of synthetic rubbers. i. non-crystalline copolymers, *Journal of Applied Chemistry* 2 (9), **1952**, 493-500.

[93]   R. Simha and R. F. Boyer, On a General Relation Involving the Glass Temperature and Coefficients of Expansion of Polymers, *The Journal of Chemical Physics* 37 (5), **1962**, 1003-1007.

[94]   G. K. Prasad, T. P. Radhakrishnan, D. S. Kumar and M. G. Krishna, Ammonia sensing characteristics of thin film based on polyelectrolyte templated polyaniline, *Sensors and Actuators B: Chemical* 106 (2), **2005**, 626-631.

[95]   T. Ishihara and S. Matsubara, Capacitive Type Gas Sensors, *Journal of Electroceramics* 2 (4), **1998**, 215-228.

[96]   J. N. Murray, Electrochemical test methods for evaluating organic coatings on metals: an update. Part III: Multiple test parameter measurements, *Progress in Organic Coatings* 31 (4), **1997**, 375-391.

[97]   A. V. Oppenheimer and A. S. Willsky, *Signal and Systems*, Prentice-Hall, Englewood Cliffs, New. Jersey, **1983**.

[98]   M. Ciureanu, S. D. Mikhailenko and S. Kaliaguine, PEM fuel cells as membrane reactors: kinetic analysis by impedance spectroscopy, *Catalysis Today* 82 (1-4), **2003**, 195-206.

[99]   F. Mansfeld, *Solartron Technical Report No. 26*, Schlumberger Technologies, UK, **1993**.

[100] G. W. Walter, A review of impedance plot methods used for corrosion performance analysis of painted metals, *Corrosion Science* 26 (9), **1986**, 681-703.

[101] F. Mansfeld, Concerning the Display of Impedance Data, *Corrosion* 44, **1988**, 558-559.

[102] X. Qian, N. Gu, Z. Cheng, X. Yang, E. Wang and S. Dong, Methods to study the ionic conductivity of polymeric electrolytes using a.c. impedance spectroscopy, *Journal of Solid State Electrochemistry* 6 (1), **2001**, 8-15.

[103] D. G. Han and G. M. Choi, Computer simulation of the electrical conductivity of composites: the effect of geometrical arrangement, *Solid State Ionics* 106 (1-2), **1998**, 71-87.

[104] A. Amirudin and D. Thieny, Application of electrochemical impedance spectroscopy to study the degradation of polymer-coated metals, *Progress in Organic Coatings* 26 (1), **1995**, 1-28.

[105] G. J. Brug, A. L. G. Van Den Eeden, M. Sluyters-Rehbach and J. H. Sluyters, The analysis of electrode impedances complicated by the presence of a constant phase element, *Journal of Electroanalytical Chemistry* 176 (1-2), **1984**, 275-295.

[106] F. Bellucci, M. Valentino, T. Monetta, L. Nicodemo, J. Kenny, L. Nicolais and J. Mijovic, Impedance spectroscopy of reactive polymers., *Journal of Polymer Science Part B: Polymer Physics* 32 (15), **1994**, 2519-2527.

[107] J. R. Macdonald and M. K. Brachman, Linear-System Integral Transform Relations, *Reviews of Modern Physics* 28 (4), **1956**, 393- 422.

[108] J. Schrama, On the Phenomenological Theory of Linear Relaxation Processes, *PhD*, University of Leiden, Leiden, Netherlands, **1957**.

[109] N. Bonanos, E. P. Butler, D. R. Franceschetti, W. B. Johnson, D. D. Macdonald, J. R. Macdonald, M. C. H. McKubre, I. D. Raistrick, B. C. H. Steele and W. L. Worrel, in ed. J. R. Macdonald, *Impedance Spectroscopy - emphasizing solid materials and systems*, Wiley, New York, **1987**.

[110] C. Ho, I. D. Raistrick and R. A. Huggins, Application of A-C Techniques to the Study of Lithium Diffusion in Tungsten Trioxide Thin Films, *Journal of The Electrochemical Society* 127 (2), **1980**, 343-350.

[111] M. A. Ratner and D. F. Shriver, Ion transport in solvent-free polymers, *Chemical Reviews* 88 (1), **1988**, 109-124.

[112] Y. Sadaoka, M. Matsuguchi, Y. Sakai and K. Takahashi, Effects of sorbed water on the dielectric constant of some cellulose thin films, *Journal of Materials Science Letters* 7 (2), **1988**, 121-124.

[113] K.-D. Kreuer, Proton Conductivity: Materials and Applications, *Chemistry of Materials* 8 (3), **1996**, 610-641.

[114] G. C. Pimentel and A. L. McClellan, *The hydrogen bond*, Freeman, San Francisco, **1960**.

[115] C. J. D. van Grotthuss, Mémoire sur la décomposition de l'eau et des corps qu'elle tient en dissolution a l'aide de l'électricité galvanique, *Annales de Chimie* 58, **1806**, 54-74.

[116] A. Bozkurt, W. H. Meyer and G. Wegner, PAA/imidazol-based proton conducting polymer electrolytes, *Journal of Power Sources* 123 (2), **2003**, 126-131.

[117] K.-D. Kreuer, A. Rabenau and W. Weppner, Vehicle Mechanism, A New Model for the Interpretation of the Conductivity of Fast Proton Conductors, *Angewandte Chemie International Edition in English* 21 (3), **1982**, 208-209.

[118] A. S. Castela and A. M. Simoes, Assessment of Water Uptake in Coil Coatings by Capacitance Measurements, *Journal of Corrosion Measurements* 1, **2001**, 1-10.

[119] D. M. Brasher and A. H. Kingsbury, Electrical measurements in the study of immersed paint coatings on metal. I. Comparison between capacitance and gravimetric methods of estimating water-uptake, *Journal of Applied Chemistry* 4 (2), **1954**, 62-72.

[120] S. A. Lindqvist, Theory of dielectric properties of heterogeneous substances applied to water in a paint film, *Corrosion* 41 (2), **1985**, 69-75.

[121] I. Thompson and D. Campbell, Interpreting Nyquist responses from defective coatings on steel substrates, *Corrosion Science* 36 (1), **1994**, 187-198.

[122] L. Tortet, J. R. Gavarri, J. Musso, G. Nihoul, J. P. Clerc, A. N. Lagarkov and A. K. Sarychev, Impedance spectroscopy of brushite composites and a scaling approach to the dispersion behavior of inhomogeneous ionic conductors, *Physical Review B* 58 (9), **1998**, 5390 LP - 5407.

[123] A. Prokopowicz and M. Opallo, Impedance study of hydrogen evolution from solid tetrabutylammonium hydroxide hydrate, *Solid State Ionics* 157 (1-4), **2003**, 209-213.

[124] G. Casalbore-Miceli, M. J. Yang, N. Camaioni, C.-M. Mari, Y. Li, H. Sun and M. Ling, Investigations on the ion transport mechanism in conducting polymer films, *Solid State Ionics* 131 (3-4), **2000**, 311-321.

[125] C. H. Hamann and W. Vielstich, *Elektrochemie II, Elektrodenprozesse, Angewandte Elektrochemie*, Verlag Chemie Weinheim, Weinheim, **1981**.

[126] M. J. Yang, Y. Li, N. Camaioni, G. Casalbore-Miceli, A. Martelli and G. Ridolfi, Polymer electrolytes as humidity sensors: progress in improving an impedance device, *Sensors and Actuators B: Chemical* 86 (2-3), **2002**, 229-234.

[127] A. J. Bard and L. R. Faulkner, *Electrochemical Methods, fundamentals and applications*, Wiley, New York, 2nd edition, **2001**.

[128] S. Trasatti and R. Parsons, Commision on Electrochemistry: Interphases in systems of conducting phases (IUPAC Recommendations 1985), *Pure and Applied Chemistry* 58 (3), **1986**, 437-454.

[129] H. Wingbrant, I. Lundstrom and A. Lloyd Spetz, The speed of response of MISiCFET devices, *Sensors and Actuators B: Chemical* 93 (1-3), **2003**, 286-294.

[130] H. Geistlinger, I. Eisele, B. Flietner and R. Winter, Dipole- and charge transfer contributions to the work function change of semiconducting thin films: experiment and theory, *Sensors and Actuators B: Chemical* 34 (1-3), **1996**, 499-505.

[131] R. P. Gupta, Z. Gergintschew, D. Schipanski and P. D. Vyas, YBCO-FET room temperature ammonia sensor, *Sensors and Actuators B: Chemical* 63 (1-2), **2000**, 35-41.

[132] L. Kelvin, Contact Electricity of Metals, *Phil. Mag.* 46, **1898**, 82-120.

[133] P. K. Schmidt, Wechselwirkung von Wasserstoff mit einer Pd(210)- und Ni(210)-Oberfläche, *PhD*, Freie Universität Berlin, Berlin, **2001**.

[134] A. Karthigeyan, R. P. Gupta, M. Burgmair, S. K. Sharma and I. Eisele, Influence of oxidation temperature, film thickness and substrate on NO2 sensing of SnO2 ultra thin films, *Sensors and Actuators B: Chemical* 87 (2), **2002**, 321-330.

[135] J. Janata, Chemical modulation of the electron work function, *Analytical Chemistry* 63 (22), **1991**, 2546-2550.

[136] H. Ishii, K. Sugiyama, E. Ito and K. Seki, Energy Level Alignment and Interfacial Electronic Structures at Organic/Metal and Organic/Organic Interfaces, *Advanced Materials* 11 (8), **1999**, 605-625.

[137] H. Gronbeck, A. Curioni and W. Andreoni, Thiols and Disulfides on the Au(111) Surface: The Headgroup-Gold Interaction, *Journal of the American Chemical Society* 122 (16), **2000**, 3839-3842.

[138] V. De Renzi, R. Rousseau, D. Marchetto, R. Biagi, S. Scandolo and U. del Pennino, Metal Work-Function Changes Induced by Organic Adsorbates: A

Combined Experimental and Theoretical Study, *Physical Review Letters* 95 (4), **2005**, 046804-046804.

[139] I. G. Hill, A. Rajagopal, A. Kahn and Y. Hu, Molecular level alignment at organic semiconductor-metal interfaces, *Applied Physics Letters* 73 (5), **1998**, 662-664.

[140] E. Bertel, The interaction of rare gases with transition metal surfaces, *Surface Science* 367 (2), **1996**, L61-L65.

[141] H. J. Freund and H. Kuhlenbeck, Band-structure determination of adsorbates, in ed. W. Eberhardt, *Applications in synchrotron radiation*, Springer Verlag, Berlin, **1995**.

[142] W. Monch, Metal-semiconductor contacts: electronic properties, *Surface Science* 299-300, **1994**, 928-944.

[143] A. Chattopadhyay, H. Yang and J. L. Whitten, Adsorption of ammonia on nickel(111), *Journal of Physical Chemistry* 94 (16), **1990**, 6379-6383.

[144] R. J. Purtell, R. P. Merrill, C. W. Seabury and T. N. Rhodin, Molecular Adsorbate Structures from Angular-Resolved Photoemission: Ammonia on Ir(111), *Physical Review Letters* 44 (19), **1980**, 1279 LP - 1281.

[145] B. A. Sexton and G. E. Mitchell, Vibrational spectra of ammonia chemisorbed on platinum (111) : I. Identification of chemisorbed states, *Surface Science* 99 (3), **1980**, 523-538.

[146] F. P. Netzer and T. E. Madey, Structure and orientation of NH3 on clean and oxygen-precovered Al(111), *Chemical Physics Letters* 88 (3), **1982**, 315-320.

[147] A. Bilic, J. R. Reimers, N. S. Hush and J. Hafner, Adsorption of ammonia on the gold (111) surface, *The Journal of Chemical Physics* 116 (20), **2002**, 8981-8987.

[148] N. A. Surplice and W. Brearley, The adsorption of carbon monoxide, ammonia, and wet air on gold, *Surface Science* 52 (1), **1975**, 62-74.

[149] B. D. Kay, K. R. Lykke, J. R. Creighton and S. J. Ward, The influence of adsorbate--absorbate hydrogen bonding in molecular chemisorption: NH[sub 3], HF, and H[sub 2]O on Au(111), *The Journal of Chemical Physics* 91 (8), **1989**, 5120-5121.

[150] R. E. Richton and L. A. Farrow, Adsorption kinetics of ammonia on an inhomogeneous gold surface, *Journal of Physical Chemistry* 85 (24), **1981**, 3577-3581.

[151] P. A. Thiel and T. E. Madey, The interaction of water with solid surfaces: Fundamental aspects, *Surface Science Reports* 7 (6-8), **1987**, 211-385.

[152] R. L. Wells and T. Fort, Adsorption of water on clean gold by measurement of work function changes, *Surface Science* 32 (3), **1972**, 554-560.

[153] M. Fleischer, E. Simon, E. Rumpel, H. Ulmer, M. Harbeck, M. Wandel, C. Fietzek, U. Weimar and H. Meixner, Detection of volatile compounds correlated to human diseases through breath analysis with chemical sensors, *Sensors and Actuators B: Chemical* 83 (1-3), **2002**, 245-249.

[154] M. Hesse, H. Meier and B. Zeeh, *Spektroskopische Methoden in der organischen Chemie*, Thieme, New York, Stuttgart, 4th edition, **1991**.

[155] H.-S. Wu, H.-C. Jone and J.-w. Hwang, Reaction of polyacrylic acid and metal oxides: Infrared spectroscopic kinetic study and solvent effect, *Journal of Applied Polymer Science* 63 (1), **1997**, 89-101.

[156] J. Ostrowska and A. Narebska, Association of the functional groups in polymers, *Colloid & Polymer Science* 257 (2), **1979**, 128-135.

[157] D. Santhiya, S. Subramanian, K. A. Natarajan and S. G. Malghan, Surface Chemical Studies on the Competitive Adsorption of Poly(acrylic acid) and Poly(vinyl alcohol) onto Alumina, *Journal of Colloid and Interface Science* 216 (1), **1999**, 143-153.

[158] T. Sugama, L. E. Kukacka and N. Carciello, Nature of interfacial interaction mechanisms between polyacrylic acid macromolecules and oxide metal surfaces, *Journal of Materials Science* 19 (12), **1984**, 4045-4056.

[159] A. Simon, M. Mücklich, D. Kunath and G. Heintz, Über raman- und ultrarotspektroskopische Untersuchungen an Hochpolymeren, *Journal of Polymer Science* 30 (121), **1958**, 201-226.

[160] W. G. Pohl and H. J. Kuhn, Über die Reaktion des Ag^+-Ions mit polyacrylsäurehaltigen Gelen, *Kolloid Zeitschrift und Zeitschrift für Polymere* 212, **1966**, 1-12.

[161] D. H. Lee, R. A. Condrate and J. S. Reed, Infrared spectral investigation of polyacrylate adsorption on alumina, *Journal of Materials Science* 31 (2), **1996**, 471-478.

[162] L. J. Bellamy, *Ultrarot-Spektrum und chemische Konstitution*, Dr. Dietrich Steinkopf Verlag, Darmstadt, 2nd edition, **1966**.

[163] J. Brandrup and E. H. Immergut, *Polymer Handbook*, Wiley, Weinheim, 3rd edition, **1989**.

[164] A. Eisenberg, H. Matsura and T. Yokoyama, Glass transition in ionic polymers: The acrylates, *Journal of Polymer Science Part A-2: Polymer Physics* 9 (12), **1971**, 2131-2135.

[165] A. Krauß, Hall-Effekt-Messungen an nanokristallinem Sensormaterial und applikationsspezifische Sensorentwicklung, *PhD*, University of Tübingen, Tübingen, **2001**.

[166] K. Bodenhöfer, Chirale Erkennung mit Schwingquarzsensoren, *PhD*, University of Tübingen, Tübingen, **1997**.

[167] B. A. Boukamp, Equivalent Circuit (EQUIVCRT.PAS), Users Manual, *PhD*, University of Twente, Department Chemical Technology, Enschede, **1989**.

[168] K. Besocke and S. Berger, Piezoelectric driven Kelvin probe for contact potential difference studies, *Review of Scientific Instruments* 47 (7), **1976**, 840-842.

[169] McAllister Technical Services, KP6500 Kelvin Probe User's Manual, **1999**.

[170] A. Arce, F. Fornasiero, O. Rodriguez, C. J. Radke and J. M. Prausnitz, Sorption and transport of water vapor in thin polymer films at 35°C, *Physical Chemistry Chemical Physics* 6, **2004**, 103-108.

[171] A. Kummer, A. Hierlemann and H. Baltes, Tuning the Sensitivity of Capacitive Chemical Microsensors, *Book of Abstracts, Eurosensors XVI*, Prag, Czech Republic, **2002**, 527-528.

[172] K. Ichikawa, T. Mori, H. Kitano, M. Fukuda, A. Mochizuki and M. Tanaka, Fourier transform infrared study on the sorption of water to various kinds of polymer thin films, *Journal of Polymer Science Part B: Polymer Physics* 39 (18), **2001**, 2175-2182.

[173] M.-J. Chang, A. S. Myerson and T. K. Kwei, The effect of hydrogen bonding on vapor diffusion in water-soluble polymers, *Journal of Applied Polymer Science* 66 (2), **1997**, 279-291.

[174] D. D. Nelson, G. T. Fraser and W. Klemperer, Does Ammonia Hydrogen Bond?, *Science* 238, **1987**, 1670-1674.

[175] R. C. Weast, *CRC Handbook of Chemistry and Physics*, The Chemical Rubber Company, Cleveland, Ohio, 53th edition, **1972**.

[176] C.-T. Lin, I. C. Paul and D. Y. Curtin, Anisotropic reaction with ammonia gas of a crystal of a carboxylic acid with linear hydrogen-bonded chains. Example of unitropic attack, *Journal of the American Chemical Society* 96 (11), **1974**, 3699-3701.

List of abbreviations

symbol	description
$\Delta\alpha$	change of thermal expansivity of T_g
ε	dielectric constant
ε_W	dielectric constant of water
Δf	QMB frequency shift due to added mass [Hz]
$\Delta f_{\text{PAA layer}}$	frequency shift due to the polymer compared with the uncovered QMB
Δf_{water}	further frequency shift due to the sorption of water
$\Delta m/A$	surface mass loading (g/cm2)
ϕ	phase shift
Φ	work function
ϕ_V	volume fraction
λ	adsorbate loading
$\lambda/2$	half of the acoustic wave length
λ_m	adsorbate loading at monolayer coverage
ρ	density
σ	conductivity
ω	radial frequency
ω_0	frequency wherein the imaginary part of the impedance is a maximum

AC IS	alternating current impedance spectroscopy
A	area
AC, ac	alternating current
APM	Acoustic Plate Mode
aq	aqueous

List of abbreviations

symbol	description
AW	Acoustic Wave
b	constant
b (as index)	bulk properties
BET	Brunauer-Emmett-Teller
C	capacitor, capacitance
c'	stiffness
C_0	initial capacitance in dry air
C_b	capacitance of the electrode structure covered with polymer as a dielectric material
C_{BET}	BET-constant
C_{dl}	double layer capacitance
CPD	contact potential difference
CPE	constant phase element
C_t	capacitance at time t
ct (as index)	charge transfer
CV	Cyclic Voltammetry
d	separation distance of the capacitor plates
dl (as index)	double layer
d_0	amplitude of the separation distance
DC	direct current
DFG	Deutsche Forschungsgemeinschaft
DSC	differential scanning calorimetry
e	elementary charge
E_0	amplitude of the potential signal
E_F	Fermi energy
E_t	potential at time t
EU-SCOEL	European Scientific Commitee on Occupational Exposure Limits
E_{VAC}	vacuum level

symbol	description
f_0	fundamental frequency of the quartz crystal [Hz]
FET	field effect transducer
FPW	Flexural Plate Wave
h_q	thickness of the quartz resonator
h_f	thickness of the polymer film
i	imaginary number
I	current
I_0	amplitude of the current signal
IC	integrated circuit
IR	infrared
IS	impedance spectroscopy
I_t	current at time t
IUPAC	International Union of Pure and Applied Chemistry
k	constant
K	constant
L	inductor
LOD	limit of detection
m	mass
n	number of multilayers
n	parameter of the constant phase element
NaPA	sodium polyacrylate
NH4PA	ammonium polyacrylate
p	pressure
P	adsorptive partial pressure
P*	saturation pressure of the adsorptive
PAA	polyacrylic acid
ppb	parts per billion
ppm	parts per million
q	charge

List of abbreviations

symbol	description
Q	charge of the condensator plates
QMB	Quarz microbalances
r	modulus of impedance
R	resistor
r.h.	relative humidity
R_b	resistance of the polymer bulk
R_{ct}	charge transfer resistance
S/N	signal to noise ratio
SAW	Surface Acoustic Wave
T	temperature
t	time
T_g	static glass transitin temperature
TRGS	Technische Regeln für Gefahrstoffe
T_{gm}	static glass transitin temperature of a mixed amorphous system
T_{gp}	glass transition temperature of the dry polymer
T_{gw}	glass transition temperature of water
TSM	thickness shear mode
V	voltage
w	weight fraction
W	Warburg impedance
w_p	weight fraction of polymer
wt %	weight percent
w_w	weight fraction of water in the polymer layer
x	P / P*
Y_0	parameter of the constant phase element
Z	impedance
Z_0	amplitude of the impedance
Z_W*	complex Warburg impedance

symbol	description
Z'	real part of the impedance
Z"	imaginary part of the impedance

List of publications

Full papers

M. Hoerter, A. Oprea, N. Bârsan, U. Weimar, Chemical interaction of gaseous ammonia and water vapour with polyacrylic acid layers, submitted to Sensors and Actuators B.

M. Hoerter, A. Oprea, N. Bârsan, U. Weimar, Kelvin Probe measurements of polymer coated gold substrates: mechanism studies, *Sensors and Actuators B*, 2008, doi:10.1016/j.snb.2008.04.048.

M. Sahm, A. Oprea, N. Bârsan, U. Weimar, Water and ammonia influence on the conduction mechanisms in polyacrylic acid films, *Sensors and Actuators B,*127, **2007**, 204-209.

M. Sahm, A. Oprea, N. Bârsan, U. Weimar, Interdependance of ammonia and water sorption in polyacrylic acid layers, *Sensors and Actuators B*, 130, **2007**, 502-507.

A.Gurlo, M.Sahm, A.Oprea, N.Bârsan, U.Weimar, A p- to n- transition on α-Fe_2O_3-based thick film sensors studied by conductance and work function change measurements, *Sensors and Actuators B*, 102, **2004**, 291-298.

A.Gurlo, N.Bârsan, A.Oprea, M.Sahm, T.Sahm, U.Weimar, A n- to p- conductivity transition induced by oxygen adsorption on α-Fe_2O_3, *Applied Physics Letters*, 85, **2004**, 2280-2282.

Diploma thesis

M. Sahm, Kombinierte Leitfähigkeits- und Austrittsarbeitsmessungen an Metalloxidsensoren, *Diplomarbeit*, Universität Tübingen, **2003**.

Conference Proceedings and Short Notes

M. Sahm, A. Oprea, N. Bârsan and U. Weimar, Water and Ammonia Influence on the Conduction Mechanisms in Polyacrylic Acid Films, *Eurosensors XX*, **2006**, 358-359, Goeteborg, Sweden, ISBN 978-91-631-9280.

M. Sahm, A. Oprea, N. Bârsan and U. Weimar, Interdependence of Ammonia and Water Sorption in Polyacrylic Acid Layers, *The 11th International Meeting on Chemical Sensors*, **2006**, Brescia, Italy.

A. Oprea, S. Riegelsberger, M. Sahm, U. Weimar, Gasempfindliche Polymer-Schichten zum Nachweis flüchtiger organischer Verbindungen: Fähigkeiten für

kapazitive Auslesung, *7. Dresdner Sensor-Symposium*, Dresdner Beiträge zur Sensorik, Band 24, TUDpress, **2005**, 25-28.

M. Sahm, A. Oprea, N. Bârsan and U. Weimar, Empfindliche Prozesse bei dünnen Polyacrylsäure-Schichten unter Ammoniak-Atmosphäre durch Impedanzspektroskopie aufgedeckt, *7. Dresdner Sensor-Symposium*, Dresdner Beiträge zur Sensorik, Band 24, TUDpress, **2005**, 267-270, Dresden.

N. Bârsan, A. Gurlo, M. Sahm, U. Weimar, Properties of indium oxide semiconducting sensors deposited by different techniques, *Partec 2004*, **2004**, Nürnberg (Germany).

M.Sahm, N.Bârsan, A.Gurlo, A.Oprea, U.Weimar, n-typ Metalloxidsensoren werden zu p-typ Halbleitern: Liegt es an Adsorptionsvorgängen oder ist es die elektronische Struktur? Messung und Interpretation, *6.Dresdner Sensor Symposium*, **2003**, 19-22, Dresden (Germany).

A.Gurlo, M.Sahm, A.Oprea, N.Bârsan, U.Weimar, Anomalous behaviour of a-Fe_2O_3-based thick film sensors studied by conductance and work function change measurements, *Eurosensors XVII European Conference on Solid-State Transducers*, **2003**, 70-71, Guimaraes (Portugal).

Acknowledgements

Meine akademischen Lehrer waren:

K. Albert, D. Christen, H.-J. Egelhaaf, H. Eckstein, G. Gauglitz, F. Gönnenwein, G. Häfelinger, M. Hanack, D. Hoffmann, V. Hoffman, W. Jäger, W. Koch, D. Krug, N. Kuhn, M.E. Maier, H.A. Mayer, H.-J. Meyer, E. Lindner, U. Nagel, H. Oberhammer, D. Oelkrug, H. Pauschmann, H. Pommer, G. Reinhardt, V. Schurig, M. Schwarz, E. Schweda, F.F. Seelig, J. Strähle, U. Weimar, K.-P. Zeller.

Curriculum Vitae

Name	Melanie Hörter, geb. Sahm
Geburtstag	17.10.1977
Geburtsort	Offenbach am Main
Familienstand	verheiratet
Staatsangehörigkeit	deutsch

Schule

09/1984 – 07/1988	**Carl-Orff-Schule** Rodgau (Grundschule)
09/1988 – 07/1997	**Marienschule der Ursulinen** in Offenbach mit dem Abschluss der Allgemeinen Hochschulreife

Studium

10/1997 – 05/2003	**Studium der Chemie** an der Eberhard-Karls-Universität Tübingen
09/1999	**Vordiplomprüfungen**
05/2003	**Diplomprüfungen**
	Diplomarbeit bei PD Dr. Udo Weimar am Institut für Physikalische und Theoretische Chemie der Eberhard-Karls-Universität Tübingen

Promotionsstudium

seit 08/2004	Anfertigung der **Dissertation** bei PD Dr. Udo Weimar am Institut für Physikalische und Theoretische Chemie der Eberhard-Karls-Universität Tübingen mit dem Titel
	"Influence of ammonia and water sorption on the chemical and electrochemical properties of polyacrylic acid and its derivates"